UNIVERSITÀ DEGLI STUDI DI TRIESTE

XXXVI CICLO DEL DOTTORATO DI RICERCA IN BIOMEDICINA MOLECOLARE

THE ROLE OF AURORA KINASE A IN THE DEVELOPMENT OF HEPATOCELLULAR CARCINOMA AND IN THE REGULATION OF PROGRAMMED DEATH-LIGAND 1

Settore scientifico-disciplinare: **BIO/11**

DOTTORANDO / A
LUCA GRISETTI

COORDINATORE
PROF. GERMANA MERONI

SUPERVISORE DI TESI
PROF. CLAUDIO TIRIBELLI

CO-SUPERVISORE DI TESI
DOTT. DEVIS PASCUT

ANNO ACCADEMICO 2022/2023

Table of contents

List of Figures

List of tables

List of abbreviations

2n - Diploid cells

4n - Tetraploid cells

>4n - Aneuploid cells with more than 4 sets of chromosomes

α-SMA - Actin α2, Smooth Muscle

AASLD - America Association for the Study of Liver Diseases

AFP - α-fetoprotein

AFP-L3 - Lens Culinaris Agglutinin A–Reactive Fraction of AFP

AJUBA - Ajuba LIM Protein

AKT - AKT Serine/Threonine Kinase

AKT1 - AKT Serine/Threonine Kinase 1

ALBI - Albumin-Bilirubin

ALD - Alcohol-associated liver disease

APASL - Asian Pacific Association for the Study of the Liver

APC- APC Regulator of WNT signaling pathway

APC/C - Anaphase-Promoting Complex/Cyclosome

aPKC - Atypical Protein Kinase C

ARID1A - AT-Rich Interaction Domain 1A

ASR - Age-standardized incidence and mortality rate

ASUGI - Azienda Sanitaria Universitaria Giuliano Isontina

ATP - Adenosine triphosphate

ATP1A1 - ATPase Na+/K+ Transporting Subunit α1

ATP5F1A - ATP synthase F1 subunit α

ATP5F1B - ATP synthase F1 subunit β

AUC - Area under the curve

AURKA - Aurora Kinase A

AURKB - Aurora Kinase B

AURKC - Aurora Kinase C

AXIN1 - Axin 1

BCL-2 - B-Cell Leukemia/Lymphoma 2

BCLC - Barcelona-Clinic Liver Cancer

BECN1 - Beclin 1

BMI - Body mass index

BMI1 – BMI1 Proto-Oncogene Polycomb Ring Finger

BORA - Protein Aurora Borealis

BRAF - B-Raf Proto-Oncogene, Serine/Threonine Kinase

BRCA1 - Breast Cancer Type 1

CBX3 - Chromobox 3

CBP - CREB Binding Protein

CDC20 - Cell Division Cycle 20

CDC25A - Cell Division Cycle 25A

CDCA7 - Cell Division Cycle Associated 7

CDE - Cell cycle-dependent element

CDK1 - Cyclin-Dependent Kinase 1

CDKNA2 - Cyclin-Dependent Kinase Inhibitor 2A

CDT1 - Chromatin Licensing and DNA Replication Factor 1

cGAS - Cyclic GMP-AMP Synthase

CHR - Cell cycle gene homology region

chrebp - carbohydrate-responsive element-binding protein

COL1A1 - Collagen Type I α1 Chain

CSC - Cancer stem cells

CT - Computed tomography

CTLA-4 - Cytotoxic T Lymphocyte-Associated Antigen 4

CTNNB1 - Catenin Beta 1

DCP - Des-Carboxy-Prothrombin

DMSO - Dimethyl sulfoxide

DREAM - DP/RB-like/E2F/MuvB

DRP1 - Dynamin-Related Protein 1

EASL - European Association for the Study of the Liver

EGF - Epidermal Growth Factor

EGFR - Epidermal Growth Factor Receptor

EHMT2 - Euchromatic Histone Lysine Methyltransferase 2

EMT - Epithelial-mesenchymal transition

ERK - Mitogen-Activated Protein Kinase

ES - Edmondson Steiner

FC - Fold change

FDA - Food and Drug Administration

FZR1 - Fizzy and Cell Division Cycle 20 Related 1

GALAD - Gender, Age, AFP-L3, AFP, and DCP

GMNN – Geminin

GSK3B - Glycogen Synthase Kinase 3β

GTEx - Genotype-tissue expression

HAVCR2 - Hepatitis A Virus Cellular Receptor 2

HBV - Hepatitis B Virus

HCC - Hepatocellular carcinoma

HCV - Hepatitis C Virus

HDAC6 - Histone Deacetylase 6

HE - Hematoxylin and eosin

List of abbreviations

HIF-1α - Hypoxia-Inducible Factor 1α

HP1γ - Heterochromatin Protein 1γ

HR – Hazard ratio

HRAS - HRas Proto-Oncogene, GTPase

ID1 - Inhibitor of Differentiation 1

IF – Immunofluorescence

IL2 - Interleukin 2

ILF3 - Interleukin Enhancer Binding Factor 3

INR - International normalized ratio

KDM4-AS1 - KDM4A antisense RNA 1

KEAP1 - Kelch Like ECH Associated Protein 1

KRAS - KRAS Proto-Oncogene, GTPase

LATS2 - Large Tumor Suppressor 2

LC50 - Lethal concentration 50

LGG - Brain lower-grade glioma

LT - Liver transplantation

MAFL - Metabolic dysfunction-associated steatotic liver

MAPK - Mitogen-Activated Protein Kinase

MASH - Metabolic dysfunction-associated steatohepatitis

MASLD - Metabolic dysfunction-associated steatotic liver disease

MCL1 – MCL-1 Apoptosis Regulator BCL2 Family Member

MRI - magnetic resonance imaging

MTOC - Microtubule-organizing center

mTOR - Mechanistic Target of Rapamycin

MTT - 3-(4,5-dimethyl thiazolyl-2)-2,5 diphenyltetrazolium

MYC - MYC Proto-Oncogene, BHLH Transcription Factor

NAFLD - Non-alcoholic fatty liver disease

NANOG - Nanog Homeobox

NDEL1 - NudE Neurodevelopment Protein 1 Like 1

NEDD9 - Neural Precursor Cell Expressed Developmentally Down-Regulated 9

NF-κB - Nuclear Factor kappa B

NFE2L2 - Nuclear Factor Erythroid 2-Related Factor 2

NFKB3 - RELA Proto-Oncogene, NF-kB Subunit

NFKBIA - NF-κB inhibitor α

NHEIII1 - Nuclear hypersensitive element III 1

NSCLC – Non-small cell lung cancer

NT5E - 5'-Nucleotidase Ecto

OCT4 - Octamer-binding protein 4

OS - Overall survival

PBMC - Peripheral blood mononuclear cell

PBS - Phosphate-Buffered saline

PCM - Peri-centriolar material

PCNT - Pericentrin

PCR - Polymerase chain reaction

PD-1 - Programmed Death-1

PD-L1 - Programmed Death – Ligand 1

PDAC - pancreatic ductal adenocarcinomas

PDCD1LG2 - Programmed Cell Death 1 Ligand 2

PDGFR - Platelet-Derived Growth Factor Receptor

PI3K - Phosphoinositide 3-Kinases

PP1 - Protein Phosphatase 1

PP6 - Protein Phosphatase 6

pparγ - proliferator-activated receptor γ

PRAD - Prostate adenocarcinoma

PRF - Perforin 1

PTEN - Phosphatase And Tensin Homolog

RAC1 - Rac Family Small GTPase 1

RAF1 - Raf-1 Proto-Oncogene Serine/Threonine Kinase

RAS - Rat Sarcoma

RNAi - RNA interference

ROC - Receiver operating characteristic

RPS6KB1 - Ribosomal Protein S6 Kinase B1

RT – Reverse transcription

RT-qPCR - Quantitative Real-Time

RTK - Receptor Tyrosine Kinases

SA-β-gal - Senescence-Associated β-galactosidase

SCLC - Small cell lung cancer

SD – Standard deviation

SIGLEC15 - Sialic Acid-Binding Ig Like Lectin 15

SiRNA - Small interfering RNA

SLD - Steatotic liver disease

SREBF1 - Sterol Regulatory Element-Binding Transcription Factor 1

srebp1 - sterol regulatory element-binding protein 1

STAT3 - Signal Transducer and Activator of Transcription 3

STING Stimulator of IFN Genes

TACC3 - Transforming Acidic Coiled-Coil Containing Protein 3

TACE - Transarterial chemoembolization

TCGA - The Cancer Genome Atlas

TERT - Telomerase reverse transcriptase

TG – Transgenic

List of abbreviations

TGFβ – Transforming Growth Factor β

THCA - Thyroid carcinoma

THPA - The Human Protein Atlas

TIGIT - T Cell Immunoreceptor with Ig and ITIM Domains

TNBC - Triple-negative breast cancer

TNM - tumor, node and metastases

TP53 - Tumor Protein P53

TPM – Transcripts per million

TPX2 - Targeting Protein for Xenopus Kinesin-Like Protein 2

US - Ultrasonography

VEGF - Vascular Endothelial Growth Factor

VEGFR - Vascular Endothelial Growth Factor Receptor

WB – Western blot

Wnt - Wingless-Related Integration Site

WT - Wild-type

YAP1 - Yes1 Associated Transcriptional Regulator

Summary

Hepatocellular carcinoma (HCC) is a global health challenge, ranking as the fourth leading cause of cancer-related deaths, and is predicted to increase in both incidence and mortality rates in the coming years. The persistent high mortality associated with HCC is primarily attributed to late diagnoses and limited therapeutic options. Recent strides in clinical practice, particularly the combination of targeted therapy and immunotherapy, have slightly improved outcomes in advanced-stage HCC. The modest progress observed can be attributed to the substantial heterogeneity of the disease. Thus, there is an urgent need for the identification of novel therapeutic targets, potentially in combination with immune checkpoint inhibitors, to address the intricate variability of the conditions for a more personalized and effective approach.

Aurora Kinase A (AURKA), belonging to the Aurora family of serine/threonine kinases, plays a pivotal role in mitosis, particularly in the G2/M transition. Beyond the canonical function, AURKA is involved in other cellular processes, including primary cilium remodeling, neuromorphogenesis, and mitochondrial fission. AURKA overexpression has been observed in numerous tumor types, including HCC, where it is implicated in critical oncogenic processes such as proliferation, survival, migration, and invasion. Recent findings in various cancer types revealed an intriguing role of AURKA in Programmed Death-Ligand 1 (PD-L1) regulation and immune response to the tumor. However, the regulatory interplay between AURKA and PD-L1 is still unexplored in HCC.

This study aims to comprehensively investigate the expression patterns of AURKA and its interactors in both HCC and precancerous conditions and to evaluate the molecular and cellular effects of inhibiting and silencing AURKA *in vitro*, with a specific focus on the regulatory influence on PD-L1. The project employed a translational approach, by integrating the analysis of human liver samples, a transgenic (TG) mouse model of HBV infection leading to HCC, and two HCC-derived cell lines (JHH6 and Huh7 cells). The human liver samples utilized in our study were sourced from HCC patients (n=56), individuals with metabolic dysfunction-associated steatotic liver disease (MASLD) (n=17), and subjects with healthy livers (n=14). The animal model was the HBV-TG mice C57BL/6J-TG(ALB1HBV)44BRI/J progressing to HCC within 12 months.

The analysis of human samples revealed significant overexpression of *AURKA* mRNA in HCC, with 75% of the tumor tissues showing elevated levels compared to adjacent non-tumor tissues. *AURKA* exhibited a consistent gradual increase with the hepatocarcinogenesis progression, demonstrating

diagnostic potential for HCC in patients with chronic liver disease. Corroborating these findings, the TG mouse model reflected a similar increase in *Aurka* expression as tumors developed when compared to pre-tumoral stages and adjacent non-neoplastic tissues. In HCC patients, *AURKA*'s expression positively correlated with several oncogenes, including *TPX2 Microtubule Nucleation Factor (TPX2), PD-L1*, and *KRAS Proto-Oncogene, GTPase (KRAS)*. This positive correlation with *TPX2* and *PD-L1* extended to pre-cancerous conditions, with the expression of both genes increasing with disease progression.

Surprisingly, AURKA protein expression exhibited a reduction in 83% of tumors compared to adjacent non-tumoral tissues. This discrepancy in expression levels might stem from differential post-transcriptional regulation, resulting in distinct isoforms of *AURKA* mRNA with varying translation efficiencies. The highest AURKA expression was observed in steatotic tissues, suggesting a potential non-canonical role of AURKA in steatosis and fibrosis. However, our analysis revealed a higher percentage of phosphorylated AURKA on the Thr288 residue specifically within the tumor tissue. This phosphorylation pattern is an indicator of heightened kinase activity in the HCC tumor microenvironment. However, the increased kinase activity did not correlate with cell proliferation, as evidenced by Ki67 staining, suggesting potential non-canonical roles to further elucidate.

PD-L1 expression increased in tumor tissues compared to adjacent non-tumoral tissues, particularly in the non-mature unglycosylated forms, while the glycosylated mature forms were stable. This can represent the initial step for subsequent membrane localization of PD-L1, promoting the immune escape of tumor cells. Alternatively, it can suggest a potential non-immunological, pro-oncogenic role of PD-L1 within tumor cells. Novel evidence observed PD-L1 involvement in epithelial-mesenchymal transition (EMT), glucose and lipid metabolism, stemness, and autophagy.

The two selected HCC-derived cell models exhibited elevated AURKA expression and displayed a strong dependency on AURKA for their growth. To efficiently inhibit AURKA kinase activity, we employed two inhibitors, alisertib and AK-01, as well as a siRNA targeting *AURKA* to modulate total AURKA expression. Both AURKA inhibitors effectively reduced AURKA enzymatic activity, with AK-01 showing superior inhibition. Interestingly, in JHH6 cells, AURKA inhibition triggered an increase in both *AURKA* mRNA and AURKA protein expression, suggesting the activation of a compensatory mechanism to generate new enzymatically active AURKA proteins in response to the inhibition of phosphorylated protein. The varied response observed in the two cell lines, particularly the higher effectiveness of AURKA inhibition treatments in JHH6 cells could be attributed to the distinct HCC subtypes of the two cell lines, emphasizing the importance of considering tumor heterogeneity in therapeutic strategies.

Summary

AURKA inhibition led to disruptions in cell mitosis, manifesting as centrosomal disorganization, defective mitotic spindle assembly, incorrect chromosome alignment, impaired chromosome separation, and incomplete cytokinesis. These disruptions induced cellular stress, resulting in a gradual reduction in cell viability over time. Despite their resistance to apoptosis, cancer cells progressed through anaphase and telophase but failed to complete cytokinesis accurately, promoting the accumulation of multiple chromosomes and the formation of aneuploid cells.

Silencing AURKA significantly reduced both AURKA mRNA and protein expression in the two cell lines. Consistent with chemical inhibition, AURKA knockdown disrupted cell mitosis, leading to an increased population of aneuploid cells and a reduction in cell viability over time.

In vitro, AURKA exerts regulatory control over PD-L1 through two distinct mechanisms. The kinase-mediated activity of AURKA is crucial in influencing PD-L1 protein glycosylation and stabilization, while the presence of AURKA protein, irrespective of its kinase activity, has a notable impact on PD-L1 transcription. Indeed, the treatment with the AURKA inhibitor AK-01 decreased PD-L1 glycosylated mature forms, triggering a compensatory mechanism that promoted new *PD-L1* transcription. Conversely, AURKA knockdown led to a decrease in PD-L1 promoter activation, *PD-L1* mRNA, and newly translated PD-L1 protein forms.

In conclusion, our study revealed the multifaceted roles of AURKA in the HCC progression, uncovering its potential as a biomarker and a therapeutic target. The intricate interplay identified between PD-L1 and AURKA presents a potential avenue for the development of more precise and effective therapeutic strategies. Combining AURKA inhibitors with immune checkpoint inhibitors holds promise, offering a synergic approach that could significantly benefit HCC patients.

Chapter 1 - Introduction

1.1 Hepatocellular carcinoma: A worsening global burden

Liver cancer is the sixth most common tumor worldwide in 2020, with more than 906.000 cases annually, and the fourth leading cause of cancer-related death, with approximately 830.000 deaths per year [1]. The highest age-standardized incidence and mortality rates (ASRs) occur in Eastern Asia (17.8 new cases and 16.1 deaths per 100,000 people), Northern Africa (15.2 new cases, 14.5 deaths), and South-Eastern Asia (13.7 new cases, 13.2 deaths). A similarity between the number of cases and deaths underlines the high mortality of this disease. The number of new cases and deaths of liver cancer per year will increase by 55.0% and 56.4%, respectively, between 2020 and 2040, with a possible 1.4 million people diagnosed and 1.3 million dying in 2040. Liver cancer has a strong male predominance, indicated by the 1.2-3.6 times higher ASR among males compared to females in all world regions [2].

Hepatocellular carcinoma (HCC) is a primary liver tumor that represents approximately 75-85% of all liver malignancies [1,2]. Its name derives from the term “hepatocytes”, the cell type from which HCC originates [3]. HCC is a progressive disease, mostly developed (>90% of cases) in patients with chronic liver inflammation, fibrosis, and cirrhosis. Despite a marked improvement in overall patient management in the last decades, HCC remains a malignancy with an unfavorable prognosis [4].

1.1.1 From risk factors and molecular mechanisms to diagnostic advances in HCC

HCC is a life-threatening malignancy triggered by chronic exposure to hepatitis B and C viruses, excessive alcohol intake, hepatic lipid droplet accumulation, and aflatoxins [5]. Long-term exposure to these risk factors determines a chronic liver inflammation that often results in cirrhosis, the main predisposing condition for HCC development [1].

The occurrence of the risk factors depends on geography, ethnicity, age, and lifestyle habits, which deeply marks a variability in the incidence of HCC worldwide [5]. Chronic infection of Hepatitis B Virus (HBV) is the major etiological factor in most parts of Asia (except Japan), Andean Latin America, and Western Africa, while Chronic Hepatitis C Virus (HCV) in Northern Africa, North America, Western Europe, Japan, and the Middle East [1] (Figure 1). Metabolic dysfunction-associated steatotic liver disease (MASLD) – formerly named Non-alcoholic fatty liver disease

(NAFLD) – has become the major cause of cirrhosis in most developed countries during the last few years (Figure 1). MASLD is defined as the presence of hepatic steatosis in conjunction with one cardio-metabolic risk factor and no other discernible cause [6,7]. Alcohol abuse is a prevalent risk factor for HCC in Central and Eastern Europe, South Latin America, and Southern Africa [1] (Figure 1). Heavy alcohol consumption (≥3 drinks/day) promotes a ~16% increase in liver malignancies [8].

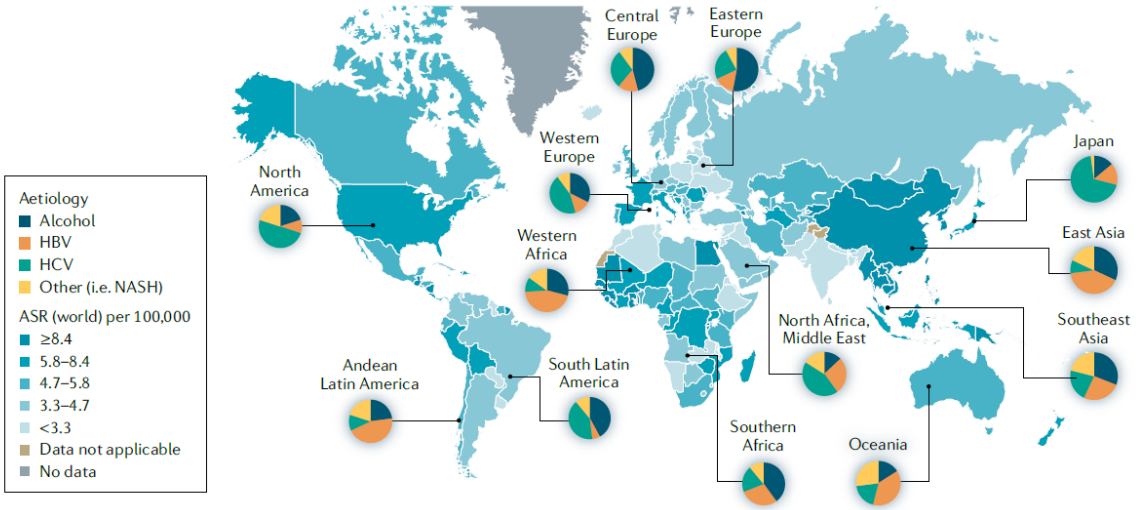

Figure 1. The global incidence of HCC and the major etiological factors involved in hepatocarcinogenesis [1]. The Hepatitis B virus (HBV) is the main risk factor in most parts of Asia, South America, and Africa; while the Hepatitis C virus (HCV) is in Western Europe, North America, and Japan. Alcohol intake represents ~50% of etiologies in Central and Eastern Europe. HBV, Hepatitis B virus; HCV, Hepatitis C virus; NASH, Non-alcoholic steatohepatitis, recently renamed MASH, Metabolic dysfunction-associated steatohepatitis; ASR, Age-standardized incidence rate.

The progression from cirrhosis to HCC is initiated by a gradual accumulation of somatic mutations and copy number variations in driver genes. Among the most frequent alterations is the reactivation of telomerase (observed in 80% of HCC cases), which occurs *via* Telomerase Reverse Transcriptase (TERT) promoter mutations, viral insertions, chromosome translocations, or gene amplifications. Another common alteration is the activation of the Wingless-related integration site (Wnt)–β-catenin signaling pathway, identified in 30–50% of cases. This activation results from mutations in key genes such as *Catenin β1* (*CTNNB1*), *AXIN1*, *or APC Regulator of WNT Signaling Pathway* (*APC*) inactivation [1]. Further alterations occur in genes involved in cell cycle control pathways, such as *Tumor Protein P53* (*TP53*) and *Cyclin-Dependent Kinase Inhibitor 2A* (*CDKNA2*), oxidative stress (*Nuclear Factor Erythroid 2-Related Factor 2* (*NFE2L2*), *Kelch Like ECH Associated Protein 1* (*KEAP1*), and chromatin modification (*AT-Rich Interaction Domain 1A* (*ARID1A*)), as well as in the pathway involving AKT Serine/Threonine Kinase (AKT), Mechanistic

Target of Rapamycin Kinase (mTOR), and Mitogen-activated protein kinase (MAPK) [1,9–11]. The high heterogeneity both at the intratumoral and inter-patient levels of HCC makes more challenging the comprehension of the molecular mechanisms of hepatocarcinogenesis [12,13].

The American Association for the Study of Liver Diseases (AASLD), the European Association for the Study of the Liver (EASL), and the Asian Pacific Association for the Study of the Liver (APASL) recommend a surveillance program for patients with a high risk of HCC development to diagnose cancer at early stages and increase the possibilities of providing curative treatments. These patients are recommended to undergo ultrasonography (US) every six months, with or without serum α-fetoprotein (AFP) analysis. US has low sensitivity (~47%) for early-stage HCC, which is partially increased by the analysis of serum AFP to 48-75% [14]. Additional diagnostic imaging tests, such as computed tomography (CT) and dynamic contrast-enhanced magnetic resonance imaging (MRI), are employed when dealing with lesions larger than 1cm in diameter or with AFP levels above 20ng/mL [1].

Beyond ultrasonography and diagnostic imaging, molecular biomarkers provide an additional way for HCC detection. Notably, the GALAD score, an acronym derived from the initials of each biomarker, integrates Gender and Age with the molecular biomarkers Lens culinaris agglutinin A–reactive fraction of AFP (AFP-L3), AFP, and Des-carboxy-prothrombin (DCP) [15]. A comprehensive meta-analysis encompassing 3,739 patients from 9 different studies investigated the overall diagnostic performance of the GALAD score in detecting early-stage HCC in patients with chronic liver diseases. The study revealed a moderate sensitivity (0.73 (95%CI: 0.66–0.79)) and high specificity (0.87 (95%CI: 0.81–0.91)) of GALAD score in HCC detection [16]. Despite advancements in technology, concerted preventive campaigns, and surveillance initiatives in recent decades, only a restricted number of patients receive an early-stage diagnosis. Most HCC patients are diagnosed at advanced tumor stages, yielding a five-year survival rate of 20-40% [14]. Thus, persists a crucial clinical need for the identification and integration of novel biomarkers for HCC diagnosis.

1.1.2 The treatment strategies for the different HCC stages: The urgency of new therapies

Novel staging systems have been developed in the last three decades to stratify HCC patients according to the severity of the disease based on tumor-related features and preserved liver function,

critical elements for the maintenance of body homeostasis, which are gradually lost during tumor progression [17]. The Barcelona-Clinic Liver Cancer (BCLC) classification is recommended by the EASL and AASLD [18] and classifies HCC patients into five stages (0, A, B, C, and D) based on tumor status (size, number, vascular invasion, lymph node, and metastases), liver function (Child-Pugh score and Albumin-Bilirubin (ALBI) score), and overall health status (Figure 2). This classification helps clinicians predict prognosis and decide the best treatment strategy for HCC patients [19]. The decision-making process considers various factors such as tumor burden, the severity of liver dysfunction, medical comorbidities, and patient preferences [14].

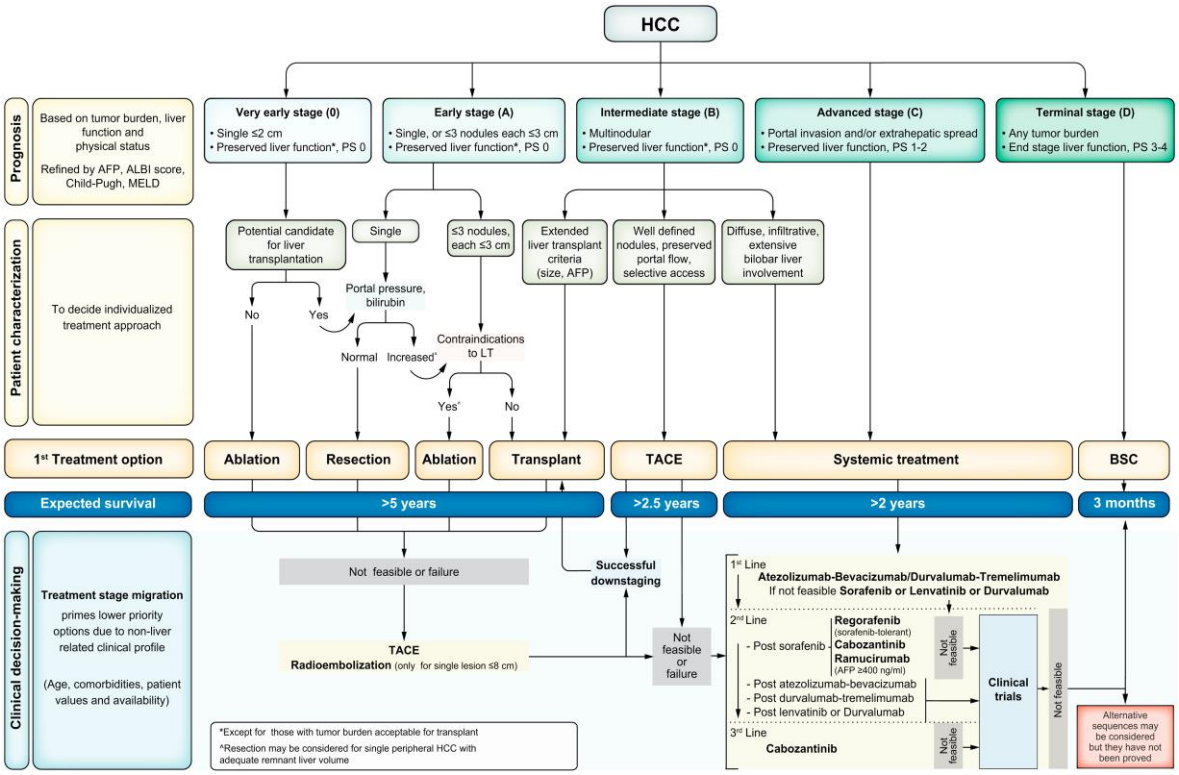

Figure 2. BCLC staging system and related treatment strategies [19]. The BCLC system establishes a prognosis and a first-line treatment recommendation in accordance with the 5 stages (0, A, B, C, and D). AFP, α-fetoprotein; ALBI, Albumin-Bilirubin; BCLC, Barcelona Clinic Liver Cancer; BSC, Best supportive care; ECOG-PS, Eastern Cooperative Oncology Group-performance status; LT, Liver transplantation; MELD, Model of end-stage liver disease; TACE, Transarterial chemoembolization.

The available treatment options for HCC remain restricted compared to other types of solid tumors. Patients diagnosed at early stages (BCLC 0/A) have a >5 years median of expected survival after treatments, which decreases to >2.5 years in intermediate stages (BCLC B), and >2 years in advanced stages (BCLC C) [19] (Figure 2). Patients diagnosed at terminal stages (BCLC D) have an expected median survival of 3 months and are only eligible for palliative therapies [1,19] (Figure 2).

The management of very early-stage (BCLC 0) and early-stage patients (BCLC A) includes potentially curative treatments (hepatic resection, liver transplantation (LT), and ablation) (Figure 2) with ~70–80% of a 5-year survival rate. The eligibility of patients for ablation, resection, or LT is determined by factors such as liver function, portal hypertension, performance status, and tumor characteristics [1]. For multifocal (≤3 nodules ≤3cm each) tumors, LT is the best option strategy boosting a survival rate of 70% and a recurrence rate of 10–15% at 5 years, while ablation and recurrence have a high risk of HCC recurrence [1,19]. The BCLC B stage can be divided into three subgroups (Figure 2), according to tumor burden and liver functions. Patients with well-defined HCC nodules are candidates for LT (Figure 2), patients with preserved portal flow and defined tumor burden are eligible for transarterial chemoembolization (TACE) (Figure 2), and patients with diffuse, infiltrative, and extensive bilobar liver involvement are recommended for systemic therapy (Figure 2). During TACE, the chemotherapy is delivered to the tumor and causes embolization of the tumor microcirculation. This therapy has a median overall survival (OS) of the patients estimated at ~30 months [1,19].

From 2007 to 2017 the only available first-line option for the treatment of BCLC C patients was the multikinase inhibitor sorafenib, which targets Vascular endothelial growth factor receptor (VEGFR)-1, VEGFR-2, and VEGFR-3, Platelet-derived growth factor receptor (PDGFR), and Raf-1 proto-oncogene serine/threonine kinase (RAF1) [14]. In 2018, the approval of the multikinase inhibitor lenvatinib represented a notable advancement. Lenvatinib demonstrated a slightly higher median OS (13.6 months) compared with Sorafenib (13.2 months) [1]. However, the current first choice as first-line treatment for BCLC C patients is the combination of an immune checkpoint inhibitor (atezolizumab) with an oncogene-targeted therapy (bevacizumab) (Figure 2) approved by the Food and Drug Administration (FDA) in May 2020 [1].

The phase III IMbrave150 study revealed a superior survival benefit of atezolizumab-bevacizumab (median OS of 19.2 months) compared to sorafenib (median OS of 13.4 months) [20]. Bevacizumab acts by selectively binding circulating Vascular Endothelial Growth Factor (VEGF), while Atezolizumab (IgG1 anti-Programmed death – ligand 1 (PD-L1)) is a drug that binds and blocks PD-L1 interaction with its receptor Programmed Death-1 (PD-1) promoting T cell response and inhibiting tumor immune evasion [21,22]. Oncogene-targeted therapies in cancer treatment can provide a high response in patients that timely leads to resistance, while immunotherapy has a relatively low response in patients but with consistent prolonged effects. Thus, the combination of

immune checkpoint inhibitors and oncogene-targeted therapy can improve the efficacy and long-term effectiveness of the treatment [23].

An alternative first-line treatment is represented by the combination of durvalumab (anti-PD-L1 monoclonal antibody) and tremelimumab (anti-Cytotoxic T Lymphocyte-Associated Antigen 4 (CTLA-4) monoclonal antibody) [19] (Figure 2). The phase III HIMALAYA trial showed that a single priming dose of tremelimumab added to durvalumab significantly prolonged the survival (median OS of 16.4 months) compared to sorafenib (13.8 months) and durvalumab as monotherapy is not inferior to sorafenib in first-line therapy [24].

The advent of recent therapies has increased advanced patients ' expected survival to two years or more. However, the demand for novel therapies that can markedly improve patient survival persists. The exploration of combining multiple drugs, particularly immune checkpoint inhibitors and oncogene-targeted therapies, represents a promising direction for further investigation.

1.2 Aurora kinase A: A protein with multifaceted roles

The Aurora kinase family is a group of serine/threonine kinases that regulates mitotic cell division (mitotic entry, spindle assembly, and cytokinesis), fundamental processes for maintaining the fidelity of genetic information [25]. Their family name originated from the observation that *aurora*-mutated *Drosophila melanogaster* cells failed to correct duplicate and separate their centrosome during mitosis. This results in the formation of defective spindles, characterized by monopolar configuration rather than the typical bipolar spindle, which resemble the *aurora borealis* phenomenon [26]. In mammals, the three members of the Aurora kinase family are Aurora Kinase A (AURKA), Aurora Kinase B (AURKB), and Aurora Kinase C (AURKC) [27]. AURKA and AURKB are expressed in most somatic cell types where they regulate cell division during mitosis, whereas AURKC is predominantly expressed in germ cells and early embryos where it regulates meiosis [10,25,26,28]. However, recent evidence showed that AURKC can also modulate mitosis [26,29].

1.2.1 AURKA protein structure

AURKA gene maps on human chromosomes 20q13.2 [27] and encodes for at least 16 known transcript variants [30]. The reference transcript encodes for a 403 amino acid (aa) protein constituted

by a kinase domain flanked by two non-catalytic domains, known as the N-terminal domain (length: 39-139aa) and the C-terminal domain (15–20aa) [27].

The AURKA kinase domain is constituted by a β-stranded N-terminal lobe and an α-helical C-terminal lobe linked together by a hinge region, and an Adenosine triphosphate (ATP)-binding pocket. The hydrogen bonds link the purine ring of adenosine to the hinge region [27]. An intermolecular trans-reaction within the two-lobed AURKA domain triggers autophosphorylation on the conserved catalytic T-loop residue (Thr288) of the C-terminal lobe, followed by a 3D conformation change of the kinase catalytic ATP-binding pocket. This conformational alteration involves the opening of the catalytic loop, thereby activating the kinase activity [31,32] (Figure 3). The C-terminal domain orchestrates the interactions with co-factors that govern protein conformation, while the N-terminal domain plays a pivotal function in the interaction with its protein partners, thereby regulating AURKA localization and function [27].

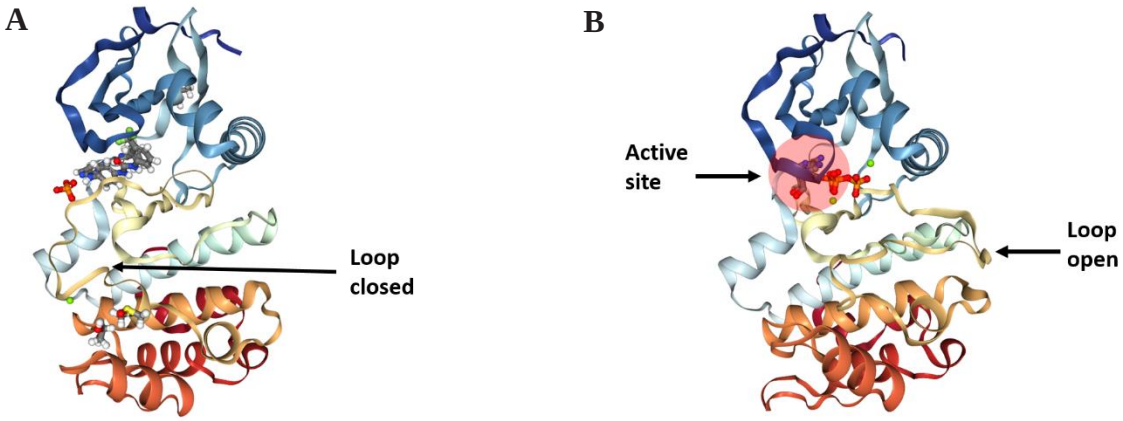

Figure 3. AURKA structure. (A) Human AURKA in a close conformation bound to the inhibitor CD532 [33], structure 4j8M, taken from the protein data bank PDB database. (B) Human AURKA in an open conformation in complex with ATP [34], structure 5DNR, taken from the protein data bank PDB database. Phosphorylation on the activation loop switches the kinase into an active T-loop conformation required to provide access to ATP and substrates.

1.2.2 The fundamental role of AURKA in mitosis

AURKA plays a pivotal role in the regulation of the mitotic process, particularly in G2/M transition, centrosome maturation, mitosis entry, and mitotic spindle formation [27,35]. AURKA levels are low in the G1 phase, but as the cell cycle progresses, there is an increase in transcription

and protein accumulation within nuclei. This elevation begins towards the end of the S phase and reaches its peak during the G2 phase [36,37].

The tight regulation of AURKA transcription during the cell cycle is orchestrated by specific elements located in its promoter region, namely the Cell cycle-dependent element (CDE) and Cell cycle gene homology region (CHR) [36]. The DP/RB-like/E2F/MuvB (DREAM) binds on the CHR facilitated by CDE playing a pivotal role in either activating or repressing transcription [38].

During mitosis, the phosphorylation on Thr288 plays a fundamental role in regulating the kinase activity of AURKA, enabling a correct mitotic process. It can be initiated by AURKA through autophosphorylation [27] or with the involvement of several co-factors, including Ajuba LIM Protein (AJUBA) [39], Targeting Protein for Xenopus Kinesin-Like Protein 2 (TPX2) [40], and Protein Aurora Borealis (BORA) [41] (Figure 4). The Thr288 phosphorylation triggers the activation of AURKA subsequently prompting the phosphorylation of its co-factor, BORA, thus increasing the kinase activity of AURKA [41]. Consequently, AURKA can phosphorylate and activate the Cyclin-Dependent Kinase 1 (CDK1)-Cyclin B complex to unlock the G2/M checkpoint [39] (Figure 4). During the G2/M transition, AURKA localizes in the centrosome and contributes to its maturation before mitotic entry [27]. The localization of AURKA at the centrosome is facilitated by two distinct mechanisms. The N-terminal domain promotes AURKA interaction with the centrosomes [42,43] and the CDK11 increase during prophase contributes to its recruitment [27].

Before spindle assembly, AURKA whose activity is maintained by AJUBA, recruits peri-centriolar material (PCM) proteins such as Centrosomin, Large Tumor Suppressor 2 (LATS2), and Breast Cancer Type 1 (BRCA1) to organize the microtubule-organizing center (MTOC) [44–46] (Figure 4). LATS2 recruits γ-tubulin and BRCA1 promotes microtubule nucleation during centrosome maturation [44,47]. At metaphase, AURKA localizes to the proximal microtubule spindle and targets microtubule-associated proteins to assemble the mitotic spindle [27] (Figure 4). During the initial spindle assembly, TPX2 allows the maintenance of AURKA's active conformation, protecting the kinase from dephosphorylation by Protein Phosphatase (PP)1 and PP6 [27,29].

The second part of the mitotic process is regulated by AURKB promoting spindle assembly checkpoint crossing, triggering sister chromatids separation, and phosphorylating some cytoskeleton regulatory proteins (including Vimentin and Desmin) at the midbody to organize the cleavage furrow for cytokinesis [27].

To enable the progress of the cell cycle, AURKA inactivation and degradation are essential processes during the phase known as "mitotic exit" [48]. These two processes operate independently, each involving different actors. The Anaphase-Promoting Complex/Cyclosome (APC/C), along with its co-activator Cell Division Cycle 20 (CDC20), recognizes TPX2 and promotes its destruction. The loss of interaction with TPX2 triggers the dephosphorylation of AURKA at Thr288, subsequently promoting PP1-mediated inactivation [49]. In the degradation process, APC/C is assisted by the coactivator Fizzy and Cell Division Cycle 20 Related 1 (FZR1). The APC/C-FZR1 complex recognizes AURKA as one of its substrates and catalyzes the transfer of ubiquitin molecules to specific lysine residues [50,51] in conjugation with two E2 ubiquitin enzymes. This ubiquitination process targets the substrate for proteasome-mediated degradation [52] (Figure 4). The inactivation and degradation of AURKA are crucial to ensure the correct progression of the cell cycle, preventing potential errors or anomalies.

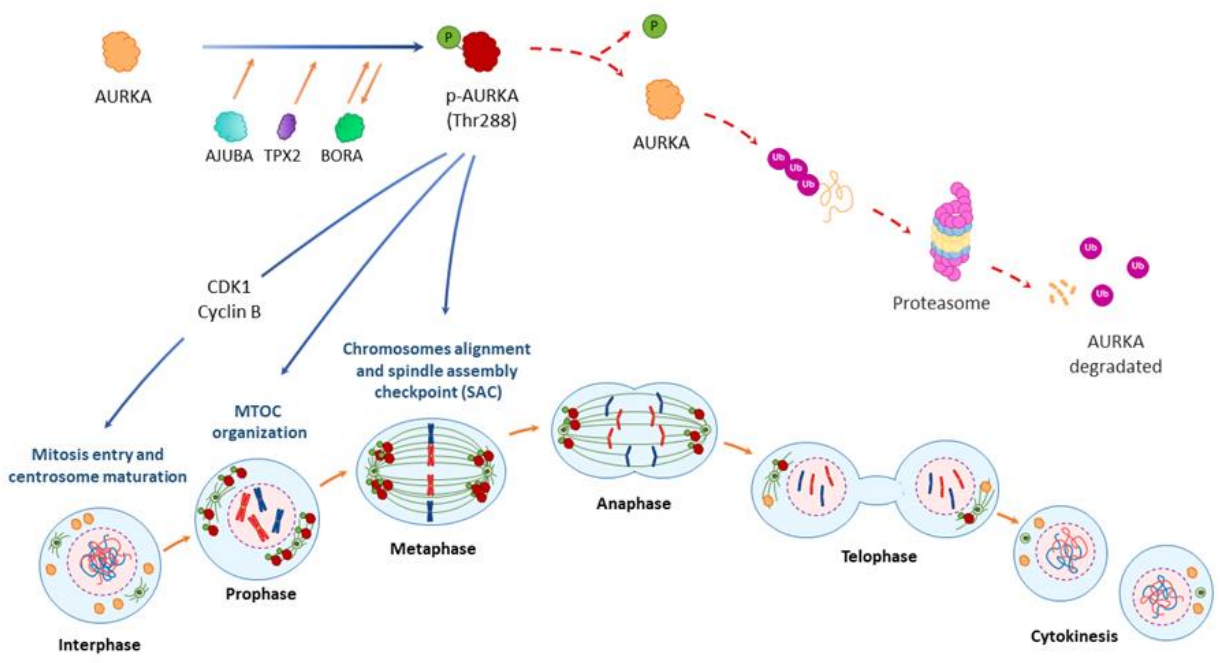

Figure 4. AURKA's roles during mitosis. AURKA is primarily activated by its auto-phosphorylation on Thr288 (phospho-AURKA (p-AURKA)), which is promoted by several co-factors including the Ajuba LIM protein (AJUBA), the Targeting Protein for Xenopus Kinesin-Like Protein 2 (TPX2), and the Protein Aurora Borealis (BORA). Once activated, AURKA phosphorylates and activates Cyclin-Dependent Kinase 1 (CDK1)-Cyclin B complex to unlock the G2/M checkpoint. In the G2/M phase, AURKA promotes centrosome maturation, mitotic entry, mitotic spindle formation, spindle assembly checkpoint (SAC) establishment, and cytokinesis. As mitosis concludes, AURKA's degradation is mediated by Anaphase-Promoting Complex/Cyclosome (APC/C) through ubiquitin-mediated proteolysis.

1.2.3 AURKA: A protein with various functions besides cell cycle regulation

AURKA mainly undergoes degradation through ubiquitin-mediated proteolysis during "mitosis exit" [50,53]. Nevertheless, recent evidence suggests the presence of an interphase pool of AURKA with diverse functions [54,55]. This pool can be preserved from proteasomal degradation, possibly due to the phosphorylation of the Ser51 residue [56]. The undegraded pool of AURKA has various non-mitotic physiological functions that vary according to the cell cycle phase, cellular localization, and cell type [54].

In the M phase, AURKA phosphorylates Geminin (GMNN) on Thr25 residue, which preserves Chromatin Licensing and DNA Replication Factor 1 (CDT1) from degradation, thus promoting the initiation of DNA replication [57,58]. During interphase, AURKA (Thr288) autophosphorylation promoted by the scaffolding protein Neural Precursor Cell Expressed Developmentally Down-Regulated 9 (NEDD9) results in Histone Deacetylase 6 (HDAC6) phosphorylation, which promotes the disassembly of the primary cilium, a process associated with the cells re-entering the cycle [59,60].

AURKA can localize in the nucleus and regulate various epigenetic factors, such as Chromobox 3 (CBX3), also known as Heterochromatin Protein 1γ (HP1γ) [61], and histone H3 [62,63]. AURKA mediates the H3S10 phosphorylation, which promotes the transcription of *Cell Division Cycle Associated 7* (*CDCA7*) and *Cell Division Cycle 25A* (*CDC25A*) and blocks the recruitment of the Euchromatic Histone Lysine Methyltransferase 2 (EHMT2) transcriptional repressor [63]. AURKA can also localize in mitochondria to regulate mitochondrial fission. It promotes the phosphorylation of Dynamin-Related Protein 1 (DRP1) on Ser616, triggering mitochondrial fission and ensuring the proper distribution of mitochondria to daughter cells [64,65].

Finally, AURKA is abundantly expressed in post-mitotic neurons, cells that undergo neurite outgrowth, playing a central role in neuromorphogenesis [66]. Atypical Protein Kinase C (aPKC) phosphorylates AURKA on Thr287, facilitating the binding of TPX2 to AURKA. This interaction promotes AURKA phosphorylation on Thr288 [67], leading to the phosphorylation of NudE Neurodevelopment Protein 1 Like 1 (NDEL1) on Ser251 residue by AURKA [68]. The aPKC/AURKA/NDEL1 pathway promotes the formation of a functional MTOC during neurite extension [67].

1.3 Aurora kinase A in hepatocellular carcinoma: A potential therapeutic target

The association between AURKA and malignant phenotypes has become increasingly evident over the years. AURKA frequently exhibits elevated levels in tumors (Figure 5), attributed to gene amplifications [69], single point mutations [70–72], and post-transcriptional regulation mechanisms, such as micro-RNAs (miRNAs) [10,73].

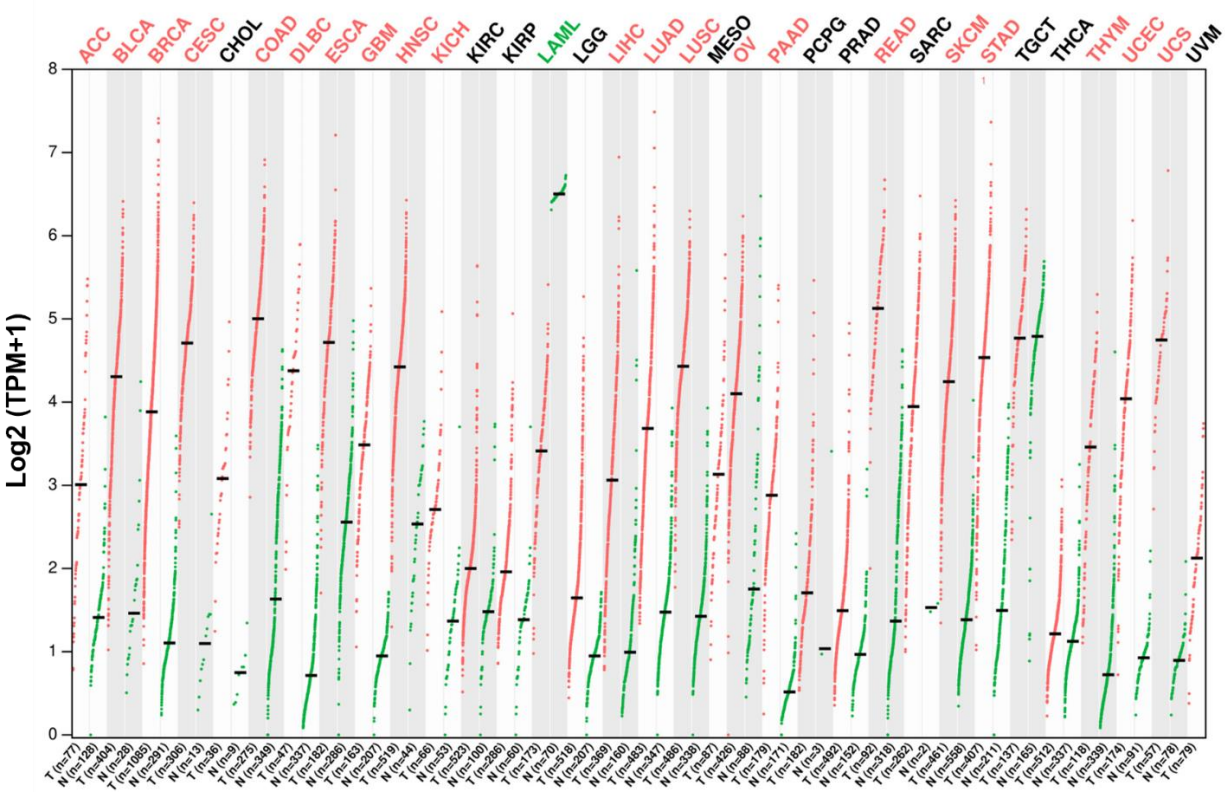

Figure 5. *AURKA* expression in tumor and paired normal tissues from the GEPIA database (http://gepia.cancer-pku.cn/). In most tumor types (T, in red), AURKA expression is significantly higher compared to paired normal tissues (T, in green), except for acute myeloid leukemia (LAML) where it is markedly decreased. ACC, Adrenocortical Carcinoma; BLCA, Bladder Urothelial Carcinoma; BRCA, Breast Invasive Carcinoma; CESC, Cervical Squamous Cell Carcinoma And Endocervical Adenocarcinoma; CHOL, Cholangiocarcinoma; COAD, Colon Adenocarcinoma; DLBC, Lymphoid Neoplasm Diffuse Large B-Cell Lymphoma; ESCA, Esophageal Carcinoma; GBM, Glioblastoma Multiforme; HNSC, Head And Neck Squamous Cell Carcinoma; KICH, Kidney Chromophobe; KIRC, Kidney Renal Clear Cell Carcinoma, KIRP, Kidney Renal Papillary Cell Carcinoma; LAML, Acute Myeloid Leukemia; LGG, Brain Lower Grade Glioma; LIHC, Liver Hepatocellular Carcinoma; LUAD, Lung Adenocarcinoma; LUSC, Lung Squamous Cell Carcinoma; MESO, Mesothelioma; OV, Ovarian Serous Cystadenocarcinoma; PAAD, Pancreatic Adenocarcinoma; PCPG, Pheochromocytoma And Paraganglioma; PRAD, Prostate Adenocarcinoma; READ, Rectum Adenocarcinoma; SARC, Sarcoma; SKCM, Skin Cutaneous Melanoma; STAD, Stomach Adenocarcinoma; TGCT, Testicular Germ Cell Tumors; THCA, Thyroid Carcinoma; THYM, Thymoma; UCEC, Uterine Corpus Endometrial Carcinoma; UCS, Uterine Carcinosarcoma; UVM, Uveal Melanoma.

According to the Genome Expression Profiling Interactive Analysis (GEPIA) database (http://gepia.cancer-pku.cn/), 82% of tumors (27 of 33 tumor types, including breast, uterus, ovaries, liver, and lung) show high levels of AURKA expression, with $\log_2$ (transcripts per million [TPM] +

1) values ≥2 (Figure 5). Conversely, only 18% of cancer types exhibit AURKA expression with $\log_2$ (TPM + 1) values <2 such as brain lower-grade glioma (LGG), prostate adenocarcinoma (PRAD), and thyroid carcinoma (THCA) [10,25] (Figure 5).

1.3.1 AURKA dysregulation in HCC

Numerous studies have investigated *AURKA* expression in HCC across publicly available gene expression datasets, collectively pointing to higher expression of *AURKA* mRNA in tumors compared to non-cancerous tissues [74–86]. *AURKA* expression is markedly increased in HBV^+ HCC samples when contrasted with the paired HBV^+ non-tumoral liver tissues in two distinct datasets, GSE14520 (HBV^+ HCC: 128.00 (78.79-219.79), HBV^+: 26.35 (22.63-33.63)) and GSE121248 (HBV^+ HCC: 227.54 (155.42-335.46), HBV^+: 80.45 (64.00-101.83)) [82]. The dysregulation of AURKA was further corroborated in a cohort of HCC patients from the National Taiwan University Hospital, where *AURKA* mRNA exhibited overexpression in 137 out of 224 (61%) tumors compared to the paired non-tumor portion of the liver [69] (Table 1).

The overexpression extends beyond the mRNA level, as the AURKA protein is frequently elevated in HCC tumors. AURKA protein was significantly upregulated in 17 out of 22 HCC patients' liver samples (77.3%) from the Tianjin Medical University Cancer Institute and Hospital [87]. Consistent findings of AURKA protein overexpression have been reported in Asian cohorts of HCC patients [88–90] (Table 1).

Table 1. Literature evidence of the AURKA expression in HCC tissues.

Molecule	AURKA expression	HCC tissues (n)	Paired non-tumor tissues (n)	References
mRNA	Up	10	10	[77]
mRNA	Up	244	199	[69]
mRNA	Up	40	40	[81]
mRNA / protein	Up	46	46	[90]
mRNA / protein	Up	3	3	[88]
Protein	Up	22	22	[87]
Protein	Up (WB) Up (IHC)	24 141	24 139	[89]

WB, Western blot; IHC, Immunohistochemistry

High levels of AURKA have been linked to clinical aggressiveness, poor outcomes, unfavorable prognoses, therapeutic resistance, and higher early recurrence risk in HCC patients [90,91]. HCC patients exhibiting high AURKA and AURKB expression (n=51) experienced significantly shorter OS and disease-free survival (DFS) rates compared to those with low expression in at least one of the two proteins (n=87) [89] (Table 1). Likewise, another study observed poor prognosis in patients with high AURKA levels (n=15) compared to patients with low AURKA expression (n=17). Higher *AURKA* mRNA expression was noted in intrahepatic metastasis (n=26) compared to primary HCC samples (n=20) [90] (Table 1).

1.3.2 AURKA regulates multiple pathways in HCC

The precise mechanisms of AURKA action in cancer, particularly in HCC, are not fully elucidated, highlighting a gap in the existing literature. However, the reported overexpression of AURKA in HCC suggests its involvement in crucial oncogenic processes within cancer cells, such as proliferation, survival, migration, and invasion. These fundamental cancer hallmarks are modulated by diverse signaling pathways, where AURKA may exert a pivotal role, contributing to malignant transformation and disease progression [92–94].

Beyond its critical role in cell cycle regulation, AURKA can also regulate cell proliferation through interactions with different oncogenes. In an *in vitro* HCC model (MHCC-97H), AURKA regulated MYC Proto-Oncogene, BHLH Transcription Factor (MYC) by binding to its Nuclear hypersensitive element III 1 (NHEIII1) region, thereby enhancing its transcriptional activity and promoting the malignant phenotype of the cells [95]. Additionally, another study revealed that AURKA contributes to MYC expression by facilitating its mRNA expression and inhibiting its protein degradation. In HCC, elevated expression of Inhibitor of Differentiation 1 (ID1) was associated with a worse prognosis. The competitive binding of ID1 to the APC/C-FZR1 complex promotes AURKA overexpression, leading to an increase in MYC expression, thereby fostering a highly malignant phenotype characterized by enhanced metastatic ability and drug resistance [96]. In a feedback loop, MYC enhances AURKA expression by binding to its promoter regions containing highly conserved E-box regions in the CpG islands, thus sustaining a malignant phenotype in HCC cell lines [95]. AURKA can additionally be regulated by the Hypoxia-Inducible Factor 1α (HIF-1α). In hypoxic conditions, HIF-1α can transcriptionally regulate AURKA by binding to the hypoxia-responsive elements in the AURKA promoter and recruiting the co-activator p300/CREB Binding Protein (CBP). AURKA promotes hyperproliferation, increased survival, and a more malignant

phenotype in HCC cell lines (HepG2 and BEL-7405 cells), by regulating downstream signaling AKT and P-38/ MAPK pathways [97].

AURKA plays a role in epithelial-mesenchymal transition (EMT) and stemness by regulating the Phosphoinositide 3-kinases (PI3K)/AKT pathway. In the context of HCC metastasis following ion radiation, stable expression of AURKA *in vitro* cell lines (HepG2 and Huh7 cells) enhanced cell invasive ability. AURKA-overexpressing cells exhibited decreased E-cadherin and increased N-cadherin and vimentin levels, markers of EMT. Simultaneously, overexpression of AURKA enhanced the levels of the markers of Cancer stem cells (CSC), such as CD133 and CD44 levels. These oncogenic processes are driven by an increase in AKT phosphorylation. Thus, AURKA knockdown suppresses radiation-enhanced cell invasiveness in HCC [90]. Additionally, interleukin enhancer binding factor 3 (ILF3), a double-stranded RNA-binding protein, was recruited by the KDM4A antisense RNA 1 (KDM4A-AS1) to promote the stability of *AURKA* mRNA, which resulted in increased activation of the PI3K/AKT signaling, consequently promoting EMT *in vitro* HCC models (Hep3B and Huh7 cells) and *in vivo* (BALB/C mice) [98].

Resistance to apoptotic signaling is a common hallmark in HCC. AURKA contributes to this resistance by dysregulating the Nuclear Factor kappa B (NF-κB) signaling pathway, a key regulator of cell death and inflammation [99]. AURKA promotes the classical activation of NF-κB signaling by phosphorylating the NF-κB inhibitor α (NFKBIA) on Ser32 and Ser36 residues, leading to the proteasomal degradation of the protein and the translocation of the NF-κB complex into the nucleus. In turn, this promotes the transcription of pro-survival target genes such as MCL1 Apoptosis Regulator BCL2 Family Member (MCL-1) and B-Cell Leukemia/Lymphoma 2 (BCL-2) [100]. Likewise, NF-κB nuclear localization promotes the expression of miR-21. This non-coding RNA negatively regulates Phosphatase And Tensin Homolog (PTEN) and obstructs Caspase-3-mediated apoptosis by upregulating antiapoptotic proteins, including p-AKT and BCL-2. Through AURKA/NF-κB/miR-21/PTEN signaling axis, dysregulated AURKA promotes a potential initiation of chemoresistance *in vitro* (HepG2, SMMC-7721, and Hep3B cells) and *in vivo* mice models [101].

1.3.3 AURKA can be a target for liver cancer therapy

AURKA is consistently overexpressed in HCC [74–90], playing pivotal roles in promoting proliferation, migration, and resistance to apoptosis [93–98,100,101]. Given its significant involvement in hepatocarcinogenesis, AURKA emerges as a potential candidate for therapeutic targeting in HCC. Recent evidence investigated the molecular mechanisms which determine the

efficacy of lenvatinib treatment in HCC. Docking algorithms predicted the non-covalent interaction between the molecular targets and the drug, based on unbound 3D structures, and AURKA was one of the possible targets of lenvatinib in HCC [102].

Several compounds able to inhibit AURKA were identified *in vitro* and some of them were further explored in preclinical or clinical trials as potential cancer therapies. The initial generation of AURKA inhibitors comprises ATP-competitive inhibitors that bind to the ATP binding pocket of AURKA. The components of this group currently are the most tested inhibitors in clinical studies [103]. Novel types of AURKA inhibitors bind to an allosteric site, impeding either the kinase activity or AURKA protein-protein interactions. Pan-Aurora kinase inhibitors target multiple Aurora family members (AURKA, AURKB, and AURKC) with moderate specificity. Recently, newly designed pan-Aurora kinase inhibitors have been tested *in vitro* and *in vivo* in preclinical studies, exhibiting potent inhibitory effects on Aurora kinase activity at low concentrations [104–106]. These inhibitors need to be evaluated in clinical studies to confirm their utility in tumor therapy.

Alisertib (MLN8237), an ATP-competitive and reversible AURKA-specific inhibitor, is the most extensively studied AURKA inhibitor. It exhibits higher selectivity (200-fold higher) for AURKA than for AURKB. Alisertib promotes the arrest of cells at the G2/M phase, mitotic spindle disorganization, and chromosome misalignment [107,108]. In multiple cancer cell lines and xenograft models, alisertib inhibits cell proliferation by impairing mitosis, blocking the EMT process, and promoting cell cycle arrest and autophagy, as well as accelerating cancer cell apoptosis and senescence [107,109]. Due to its potent efficacy in preclinical studies, alisertib underwent Phase I/II clinical trials for several cancers, including lymphomas, leukemia, gastric, ovarian, and breast tumors. However, phase III trials were halted in 2015 due to the lack of significant effects on patient survival and the presence of strong side effects including hematologic- and gastrointestinal-related toxicities, commonly observed in single-agent alisertib studies [110,111]. Therefore, alisertib has undergone testing in combination therapies aimed at enhancing its anti-tumor efficacy while minimizing toxicity and managing adverse effects. A phase I clinical trial established that the combination of alisertib and docetaxel was well-tolerated and demonstrated antitumor activity across diverse cancer types, including prostate cancer and upper gastrointestinal adenocarcinomas [112,113]. Additionally, combining alisertib with paclitaxel has shown promising results in ovarian cancer, resulting in increased disease-free survival compared to paclitaxel monotherapy [114].

AK-01 (LY3295668) is a reversible ATP-competitive inhibitor, exhibiting an over 2000-fold selectivity for AURKA over AURKB. First introduced in clinical trials in 2014, AK-01 features a fluorine atom within the pyrimidine ring, strategically positioned to bring the carboxylate of AK-01 in closer proximity to Thr217 of AURKA, thus facilitating inhibition [115,116]. AK-01 exhibited promising efficacy in affecting cell proliferation and viability *in vitro*, thus it is currently undergoing phase II clinical trials (NCT03092934) in patients with small-cell lung cancer (SCLC), breast cancer, and other solid tumors [115].

To gain a deeper understanding of how AURKA inhibitors combat hepatocarcinogenesis, both AK-01 and alisertib have undergone pre-clinical testing specifically in HCC models. AK-01 blocks proliferation in a time-dependent manner and influences cell viability in HCC-derived cell lines as well as in a broad range of cancer cells. Alisertib reduces the proliferative capacity and survival of the HCC cells compared to lenvatinib treatment alone and increases the cytotoxic effects and anti-metastatic activity of lenvatinib *in vitro* HCC cell line (HepG2 cells). The combination of lenvatinib and alisertib can also inhibit DNA damage response pathways [87,115].

1.3.4 Modulation of the immune response by AURKA: A possibility for therapy combination

Numerous studies have unveiled the regulatory function of oncogenes in modulating the immune microenvironment. The role of AURKA in immune checkpoint regulation and immune response to the tumor remains a subject of debate due to conflicting evidence [117–120]. However, regardless of its specific function in immune regulation, the combined inhibition of AURKA and PD-L1 has been shown to promote immune infiltration and the cytotoxic elimination of tumor cells.

In triple-negative breast cancer (TNBC), AURKA enhances PD-L1 levels facilitating the immune escape for tumor cells [117,118]. Overexpression of AURKA in a TNBC cell line (MDA-MB-231 cells) promotes PD-L1 expression through the activation of the MYC signaling pathway. Elevated PD-L1 levels in cancer patients are associated with high malignancy and poor clinical prognosis. *In vitro,* AURKA knockdown enhances immune response by promoting the proliferation and activity of $CD8^+$ T cells. *In vivo* (4T1 engrafted BALB/c mouse), AURKA positively correlates with tumor growth, and negatively with the enrichment and activity of tumor-infiltrating $CD8^+$ T cells [117]. The treatment of MDA-MB 231/LM xenograft mice with alisertib reduces CD44 levels and PD-L1 expression, promoting CD8+ T cell infiltration. Combining alisertib with the anti-PD-L1 inhibitor

atezolizumab in xenograft mice results in decreased expression of the EMT marker vimentin, associated with a lack of organ metastasis [118].

Novel studies have suggested a relevant role of AURKA in the negative regulation of PD-L1 expression in tumors through various pathways, enhancing immune cell infiltration and the immune response [119,120]. In diverse solid tumor cell lines (BxPC3, A549, HCT116, and T24 cells), AURKA directly phosphorylates Cyclic GMP-AMP Synthase (cGAS), suppressing PD-L1 expression. Alisertib-induced AURKA inhibition activates the cGAS/Stimulator of IFN Genes (STING)/NF-κB pathway, promoting PD-L1 expression [120]. In a breast cancer cell line (SKBR3 cells), alisertib promotes PD-L1 expression in a time- and concentration-dependent manner through the phosphorylation of with Signal Transducer and Activator of Transcription 3 (STAT3) on the Tyr705 residue [119]. AURKA overexpression promotes STAT3 nuclear translocation with the consequent activation of the transcription activity [121]. *In vivo* (4T1-breast tumor xenograft mouse), treatment with alisertib decreases the $CD3^+$ and $CD8^+$ T cell infiltration. Considering that alisertib suppresses the anti-tumor immune function of T cells by upregulating PD-L1, an anti-PD-L1 antibody could promote the immune response against the tumor. Thus, the combination of alisertib with anti-PD-L1 antibody can enhance the efficacy of the immunotherapy, significantly increasing $CD3^+$ and $CD8^+$ T cell infiltration in tumor tissues, accompanied by the reduction of the tumor volume in the MC38-colorectal cancer xenograft tumor model [119].

The role of AURKA in the regulation of the immune microenvironment in HCC remains to be fully elucidated. The elevated expression of a cluster of genes containing *AURKA* and 8-related genes is associated with the increased expression of the immune checkpoints such as *PD-L1, Sialic Acid-Binding Ig Like Lectin 15 (SIGLEC15), T Cell Immunoreceptor with Ig and ITIM Domains (TIGIT), Hepatitis A Virus Cellular Receptor 2 (HAVCR2), and Programmed Cell Death 1 Ligand 2 (PDCD1LG2),* along with a higher percentage of immune cell infiltration ($CD4^+$ T cells, macrophages, neutrophils, and dendritic cells) [74]. According to the TIMER database (https://cistrome.shinyapps.io/timer/), *AURKA* expression positively correlates with the infiltration of several immune cells in the HCC microenvironment, including B cells, $CD4^+$ T cells, macrophages, dendritic cells [122,123], $CD8^+$ T cells and neutrophils [122]. The combination of AURKA expression and macrophage levels demonstrates promising prognostic value for HCC patients (The Cancer Genome Atlas (TCGA), n=362), with a high macrophage number predicting significantly shorter OS in the high-AURKA group [123].

While AURKA may promote immune recruitment at the tumor level, the expression and localization of immune checkpoints on the cell surface protect tumor cells from degradation. Thereby, the tumor microenvironment enriched in immune cells fosters chronic inflammation and tissue remodeling, promoting tumor growth and metastasis [121]. AURKA represents an intriguing therapeutic target in HCC due to its role in immune recruitment and regulation within the tumor microenvironment. Considering that immune checkpoint inhibitors can enhance the activity of oncogene-targeted therapy, exploring the combination of AURKA-targeted therapy and immune checkpoint inhibitors, specifically anti-PD-L1 therapy, is an option warranting further investigation in hepatocarcinogenesis.

Chapter 2 - Aims of the study

HCC is one of the most prevalent tumors globally and ranks as the fourth leading cause of cancer-related deaths, with both the incidence and mortality expected to increase in the coming years. Despite the notable progress in HCC treatment, the persistently high mortality rate is mainly attributed to late-stage diagnoses and limited therapeutic efficacy. In advanced stages, the combination of oncogene-targeted therapy and immunotherapy became the first-line treatment in the last years, demonstrating slightly improved outcomes compared to previous therapies. The modest improvement observed can be attributed to the substantial heterogeneity of the disease, resulting in each patient being distinctly unique. Consequently, there is an urgent need to identify novel therapeutic targets, potentially in combination with immune checkpoint inhibitors, to address the intricate variability of the condition.

AURKA has emerged as a relevant oncogene in HCC, showing substantial overexpression and playing a crucial function in key tumorigenic processes, including proliferation, survival, migration, invasion, and resistance to apoptosis. Thus, AURKA can be a promising candidate for targeted therapy in HCC, especially considering the ongoing clinical trials involving AURKA inhibitors in cancer treatments.

Furthermore, recent studies have unveiled the role of AURKA in PD-L1 regulation, adding an intriguing novel layer to its role in cancer. This discovery not only deepens the understanding of AURKA's multifaceted functions in cancer but also creates exciting prospects for combination therapies. The potential synergic effects of AURKA inhibitors with immune checkpoint inhibitors further underscore the need to investigate AURKA as a possible therapeutic target, offering potential enhancements in treatment outcomes for HCC.

Considering the lack of information available on AURKA in liver disease, this project aims to comprehensively investigate the expression of the kinase and its interactors in both HCC and precancerous conditions and assess the molecular and cellular effects of AURKA inhibition and knockdown, with a particular focus on PD-L1 regulation.

The experimental setup was organized into three major tasks:

1. Analysis of AURKA expression in HCC human samples: Investigate the changes in the kinase expression throughout hepatocarcinogenesis and establish correlations with TPX2 and PD-L1.

2. Confirmation of AURKA expression changes in a mouse model: Validate the modifications in the kinase expression using an animal model recapitulating hepatocarcinogenesis.
3. Identification of AURKA's role in PD-L1 regulation: Elucidate the possible functions of AURKA in regulating PD-L1 through *in vitro* experiments.

This study could enhance the understanding of the intricate dynamics of AURKA and its interactions in the context of HCC. This knowledge could pave the way for the development of a synergic therapeutic approach through the combination of AURKA inhibitors and PD-L1 inhibitors, such as atezolizumab, as a promising strategy for HCC treatment.

Chapter 3 - Materials and methods

3.1 Human clinical tissue samples

3.1.1 HCC patients

Fifty-six consecutive patients diagnosed with HCC according to the EASL criteria were enrolled. Patients underwent partial hepatectomy (liver resection) between December 2008 and January 2023 at the Surgery department of the University Hospital of Trieste, Italy. The inclusion criteria were restricted to adult patients with a confirmed diagnosis of HCC, while exclusion criteria encompassed those with concurrent hepatic malignancy or other malignant diseases, as well as pediatric HCC patients.

From each patient, different portions of the diseased liver were collected, including tumor nodules and paired adjacent non-tumoral tissues. A standardized sample collection procedure (size, type of tissues, and storage condition) was executed. Fresh liver tissues were meticulously collected and stored using either RNAlater stabilization solution (M7021, Invitrogen™, Waltham, MA, USA) or snap-frozen in liquid nitrogen and then stored at −80◦C. Simultaneously, corresponding portions were fixed in formalin, embedded in paraffin, cut in serial sections, and subjected to comprehensive histological analysis, including hematoxylin and eosin (HE) staining, performed by Azienda Sanitaria Universitaria Giuliano Isontina (ASUGI), Trieste, Italy

The population with a median age of 69.95 [62.33-74.48] consists of 44 males and 12 females. The etiology of the malignancy varied, with 11% (5/56) attributed to HBV, 30% (17/56) to HCV, 38% (21/56) to MASLD or/and Alcohol-associated liver disease (ALD), and 9% (5/56) with mixed etiologies (Table 2). Edmondson Steiner (ES) HCC grading, tumor parameters, laboratory results, and other clinical variables were evaluated based on international criteria. Complete demographic, clinical, and pathological features of the study cohorts are listed in Table 2 and Table 3. The median follow-up for the cohort was 35.50 [17.25-59.00] months. During this period, 27 patients (48%) experienced tumor recurrence, with a median recurrence time of 18.00 [7.00-50.75] months, and 27 (48%) died.

Table 2. Pathological variables of HCC patients.

Variables	HCC (N=56)
Etiology (HCV/HBV/MASLD or/and ALD/Mix)	17/6/21/5
Fibrosis Score (F0-F4/F5-F6)	16/38
Child-Pugh Score (A/B/C)	53/3/0
BCLC classes (0-A/B/C)	38/13/5
Cirrhosis (Y/N)	43/13
Grading (Well/Medium/Poor/Not diff.)	15/28/8/1

Variables were represented by the number of patients. ALD, Alcohol-associated liver disease; HBV, Hepatitis B Virus; HCV, Hepatitis C Virus; MASLD, Metabolic dysfunction-associated steatotic liver disease; N, No; Y, Yes.

The study was approved by the Comitato Etico Regionale Unico of Friuli Venezia Giulia, Prot. No. 18854. Informed consent was diligently obtained from each patient or their legal representative, and sensitive data were meticulously protected through anonymization.

Table 3. Demographic and clinical variables of HCC and MASLD patients.

Variables	HCC (N=56)	MASLD (N=17)
Gender (M/F)	44/12	9/8
Age	69.95 [62.33-74.48]	53.00 [39.00-58.00]
BMI		41.51 [38.82-45.60]
Hemoglobin (g/dl)	14.15 [13.45-15.35]	
Platelet Count ($X10^3/mm^3$)	165.00 [110.75-220.75]	266.00 [196.00-313.50]
AST (U/l)	31.00 [24.00-57.75]	29.00 [19.5-46.00]
ALT (U/l)	29.50 [19.00-56.75]	40.00 [29.5-66.00]
Pseudocholinesterase (U/l)	6650.50 [5311.00-7472.75]	
Total Bilirubin (mg/dl)	0.85 [0.59-1.03]	0.53 [0.41-0.75]
Direct Bilirubin (mg/dl)	0.20 [0.14-0.28]	0.10 [0.08-0.14]
Albumin (g/dl)	4.10 [3.88-4.39]	4.24 [4.13-4.43]
Creatinine (mg/dl)	0.82 [0.73-0.96]	
INR	1.09 [1.03-1.15]	1.03 [0.96-1.09]
AFP (ng/ml)	9.80 [3.63-127.90]	
AFP classes (<20 / 20-40 />400ng/ml)	35/10/7	

Categorical variables were represented by the number of patients. Continuous variables are represented as median [IQR-IIIQR]. AFP, α-fetoprotein; ALT, Alanine transaminase; AST, Aspartate aminotransferase; BMI, Body mass index; F, Female; HCC, Hepatocellular carcinoma; INR, International normalized ratio; M, Male; MASLD, Metabolic dysfunction-associated steatotic liver disease.

3.1.2 MASLD subjects

Seventeen patients diagnosed with MASLD and with fibrosis stage F0-F4 were selected for this study from a cohort of morbidly obese individuals enrolled in a bariatric surgery program. Inclusion criteria for the program involved adult individuals, with a body mass index (BMI) exceeding 40 kg/m^2 (or >35 kg/m^2 if obesity-related comorbidities were present), acceptable operative risks, a lack of response to nonsurgical treatments, and a commitment to lifelong medical surveillance. Exclusion criteria were the coexistence of chronic liver disease, including suspected/confirmed HCC, alcoholic liver disease (>25 g/day alcohol consumption), positivity for HBV, HCV, and HIV, and the use of drugs potentially affecting the liver. The liver biopsy was performed at the time of the surgical procedure. Fresh liver tissues were collected and stored at 4°C and processed within 1 hour.

The patient group consisted of 9 male and 8 female patients, with a median age of 53.00 [39.00-58.00] years. Among the patients, 41% (7/17) showed metabolic dysfunction-associated steatotic liver (MAFL), while 59% (10/17) had metabolic dysfunction-associated steatohepatitis (MASH) (Table 4). The histological diagnosis of MAFL/MASH and fibrosis was determined according to Kleiner-Brunt criteria [124]. Laboratory results and other clinical findings were assessed based on international criteria and are detailed in Table 3 and Table 4.

Table 4. Pathological variables of MASLD patients.

Variables	MASLD (N=17)
Steatosis (0/1/2/3)	0/0/10/6
Lobular Inflammation (0/1/2/3)	3/11/3/0
Portal Inflammation (0/1/2/3)	6/11/0/0
Ballooning (0/1/2/3)	6/9/2/0
MAFL/MASH	7/10
Fibrosis Score (F0/F1/F2/F3/F4)	9/0/0/6/2

Categorical variables were represented by the number of patients. MAFL, Metabolic dysfunction-associated steatotic liver; MASH, Metabolic dysfunction-associated steatohepatitis; MASLD, Metabolic dysfunction-associated steatotic liver disease.

The study received ethical approval from the local Ethical Committee under protocol N. 22979 (Comitato Etico Regionale Unico, FVG, SSN, Italy). Informed consent to participate in the study was obtained from each patient or their legal representative, with sensitive data meticulously safeguarded through anonymization.

3.1.3 Healthy individuals

In this study, healthy liver tissues from 14 donors were included. These samples, obtained through collaboration with partners in Rome, Italy, were subjected to the exclusion criterion of the presence of liver diseases. Post-surgery, tissue samples were promptly snap-frozen and stored at -80°C. The median age of the subjects is 17.50 [6.75-27.75] years old.

3.2 Mouse liver tissue samples

An animal model, specifically the HBV-transgenic (TG) mice C57BL/6J-TG(ALB1HBV)44BRI/J [125], was employed in this study to investigate the expression of target genes and proteins during the process of liver damage and carcinogenesis. The C57BL76J wild-type (WT) mouse was used as a control. TG mice showed various stages of liver damage, including inflammation, early hepatic injury, pre-neoplastic lesions, early neoplasia, and advanced neoplasia at 3, 6, 9, 12, and 15 months of age, respectively.

Corresponding protocols and animal studies were reviewed and approved by the ethics committee of the University of Trieste and the responsible administration of the Ministry of Health of the Republic of Italy (D.M. 57/2012-B). The mouse models were housed and maintained at the animal facility of the University of Trieste. The research experiments were conducted following the Guide for the Care and Use of Laboratory Animals.

Male heterozygote TG and male WT mice were maintained until they reached specific age points. A total of 21 TG and 21 WT mice were sacrificed at 3, 6, 9, 12, and 15 months of age. During the procedure, at least three liver sections were harvested and cut from both the right and left liver lobes of each mouse. In the cases where visible nodules were present (at 12 and 15 months), HCC and non-HCC sections were collected. Tissues were stored on ice during the procedures and preserved at -80°C for further analysis.

3.3 Cell culture

Two distinct HCC cell lines were carefully selected for this study: JHH6 (JCRB1030) and Huh7 (JCRB0403) cells. Both the cell lines were obtained from the Japan Health Science Research

Resources Bank (HSRRB) in Tokyo, Japan. JHH6, a mesenchymal-like, undifferentiated HCC cell line, originated from a 58-year-old Asian female patient. Huh7 is a hepatoblast-like and well-differentiated HCC cell line derived from a 57-year-old Asian male patient. These cells represent different subtypes of HCC tumors: JHH6 is classified under subtype 1/Transforming Growth Factor β–Wingless Related Integration Site (S1/TGFβ-Wnt) activated subtype and Huh7 (JCRB0403) was classified as subtype 2 (S2)/ progenitor subtype [126].

The culture media employed for these cell lines were Williams' E medium (Gibco, Thermo Fisher Scientific, Waltham, MA, USA) for JHH6 cells and high glucose Dulbecco's modified eagle medium (DMEM) (Gibco, Thermo Fisher Scientific, Waltham, MA, USA) for Huh7 cells. The culture media were supplemented with 10% (v/v) fetal bovine serum (FBS), 1% L-glutamine 100X, and 1% penicillin/streptomycin (10.000 U/mL Penicillin and 10 mg/mL Streptomycin). The cells were maintained in a humidified 5% CO_2 incubator at 37°C.

Routine cell expansion involved using 0.05% trypsin for detachment when the cells reached 80% confluency. In the experimental setups, JHH6 cells were seeded at a concentration of 3,000 cells/cm^2, while Huh7 cells were at 6,000 cells/cm^2 unless further specified.

3.4 Chemical compounds treatments

AURKA inhibition was conducted using two ATP-competitive and reversible AURKA inhibitors: Alisertib (MLN8237, Catalog No. A10004, Adooq Bioscience, Irvine, CA, USA) and AK-01 (LY-3295668, CAS No. 1919888-06-4, ChemieTek, Indianapolis, IN, USA). Both compounds were dissolved in 100% dimethyl sulfoxide (DMSO) (Sigma-Aldrich, St. Louis, MO, USA). According to the data from the literature [115,116,127], both the cell lines were treated with concentrations ranging from 0.001μM to 10μM for Alisertib and 0.01μM to 30μM for AK-01. The treatment with the vehicle (DMSO) served as the negative control. Both the cell lines were seeded as previously reported, and 24 hours later, they were exposed to the inhibition treatments for durations of 24, 48, and 72 hours.

Interferon-gamma (IFN-γ) (Z02915, Genscript Biotech, Piscataway, NJ, USA) was employed to induce PD-L1 expression in JHH6 cells. The compound was dissolved in nuclease-free H_2O. According to the literature [128], concentrations between 25ng/ml and 300ng/ml were chosen. The vehicle (nuclease-free H_2O) was employed as the negative control in the treatment. The cells were

seeded at a concentration of 8,000 cells/cm^2, and 24 hours after, they were subjected to the IFN-γ treatment for durations of 6 and 24 hours.

3.5 *AURKA* and *PD-L1* gene silencing

Gene-silencing experiments were performed using small interfering RNA (siRNA) targeting *AURKA* (siR-AURKA, Silencer Select siRNA s197, Invitrogen™, Waltham, MA, USA) and *PD-L1* (siR-PD-L1, Silencer Pre-designed siRNA AM16708, Thermo Fisher, Waltham, MA, USA). As the negative control, siR-CTRL (Negative Control No. 2 siRNA, AM4613, Invitrogen™, Waltham, MA, USA) was employed. All siRNAs were dissolved in nuclease-free H_2O, with a final concentration of 1nM and 20nM for siR-AURKA and siR-PD-L1, respectively.

siLentFect™ Lipid Reagent (170–3362, Bio-Rad, Hercules, CA, USA) was used as the transfection reagent, following the manufacturer's protocols (0.1% dilution in the culture medium). In brief, both cell lines were seeded as previously reported, and 24 hours later, the culture medium was replaced with the respective fresh antibiotic-free medium 1 hour before transfection. The mixture of siLentFect Lipid Reagent and siR-AURKA, siR-PD-L1, or siR-CTRL was prepared in an antibiotic-free and serum-free medium. After 30 minutes of incubation, the resulting complexes were added to the cultured cells. Following a 24-hour incubation, the medium was replaced with the corresponding fresh complete medium. The effects of the silencing were evaluated at 24, 48, 72, and 144 hours post-silencing. For the 144-hour silencing, a second silencing process using the same procedure was performed 72 hours after the initial one.

3.6 MTT assay and LC50

Cytotoxicity experiments were conducted to determine the lethal concentration 50 (LC50) and the working concentrations of the studied compounds. Cell viability was assessed after 24, 48, and 72 hours of exposure to the chemical compounds and silencing agents using the 3-(4,5-dimethyl thiazolyl-2)-2,5 diphenyltetrazolium (MTT) assay (Sigma-Aldrich, St.Louis, MO, USA). Each treatment was performed in duplicate. After treatment, cells were incubated in MTT solution (0.5% MTT in culture medium with 10% (v/v) Phosphate-Buffered saline (PBS; 137 mM NaCl, 10 mM phosphate, 2.7 mM KCl; pH 7.4)) for 1 hour. The solution was replaced with DMSO to lyse cells and

dissolve the formazan salts resulting from cellular metabolic activity. Absorbance was evaluated at 562nm through the Spectrophotometer EnSpire™ Multimode Plate Reader (PerkinElmer Inc, Waltham, MA, USA). Absorbance values were normalized to the negative controls to calculate the percentage of viable cells for each experimental condition.

3.7 Total RNA extraction from solid tissue samples and cell lines

Total RNA extraction from human and mouse samples was carried out using Tri Reagent® (Sigma–Aldrich, St Louis, MO, USA), while TriFast™ (EMR517100, Euroclone S.P.A, Milan, Italy) was employed for both cell lines. Extraction procedures were performed following the respective manufacturer's protocols.

Cells were harvested using cell scrapers, while tissues underwent a homogenization process. Frozen human and mouse samples were homogenized through homogenizer beads (1.4mm Ceramic Beads Bulk, 325g with 651mg per tube, Omni International, Kennesaw, GA, USA) using Bead Ruptor 4 (Omni International, Kennesaw, GA, USA) at maximum speed for 60 seconds or potter-Elvehjem tissue grinders. Regardless of the samples' origin (tissues or cell lines), chloroform was then added to the homogenates and RNA was precipitated by isopropanol and washed with 75% ethanol. The RNA pellet was dissolved in nuclease-free water and stored at -80°C until further analysis.

Quantification of RNA was performed at a wavelength of 260 nm using the ONDA touch UV-31 scan UV/VIS Spectrophotometer (Vetrotecnica, Padova, IT) with a quartz cuvette MICRO-100µl, 10mm (ONDA). RNA purity was assessed according to the Minimum information for publication of quantitative Real-Time polymerase chain reaction (PCR) experiments (MIQE) guidelines by measuring the A_{260}/A_{280} ratio [129]. The integrity of the RNA was evaluated on a standard 2% agarose electrophoresis gel stained with GelRed (41003, Biotium, Landing Pkwy, Fremont, CA, USA), and the bands were visualized under UV lights.

3.8 Reverse transcription and quantitative real-time PCR

Reverse transcription (RT) was conducted to synthesize cDNA from 1 µg of purified RNA using the High-Capacity cDNA Reverse Transcription Kit (Applied Biosystems, Waltham, MA, USA). The kit components included 10x RT Buffer, 25x dNTP Mix (100mM), 10x RT Random Primers, Reverse

Transcriptase, and Nuclease-free H_2O. The RT process followed the manufacturer's protocol and was performed in the T100 Thermal Cycler (Bio-Rad, Hercules, California, USA). The RT protocol (High Capacity) includes annealing for 25 minutes at 25°C, synthesis for 120 minutes at 37°C, and enzyme inactivation for 5 minutes at 85°C. The resulting cDNA was stored at -20°C until further use.

The amplification of cDNAs was carried out using quantitative Real-Time PCR (RT-qPCR). The 25µL reaction included cDNA (human samples: 25.00ng, excluding 1.00ng for 18S; mouse samples: 13.70ng; cell lines: 6.25ng), SYBR Sso advanced 2x master-mix (Bio-Rad Laboratories, Hercules, CA, USA), and 250nM gene-specific forward and reverse primers (100nM for 18S). PCR reactions were performed in duplicate in 96-well plates following a protocol that included pre-incubation/activation (30 seconds, 95°C), and 50 cycles of denaturation (5 seconds, 95°C) and annealing/extension (20 seconds, 60°C).

The melting curve analysis was conducted to assess primer/product specificity. Standard curves for each gene were utilized to determine primer pair efficiency. Relative quantification was computed using Bio-Rad CFX maestro version 2.2 (Bio-Rad Laboratories, USA), and Ct values for each sample were obtained by calculating the arithmetic mean average of the duplicates. Finally, gene expression was evaluated by using the Pfaffl modification of the ΔΔCt equation, considering the efficiencies of individual genes. The results were normalized to the housekeeping genes: *18S* for human samples (human tissues and cell lines), while *Actin β (Actb)* and *Glyceraldehyde-3-phosphate dehydrogenase (Gapdh)* for mouse samples. The initial amount of template for each sample was determined as a relative expression compared to the expression of the sample selected as the reference.

The primer sequences were designed using Beacon Designer 7.9 Software (PREMIER Biosoft International, Palo Alto, CA, USA) for the detection of the target genes and are listed in Table 5 and Table 6.

Table 5. Primers for detection of human genes.

Genes	Accession Number	Forward Primer	Reverse Primer
AKT1	NM_005163.2	GATTGTGTCAGCCCTGGA	ATCTTAATGTGCCCGTCC
ATP1A1	NM_000701.7	AACTTAGCCTTGATGAACTTC	AATCGCTCCAATCCACAG
AURKA	NM_198433	GAGAATTGTGCTACTTATACTG	GGTACTAGGAAGGTTATTGC
BRAF	NM_004333.6	CTTGTATCACCATCTCCATA	GGCGTGTAAGTAATCCAT
C-MYC	NM_002467.6	GAGGAGACATGGTGAACC	ATACAGTCCTGGATGATGATG
EGFR	NM_005228.5	TTGGAAATTACCTATGTG	TAGTTAGATAAGACTGCTA
GSK3B	NM_002093.4	ATGCTCAGTCAAACCAAATCA	TCTATCAACGCCACTACCTT
HRAS	NM_005343.4	CATCAACAACACCAAGTCTT	GTCATCCGAGTCCTTCAC
KRAS	NM_033360.4	TTGCTACGATTCCACTGA	TGAATATCTGACATACACCTTAA
NFKB3	NM_021975.4	GAATGCTGTGCGGCTCTG	CACGATTGTCAAAGATGGGATG
NFKBIA	NM_020529.3	CGTCTTATTGTGGTAGGA	CTCAGAATTTCAATGATCTTTC
PD-L1	NM_001314029.2	AAGTCCTGAGTGGTAAGA	CATTAGTTGTTGTGTTGATTC
PTEN	NM_000314.8	GCAGATAATGACAAGGAATA	CTGGTGTTACAGAAGTTG
TPX2	NM_012112.5	GCTCAGAAGGATTTGGAACAG	TGATTACAGGAGTGGCACAT
YAP1	NM_006106.5	GTGAGTAGGTTCATAATGTG	ATAGAAGTAGGAGCAAGTC
18S	NR_003286.2	CGTCTGCCCTATCAACTTTCG	GCCTGCTGCCTTCCTTGG

AKT1, AKT Serine/Threonine Kinase 1; ATP1A1, ATPase Na+/K+ Transporting Subunit α1; AURKA, Aurora Kinase A; BRAF, B-Raf Proto-Oncogene, Serine/Threonine Kinase; C-MYC, MYC Proto-Oncogene, BHLH Transcription Factor; EGFR, Epidermal Growth Factor Receptor; GSK3B, Glycogen Synthase Kinase 3β; HRAS, HRas Proto-Oncogene, GTPase; KRAS, KRAS Proto-Oncogene, GTPase; NFKB3, RELA Proto-Oncogene, NF-kB Subunit; NFKBIA, NFKB Inhibitor α; PD-L1, Programmed Cell Death Ligand 1, CD274; PTEN, Phosphatase And Tensin Homolog; TPX2, TPX2 Microtubule Nucleation Factor; YAP1, Yes1 Associated Transcriptional Regulator.

Table 6. Primers for detection of mouse genes.

Genes	Accession Number	Forward Primer	Reverse Primer
Aurka	NM_011497.4	AGAAGACCGAAGACACAA	GCCAAGTAGACATTTCCAA
Cd274	NM_021893.3	TTGTTCCTCATTGTAGTGT	TATCTTCAACGCCACATT
Myc	NM_001177352.1	CACCACCAGCAGCGACTC	TTGCCTCTTCTCCACAGACAC
Tpx2	NM_001141977.1	GAGACTTGAGAACTTGATT	TTCCAGGATTCTAATACTCT
Actb	NM_007393.5	CCTTCTTGGGTATGGAATCCTGTG	CAGCACTGTGTTGGCATAGAGG
Gapdh	NM_008084.3	CCAGTATGACTCCACTCACG	CTCGCTCCTGGAAGATGGTG

Aurka, Aurora Kinase A; Cd274, CD274 antigen, Programmed cell death ligand 1; Myc, Myelocytomatosis oncogene; Tpx2, TPX2, microtubule-associated; Actb, Actin β; Gapdh, Glyceraldehyde-3-phosphate dehydrogenase.

3.9 Tissue homogenization and protein extraction

Tissue homogenization and protein extraction were conducted using multiple methodologies.

Frozen HCC human samples and mouse samples underwent homogenization in Tissue Homogenization buffer (0.25M sucrose, 9.8mM K2HPO4, 40.2mM KH2PO4, 1mM Ethylenediaminetetraacetic acid (EDTA), and 0.1mM Dithiothreitol (DTT) in H2O; pH 7.4) with homogenizer beads and the Bead Ruptor 4 (Omni International, Kennesaw, GA 30144, USA) at maximum speed for 1 minute. Fresh MASLD samples were homogenized in HNTG lysis buffer (50mM HEPES, 150mM NaCl, 10% glycerol, 1% Triton X-100, pH 7.5) with 100 µM of Phenylmethylsulfonyl fluoride (PMSF) (P7626, Sigma-Aldrich, St. Louis, MO, USA), a protease inhibitor, using Potter-Elvehjem tissue grinders. For samples from healthy donors, proteins were extracted from the organic phase of TRI Reagent® following the manufacturer's protocol. Protein precipitation was facilitated by adding isopropanol, followed by washing with Guanidine hydrochloride 0.3M in 95% ethanol and 100% ethanol. The retrieved protein pellet was resuspended in 1.0% sodium dodecyl sulfate (SDS).

For cell lines, samples were detached using trypsin, washed twice with cold PBS, and lysed in Cell lysis buffer 1X (#9803, Cell Signaling, Danvers, MA, USA) on ice for 5 minutes. They were briefly sonicated (1 pulse of 15s at 10W) using a sonicator UW3100 (Bandelin Electronics, Berlin, Germany) to facilitate the extraction of DNA, RNA, and protein contents from the cells. Purification was achieved by centrifugation at 14,000 x g for 10 min at 4°C, and the supernatant was collected.

Protein quantification was performed using the Bicinchoninic acid (BCA) method, and the samples were stored at -80°C until further use.

3.10 Western blot analysis

Protein expression was assessed through Western blot (WB) analysis. Protein lysates (50-80µg) were solubilized in Laemmli Buffer 5X and 10% β-mercaptoethanol, then heated at 95°C for 5 minutes to facilitate denaturation. Samples were loaded onto the stacking gel of a 12% polyacrylamide sodium dodecyl sulfate-polyacrylamide gel electrophoresis (SDS-PAGE). Electrophoresis was initially conducted at 80V for 20 minutes for the protein accumulation in the stacking gel followed by 180V for 90 minutes for the run. The samples were wet transferred onto a polyvinylidene difluoride (PVDF) membrane through electroblotting at 100V for 2 hours using a transfer buffer composed of 25mM Tris base, 190mM glycine, and 20% methanol.

PVDF membranes were incubated in blocking solutions for 1 hour using 4% milk or 5% Albumin BSA Fraction V Albumin (BSA) Fraction V (pH 7.0) (A1391, Panreac AppliChem ITW Reagents, Monza, Italy) in PBS-Tween 0.1% (T-PBS) or Tris-Buffered Saline (TBS; 20mM NaCl and 150mM)-Tween 0.1% (T-TBS) to saturate non-specific binding sites. The blocking solutions are listed in Table 7.

Table 7. Dilutions of the antibodies and blocking solutions used in Western Blot experiments.

Targets	Human Tissues	Mouse Tissues	Cell Lines
AURKA (SC-398814)	4% milk in T-PBS 1:1000 (primary) 1:2000 (anti-mouse)		4% in T-PBS 0.1% 1:250 (primary) 1:500 (anti-mouse)
AURKA (AB52973)	5% BSA in T-PBS 1:1,000 (primary) 1:1,000 (anti-mouse)		
AURKA (66757-1-Ig)		5% BSA in T-TBS 1:1,000 (primary) 1:1,000 (anti-mouse)	
PD-L1/CD274 (66248-1-Ig)	5% BSA in T-PBS 1:2,500 (primary) 1:2,500 (anti-mouse)		5% BSA in T-PBS 1:2,500 (primary) 1:2,500 (anti-mouse)
pAURKA (Thr288) (MA5-14904)	5% BSA in T-TBS 1:300 (primary) 1:500 (anti-rabbit)		
pLATS2 (Ser83) (MAB0009)	5% BSA in T-PBS 1:667 (primary) 1:1,000 (anti-mouse)		5% BSA in T-PBS 1:667 (primary) 1:1,000 (anti-mouse)
Actin (A2066)		5% BSA in T-TBS 1:2,000 (primary) 1:2,000 (anti-rabbit)	
B-Actin (A5441)	4% milk in T-PBS 1:2,000 (primary) 1:2,000 (anti-mouse)		4% milk in T-PBS 1:2,000 (primary) 1:2,000 (anti-mouse)

AURKA, Aurora Kinase A; PD-L1/CD274, Programmed cell death ligand 1; pAURKA, phosphorylated AURKA; pLATS2, phosphorylated Large tumor suppressor kinase 2; T-PBS, PBS-Tween; T-TBS, TBS-Tween.

Membranes were incubated overnight with primary antibodies against the following proteins: AURKA (sc-398814, Santa Cruz Biotechnology, Dallas, TX, USA; ab52973, Abcam, Waltham, MA, USA; 66757-1-Ig, Proteintech, Rosemont, IL, USA), pAURKA (Thr288) (MA5-14904, Invitrogen™, Waltham, MA, USA), PD-L1/CD274 (66248-1-Ig, Proteintech, Rosemont, IL, USA),

pLATS2 (Ser83) (MAB0009, Abnova, Taipei, Taiwan). β-Actin (A5441, Sigma-Aldrich, St. Louis, MO, USA) and Actin (A2066, Sigma-Aldrich) served as housekeeping proteins. Secondary antibodies included anti-mouse IgG HRP (p0260, Dako A/S, Glostrup, Denmark) and anti-rabbit IgG HRP (p0448, Dako A/S, Glostrup, Denmark), depending on the primary antibody. Primary and secondary antibody dilutions are detailed in Table 7.

Membranes were exposed to Immobilon Classico western HRP substrate (WBLUC, Merck Millipore, Burlington, MA, USA) for 1-5 minutes to obtain a peroxidase reaction. The blots were visualized using a C-Digit blot scanner and the densitometry analyses were performed using Image Studio™ Version 5.2 Acquisition software (LI-COR Biosciences, Lincoln, NE, USA). Protein relative quantifications were computed using β-Actin or Actin as housekeeping proteins.

3.11 The immunohistochemical assay

The expression and distribution of AURKA, PD-L1, and Ki67 (a cell proliferation marker) proteins were examined in paraffin-embedded sections from 12 subjects, including 8 HCC patients, 2 MASLD individuals, and 2 subjects with a healthy liver. For HCC patients, both HCC and paired non-HCC tissues were stained.

The immunohistochemical assay for AURKA involved the following steps. Tissues were deparaffinized by incubating in xylene and hydrated with decreasing concentrations of ethanol. Antigen retrieval was executed using Sodium Citrate Buffer (10mM Sodium Citrate, 0.05% Tween 20, pH 6.0), and endogenous peroxidase was inhibited using 3% hydrogen peroxide. The staining was performed using the VECTASTAIN® Universal Quick HRP Kit (PK-8800, Vector Laboratories, Newark, CA, USA) and ImmPACT® DAB Substrate Kit (SK-4105, Vector Laboratories, Newark, CA, USA), following the manufacturer's protocols. Slices were incubated in blocking solution (5% horse serum in PBS) for 1 hour to saturate non-specific binding sites, and then overnight in AURKA primary antibody (sc-398814, Santa Cruz Biotechnology, Dallas, TX, USA) diluted in blocking solution (1:500). The Biotinylated Pan-Specific Universal Antibody functioned as a secondary antibody, followed by incubation with the Streptavidin/Peroxidase complex and its sensitive colorimetric DAB substrate, resulting in the generation of a brown product in the presence of the protein of interest. Counterstaining with hematoxylin facilitated the detection of nuclei, and dehydration was performed by washing in increasing concentrations of ethanol and xylene.

The staining of PD-L1 (Clone SP263, VENTANA, Roche Diagnostics, Basel, Switzerland) and Ki67 (Clone 30-9, VENTANA, Roche Diagnostics, Basel, Switzerland) was performed by an automated system at ASUGI.

The stained section images were collected using an automated slide scanner (D-Sight FLUO (Combo), A. Menarini Diagnostics, Firenze, Italy) and analyzed by an expert anatomic pathologist from ASUGI.

3.12 Flow cytometry assay

The chromatin content was estimated in both cell lines through flow cytometry analysis, using the following procedure. Cells were detached by trypsin, washed with PBS, resuspended in 0.5ml of PBS, and fixed in 4.5ml of 70% ethanol to achieve a single-cell suspension. The samples were preserved at -20°C for later use. Upon usage, the cells were pelleted and resuspended in a Propidium Iodide (PI)/TritonX-100 staining solution for 30 minutes to stain DNA. The staining solution consisted of TritonX-100 0.1% v/v in PBS, 0.2mg/mL of RNAse A (6513, Sigma-Aldrich, St. Louis, MO), and 0.02mg/mL of PI (P4864, Sigma-Aldrich, St. Louis, MO), a fluorescent intercalating agent. As a negative control, cells resuspended in TritonX-100 0.1% v/v in PBS without PI were used.

Flow cytometric analysis was immediately performed through the Flow Cytometer BD Accuri™ C6 Plus (BD Biosciences, Franklin Lakes, New Jersey, USA), considering at least 10,000 events for each sample. Data were analyzed with FlowJo™ 10.8.1 version (FlowJo™ Software, Ashland, OR, USA), utilizing different gates to distinguish the percentage of cells with specific chromosome content: Diploid cells (2n), tetraploid cells (4n), or aneuploid cells with more than 4 sets of chromosomes (>4n).

3.13 Immunofluorescence assay

The organization of chromatin and Tubulin-α protein, along with the localization of Pericentrin (PCNT) protein (a centrosome marker), was evaluated in the cell lines through an immunofluorescence (IF) assay.

The cells were fixed and permeabilized with Paraformaldehyde (PFA) 3% in PBS for 20 minutes. They were incubated in a blocking solution for 90 minutes to saturate non-specific binding sites and favor the complete permeabilization of cell membranes. The blocking solution consisted of Albumin (BSA) Fraction V (pH 7.0) (A139, PanReac AppliChem, Monza, Italy) at 1% v/v in PBS, Triton X-100 0.3% (X100, Sigma-Aldrich, St. Louis, Missouri, USA), and Normal goat serum (NGS) 5% (G9023, St. Louis, MO). The fixed cells were incubated with the primary antibody against Tubulin α (sc32293, Santa Cruz Biotechnology, Dallas, TX, USA) and the corresponding secondary antibody, anti-mouse green-fluorescent dye, AlexaFluor 488 (A21202, Invitrogen™, Waltham, Massachusetts, USA), for 1 hour each. This procedure was then repeated for PCNT (CSB-PA017627LA01HU, Cusabio, Houston, TX, USA), followed by anti-rabbit orange-fluorescent dye, AlexaFluor 546 (A11035, Invitrogen™, Waltham, Massachusetts, USA). All the antibodies were diluted in the blocking solution, and the concentrations are listed in Table 8.

Table 8. The antibody dilutions and blocking solution used in the immunofluorescence experiments.

Targets	Dilutions
Tubulin α (SC-32293)	1% BSA 0.3% Triton X-100, and 5% NGS in PBS 1:100 (primary) 1:1000 (AlexaFluor 488)
PCNT (CSB-PA017627LA01HU)	1% BSA 0.3% Triton X-100, and 5% NGS in PBS 1:500 (primary) 1:1000 (AlexaFluor 546)

PCNT, Pericentrin.

Finally, the samples were counterstained with Hoechst 33258 nucleic acid stain (H3569, Thermo Fisher Scientific, Waltham, MA, USA) for 10 minutes at room temperature, protected from direct light. Using Fluorescent Mounting Media (JA1750, Calbiochem, Germany), coverslips were mounted onto glass slides. The samples were analyzed under a Fluorescence Microscope (Leica DM2000, Germany), and images were captured using LAS X software (Leica Application Suite X software, Leica, Germany).

3.14 Gene reporter assay

A gene reporter assay was conducted in JHH6 cells to investigate the influence of AURKA on PD-L1 transcription.

Cells were transfected (minimum 24 hours before the assay) with pGL3-Basic PD-L1 promoter (-1000~+200) (PVTB00385-2a, Lifescience Market, Hong Kong, China) (Figure 6) and pRL-CMV Renilla luciferase at a ratio of 49:1, achieving a final concentration of 170ng/ml. Transfection was performed using TransFectin™ Lipid Reagent (1703350, Bio-Rad, Hercules, CA, USA) diluted to 0.6% in an antibiotics-free culture medium, following the manufacturer's protocol. The culture medium was replaced with the respective fresh antibiotic-free medium 1 hour before the transfection. The mixture of TransFectin™ Lipid Reagent and plasmids was prepared in an antibiotic-free and serum-free medium, and after 30 minutes of incubation, the complexes were added to the cells. The medium containing the complexes was replaced with a fresh complete medium 24 hours later.

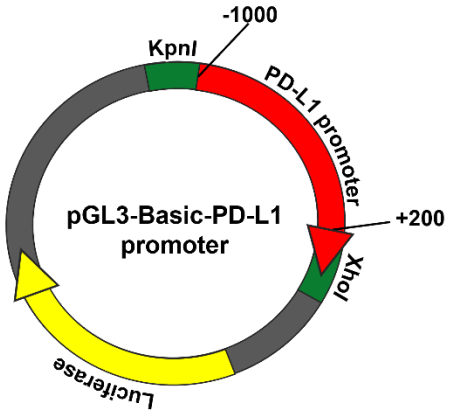

Figure 6. The construction scheme of the luciferase reporter vector plasmid containing the pGL3-Basic PD-L1. The luciferase reporter vector includes the promoter sequence (spanning from nucleotide -1,000 to +200) flanked by two cloning sites, KpnI at the 5' end and XhoI at the 3' end. The luciferase coding sequence is positioned downstream of the PD-L1 promoter. The backbone size without the insert is 4818 base pairs (bp). KpnI serves as a cloning site for the Type-II restriction enzyme KpnI (*Klebsiella pneumoniae*), and XhoI functions as the cloning site for the Type-II restriction enzyme XhoI (*Xanthomonas vasicola*).

The gene reporter assay utilized the Dual-Luciferase Reporter Gene Assay Kit (KA3784, Abnova, Taipei, Taiwan) following the manufacturer's protocol. This assay allows for the sequential measurement of the activity of two different luciferases, firefly (FFL) and Renilla (RL), in a single sample. The procedure involved washing cells with PBS and lysing them with Lysis Buffer for 15 minutes. A total of 12.5µL of cell lysate was dispensed in a 384-well plate. FFL reagent (2mg/ml FFL in Assay Buffer, 25µL) was added to the lysate, and the FFL luciferase luminescence was measured at 560 nm using The EnSpire Multimode Plate Reader (PerkinElmer, Waltham, MA, USA). Subsequently, RL reagent (35 mg/ml RL in Assay Buffer, 25µL) was added to the same well, quenching the FFL luciferase luminescence and initiating the RL luciferase reaction. The RL

luminescence was measured at 480 nm using the same plate reader. The Relative Light Unit (RLU) was calculated using the following formula:

RLU = FFL Luminescence / RL Luminescence

3.15 Online databases and bioinformatic tools

The GEPIA database (http://gepia.cancer-pku.cn/) was employed to investigate gene expression and correlation in both disease patients (utilizing data from TCGA) and healthy samples (utilizing data from both TCGA and Genotype-tissue expression (GTEx)). GEPIA facilitates the exploration of the gene expression changes based on the disease stage and provides information on OS and DFS according to gene expression. The Human Protein Atlas (THPA) (https://www.proteinatlas.org/) was employed to collect images of immunohistochemical sections from HCC tissues.

The DepMap portal (https://depmap.org/portal/) can assess gene expression in numerous cell lines (Expression Public 23Q4) and provides valuable insights into the dependency of a cell line on a specific gene using RNA interference (RNAi) and Clustered regularly interspaced short palindromic repeats (CRISPR)-Cas9 knockdown.

3.16 Statistical analysis

Statistical analyses were conducted using GraphPad Prism Software version 9.2.0 (GraphPad Software, San Diego, CA) and NCSS 11 Statistical Software (2016) (NCSS, LLC, Kaysville, UT, USA). Initially, the normal distribution of the data was assessed. The significance level was set at 0.05 (* $p < 0.05$, ** $p < 0.01$, *** $p < 0.001$).

For the patients' data, which exhibited a non-Gaussian distribution, results were presented as median [IQR-IIIQR]. The differences in mRNA and protein expression between human and mouse groups were analyzed as follows. Statistical significance was calculated employing Wilcoxon signed-rank tests to examine the disparities between HCC and paired non-HCC tissues in both human and mouse samples, Kruskal-Wallis tests to assess the differences among multiple groups of samples, and Mann-Whitney U for non-paired tissues in humans (HCC, MASLD, and healthy samples) and mice (TG mice *vs.* WT mice or groups from different time points).

The potential impact of clinical and pathological variables on gene expression was assessed through regression analysis. Correlations were calculated using Spearman's rank correlation test. The statistical significance of the differences between categorical variables in each group was calculated using Fisher’s exact test. OS and DFS analyses related to a single gene were conducted using the log-rank Mantel-Cox test. Survival analyses related to the combinations of multiple genes were assessed by Cox proportional-hazards regression analysis. The receiver operating characteristic (ROC) curve was used to assess the overall diagnostic performance of a variable.

For *in vitro* analyses, each experiment was conducted in a minimum of three independent replicates. The results were presented as mean ± standard deviation (SD) since the data exhibited a Gaussian distribution. Unpaired t-tests were employed to assess the statistical significance of the differences in mRNA, protein, and chromatin content between two sample groups (treatment *vs.* vehicle).

Chapter 4 – Results

4.1 *In silico* evaluation of *AURKA* expression

Freely accessible data repositories are valuable sources of information and offer beneficial support for research. Among all, GEPIA is a comprehensive platform offering extensive gene expression data, enabling diverse comparisons and analyses.

By analyzing HCC data from GEPIA, a marked *AURKA* mRNA overexpression was observed in tumors, compared to normal tissues (median: 7.35 TPM *vs*. 0.99 TPM, $p \leq 0.05$), with a fold change (FC) of 7.42 (Figure 7.A). A deeper exploration revealed a progressive increase in *AURKA* expression from stage I to stage III, followed by a decrease in stage IV (F value = 3.58, p = 0.014) (Figure 7.B). The impact of elevated AURKA levels in tumors extended to clinical outcomes, revealing an association between high levels of *AURKA* expression in tumors and a shorter OS rate ($p < 0.001$), or heightened likelihood of early recurrence (p = 0.001) (Figure 7.C-D). Moreover, the database revealed a positive correlation between *AURKA* and *PD-L1* expression in both HCC (Spearman r = 0.18, $p < 0.001$) and normal liver tissues (Spearman r = 0.39, $p < 0.001$) (Figure 7.E-F).

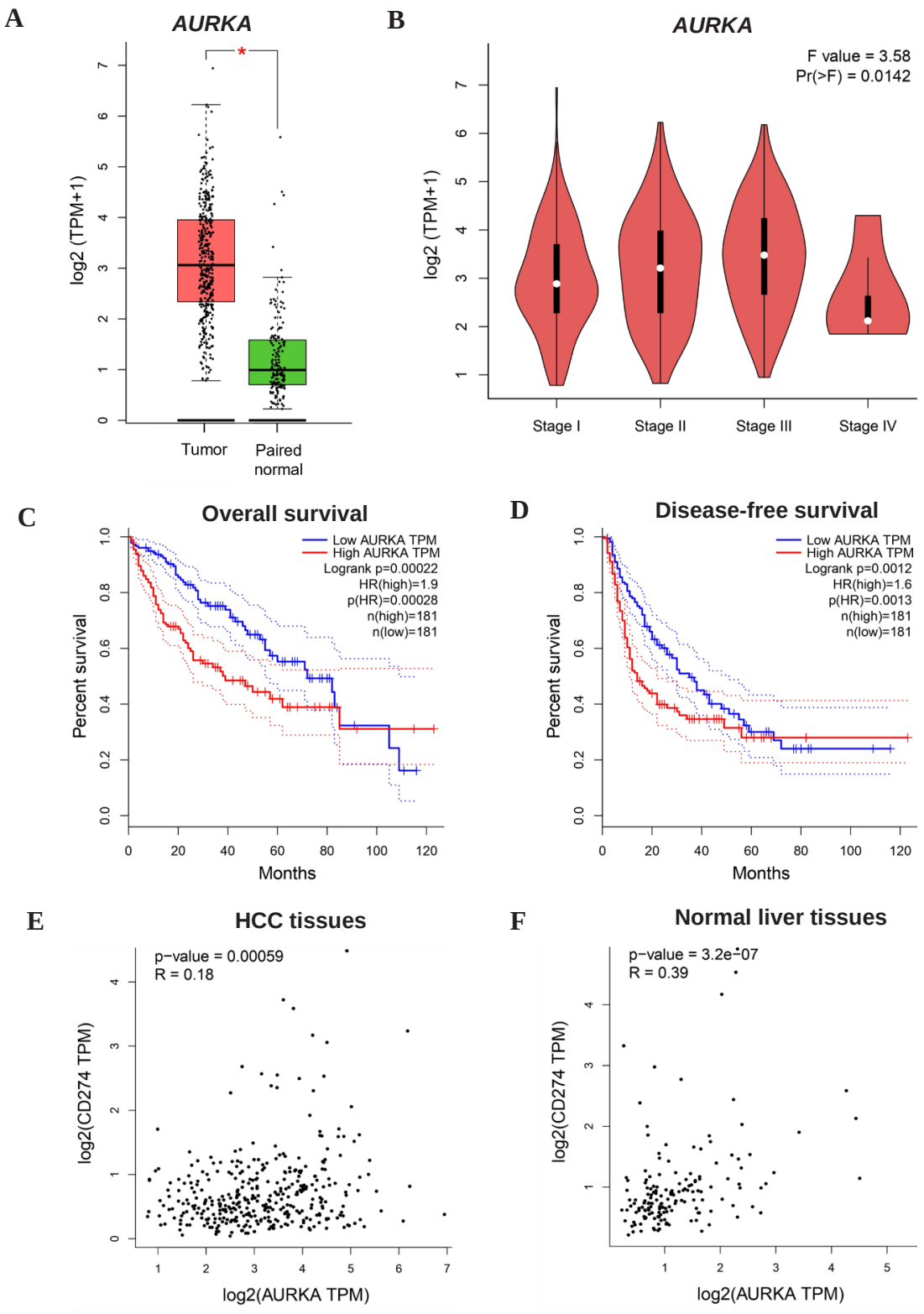

Figure 7. The expression of *AURKA* in HCC according to the GEPIA database (http://gepia.cancer-pku.cn/). (A-B) *AURKA* mRNA expression (A) in HCC (n=369) *vs.* normal LIVER tissues (n=160) and (B) in the different stages of the disease. (C) OS and (D) DFS curves based on *AURKA* expression level in HCC patients. (E-F) Correlation between *AURKA* and *PD-L1* in (E) HCC tissues and (F) normal liver tissues. * p <0.05. TPM, Transcripts per million.

4.2 The cellular and molecular alterations determined by *in vitro* AURKA inhibition or knockdown

4.2.1 AURKA expression in human cell lines

AURKA mRNA expression is prominent across various human cell lines, as evidenced by the Expression Public 23Q4 dataset from DepMap Portal. Over 400 cell lines exhibited expression levels ranging from 72.52 to 110.42 TPM, including JHH6 (81.71 TPM) and Huh7 (96.68 TPM) cells (Figure 8.A). The examination through qRT-PCR unveiled comparable *AURKA* mRNA expression levels in JHH6 and Huh7 cells (Ct: 24.18±0.49 *vs.* 24.15±0.20, p = 0.930) (Figure 8.B).

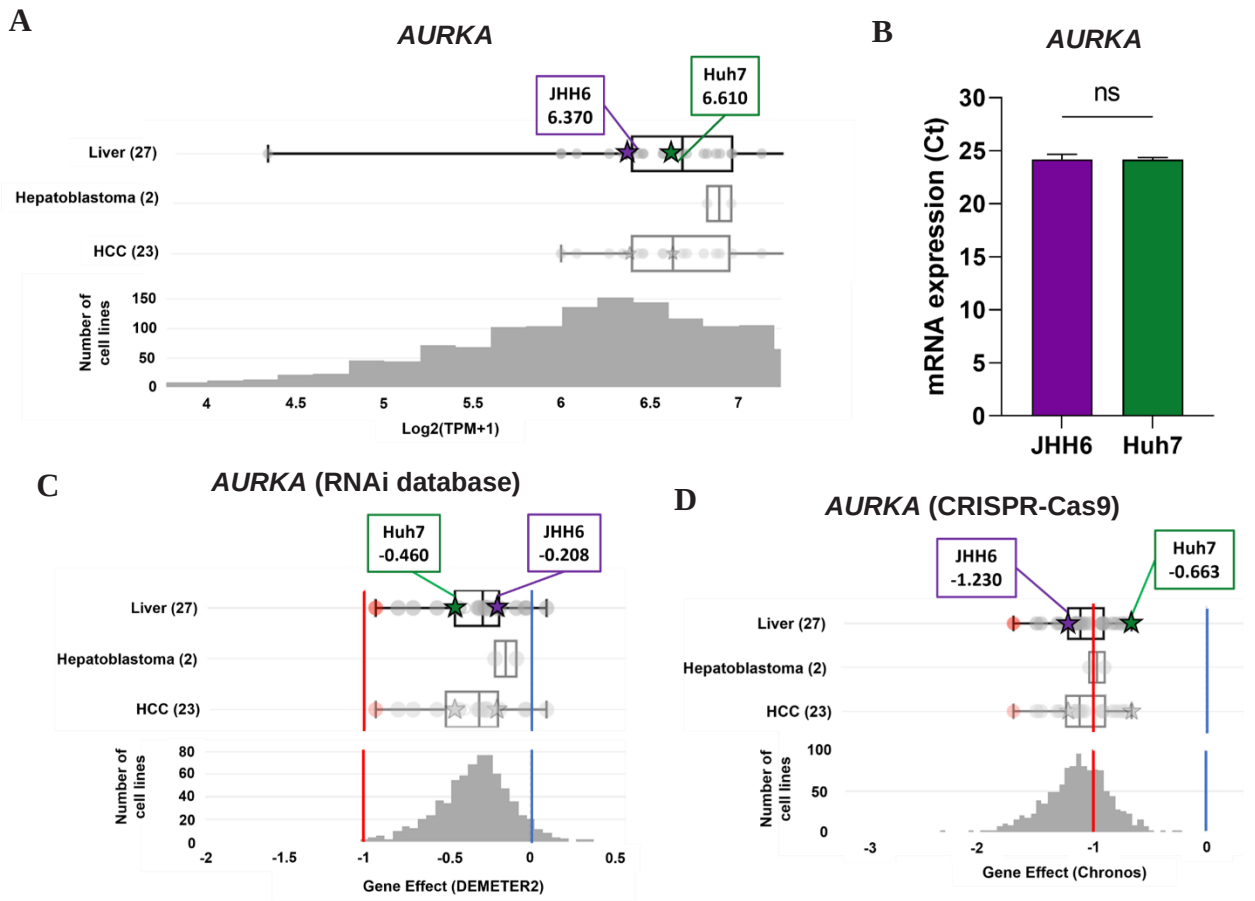

Figure 8. The expression of *AURKA* in JHH6 and Huh7 cell lines. (A) *AURKA* expression in human cell lines according to the Expression Public 23Q4 dataset from DepMap Portal (https://depmap.org/portal/). (B) *AURKA* expression in JHH6 and Huh7 by qRT-PCR expressed in Ct (n=4). Statistical analyses were calculated using the student's t-test. Ns, not significant. (C-D) Dependency of the human cell lines on the expression of *AURKA* using (C) RNAi database and (D) CRISP-Cas9 database from DepMap Portal (https://depmap.org/portal/).

However, the dependency of these two cell lines on the AURKA gene varied, as indicated by data from the DepMap portal. In this context, a score of 0 implies a non-essential gene for cell growth, while a score near -1 signifies essentiality. According to RNAi databases (Achilles, DRIVE, Marcotte, and DEMETER2), both JHH6 (-0.208) and Huh7 (-0.460) demonstrated a moderate dependency on *AURKA* mRNA expression, albeit to different extents (Figure 8.C). These findings were further strengthened by querying databases collecting results from CRISPR-Cas9 experiments (22Q4+Score, Chronos). The database analysis revealed the essential role of AURKA in both cell lines, with more pronounced effects on JHH6 (scores: -1.230 and -0.663 for JHH6 and Huh7, respectively) (Figure 8.D).

4.2.2 Determining the optimal working concentration for the in vitro experiments

AURKA inhibition was performed using two ATP-competitive and reversible AURKA inhibitors: Alisertib and AK-01. We selected concentrations ranging from 0.001μM to 10μM for Alisertib and from 0.01μM to 30μM for AK-01 to test cell viability after 72 hours of treatment. The MTT assay was employed to determine the optimal dose-response curve models for cell survival, consisting of the rational model for Alisertib and the Weibull model for AK-01 in JHH6 cells, and the modified Hoerl model and the Hoerl model in Huh7 cells (Figure 9.A-D). Based on these models, LC50 values were calculated for each compound-cell line combination (Table 9).

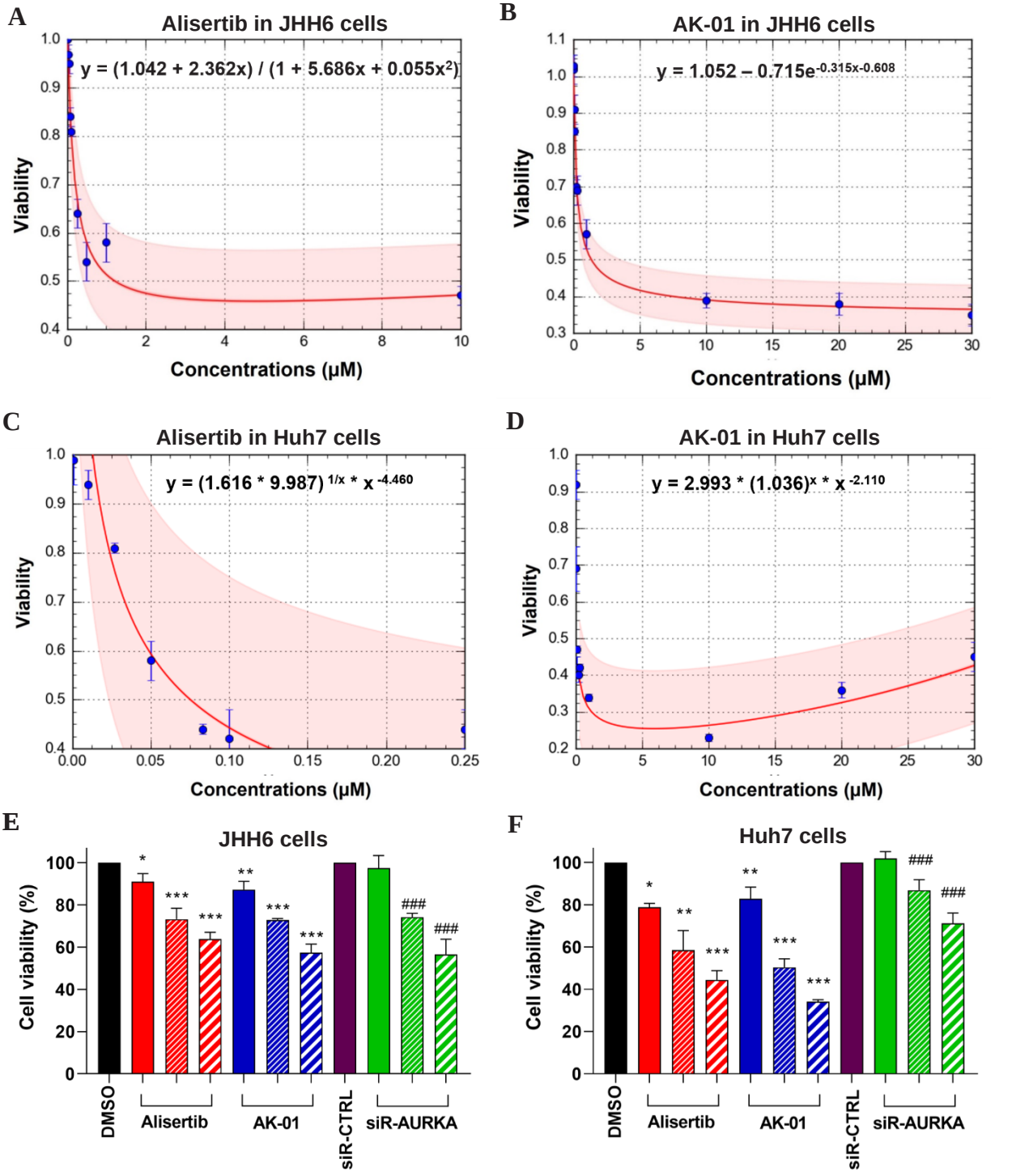

Figure 9. The effects of AURKA inhibition or knockdown on cell viability. (A-B) Dose-response curves of JHH6 cells treated with (A) alisertib and (B) AK-01 for 72h (n=3). (C-D) Dose-response curves of Huh7 cells treated with (C) alisertib and (D) AK-01 for 72h (n=3). (E-F) Relative (E) JHH6 and (F) Huh7 cell viability assessed at 72h post treatments with 0.25μM of alisertib, 1.00μM of AK-01, and 1nM of siR-AURKA. Statistical significance was calculated using the student's t-test relative to DMSO for AURKA inhibition (* p <0.05, ** p <0.01, *** p <0.001) and to siR-CTRL for AURKA knockdown (# p <0.05, ## p <0.01, ### p <0.001).

Taking into account the existing literature, the LC50 values derived from our cellular models, and the documented decrease in target specificity of alisertib and AK-01 at concentrations higher than 0.25μM and 1.00μM, respectively, we selected 0.25μM for Alisertib and 1.00μM for AK-01 as the optimal working concentrations (Table 9). It is necessary to mention that 1.00μM represents the highest concentration of AK-01 specifically inhibiting the enzymatic activity of AURKA without affecting AURKB activity [115].

Table 9. LC50 and working concentrations of treatment with alisertib and AK-01 for 72 hours in JHH6 and Huh7 cells.

AURKA inhibitors	JHH6 cells	Huh7 cells	Working concentrations
Alisertib	1.05μM	0.08μM	0.25μM
AK-01	1.30μM	0.09μM	1.00μM

The working concentration for siR-AURKA was determined to be 1.00nM. This choice was supported by consistent findings across all tested concentrations (1.00nM, 5.00nM, and 20.00nM), revealing a comparable decrease in *AURKA* mRNA expression 72 hours post-transfection.

4.2.3 The reduction in cell viability following AURKA inhibition or knockdown

The two AURKA inhibitors determined a gradual decline in the viability of both cell lines, with a more substantial impact observed in Huh7 (Table 10 and Figure 9.D-E). AK-01 demonstrated a greater reduction in cell viability compared to alisertib in both JHH6 and Huh7 cell lines (Table 10).

Table 10. Cell viability following treatments with AURKA inhibitors in JHH6 and Huh7 cells.

Treatment Times	Alisertib in JHH6 cells	P-value	Alisertib in Huh7 cells	P-value	AK-01 in JHH6 cells	P-value	AK-01 in Huh7 cells	P-value
24 hours	91.02±3.81	0.015	78.75±1.87	<0.001	87.21±3.95	0.005	82.85±5.46	0.006
48 hours	73.15±5.29	<0.001	58.54±9.22	0.002	72.79±0.78	<0.001	50.34±4.06	<0.001
72 hours	63.83±3.19	<0.001	44.45±4.37	<0.001	57.45±4.00	<0.001	34.11±0.93	<0.001

Conversely, AURKA knockdown exerted a more pronounced effect on JHH6 cell viability, reaching its maximum impact at 72 hours post-transfection (Table 11 and Figure 9).

Table 11. Cell viability following AURKA silencing in JHH6 and Huh7 cells.

Treatment Times	JHH6 cells	P-value	Huh7 cells	P-value
24 hours	97.39±6.01	0.420	101.90±3.26	0.230
48 hours	74.20±1.82	<0.001	86.86±4.94	<0.001
72 hours	56.60±7.18	<0.001	71.18±4.83	<0.001

4.2.4 The effects of AURKA inhibition and knockdown on AURKA expression and activity

The efficacy of the treatments was verified by assessing both AURKA expression and kinase activity, using LATS2 phosphorylation (Ser83) as the marker for the enzymatic activity of AURKA, as evidenced by various studies [10,164,165]. Additionally, changes in *TPX2* mRNA expression, a known co-activator/interactor of AURKA, were examined.

In JHH6 cells, both alisertib and AK-01 resulted in an increase in *AURKA* mRNA expression at 24 hours (2.12±0.48, p = 0.005; 2.92±1.59, p = 0.052), 48 hours (1.80±0.55, p = 0.028; 5.10±1.27, p <0.001), and 72 hours (1.64±0.30, p = 0.005; 5.59±1.90, p = 0.004) (Figure 10.A). Conversely, AURKA knockdown significantly decreased AURKA mRNA expression at all three selected time points (0.14±0.02, p <0.001; 0.16±0.04, p <0.001; 0.29±0.07, p <0.001) (Figure 10.A).

The protein expression was assessed at 72h and 144 hours after the silencing treatment. The selection of these time points aligns with the estimated half-life of some AURKA targets (i.e. PD-L1), ensuring a comprehensive evaluation of the treatment effects over a duration corresponding to the stability and dynamics of these relevant AURKA interactors. Consistently with the previous results, both alisertib and AK-01 increased AURKA protein expression at 72 hours (3.48±0.84, p = 0.001; 4.50±1.76, p = 0.007), while AURKA knockdown decreased AURKA protein expression at 72 hours (0.00±0.01, p <0.001) and 144 hours (0.00±0.01, p <0.001) (Figure 10.C and E). A moderate reduction in LATS2 phosphorylation (Ser83) was observed after AURKA silencing at both time points, with significant results at 72 hours (0.69±0.18, p = 0.040) (Figure 10.D-E). In contrast, kinase activity inhibition led to a pronounced reduction in LATS2 phosphorylation (Alisertib: 0.52±0.21, p <0.001; AK-01: 0.41±0.12, p <0.001) (Figure 10.D-E).

Regarding *TPX2* mRNA expression, both AK-01 and siR-AURKA treatments increased its expression at 48 hours (3.32±1.34, p = 0.013; 1.42±0.14, p = 0.001) and 72 hours (5.11±2.23, p =

0.012; 1.88±0.32, p = 0.002), whereas alisertib showed an increase only at 24 hours (2.91±1.70, p = 0.066) (Figure 10.B).

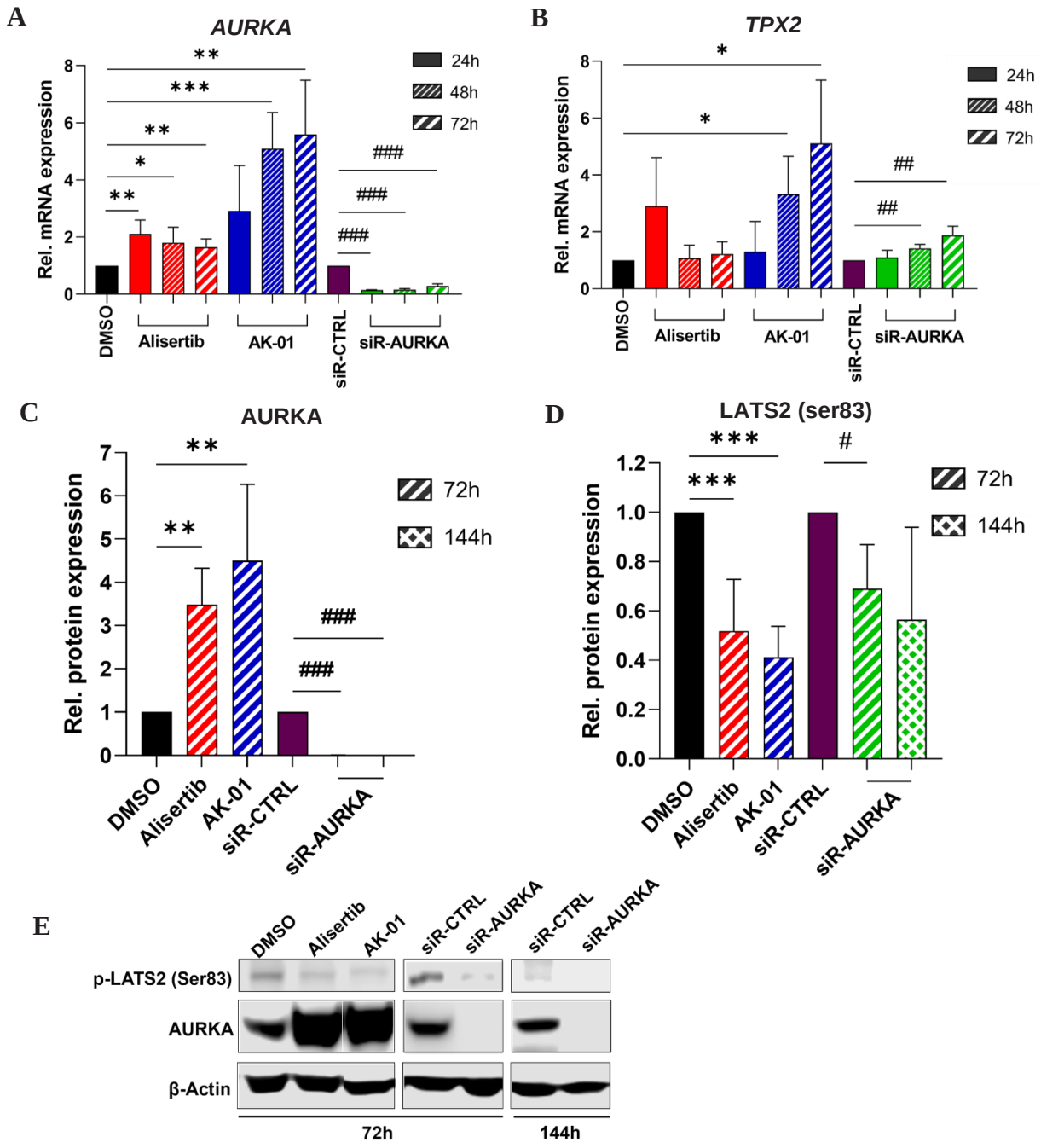

Figure 10. The effects of AURKA inhibition or knockdown on AURKA and *TPX2* expression and AURKA activity in JHH6 cells. (A-B) Relative (A) *AURKA* and (B) *TPX2* mRNA expression at 24h, 48h, and 72h post inhibition or knockdown (n=5). (C-D) Relative expression of (C) AURKA protein and (D) phospho-LATS2 (Ser83) at 72h post inhibition or knockdown and 144h post knockdown (n=4). (E) Representative protein blots of LATS2 (Ser83) phosphorylation, AURKA, and β-Actin post inhibition or knockdown. Statistical significance was calculated using the student's t-test relative to DMSO for AURKA

inhibition (* p <0.05, ** p <0.01, *** p <0.001) and siR-CTRL for AURKA knockdown. (# p <0.05, ## p <0.01, ### p <0.001)

In Huh7 cells, the treatment with alisertib and AURKA knockdown resulted in decreased *AURKA* (0.86±0.05, p = 0.010; 0.10±0.01, p <0.001) and *TPX2* (0.92±0.03, p = 0.015; 0.62±0.02, p <0.001) mRNA expression at 72 hours (Figure 11.A-B). In contrast, both inhibitors induced an elevation in AURKA protein expression (alisertib: 1.37±0.49, p = 0.259; AK-01: 2.02±0.24, p = 0.002) and a reduction in LATS2 phosphorylation (Ser83) (0.82±0.29, p = 0.344; 0.82±0.10, p = 0.032), with statistically significant results observed solely in the case of AK-01 treatments (Figure 11.C-E).

AURKA knockdown decreased AURKA protein expression and LATS2 phosphorylation (Ser83) at both 72 hours (AURKA: 0.03±0.05, p <0.001; pLATS2 (Ser83): 0.70±0.23, p = 0.090) and 144 hours (0.01±0.00, p <0.001; 0.84±0.03, p = 0.003) (Figure 11.C-E).

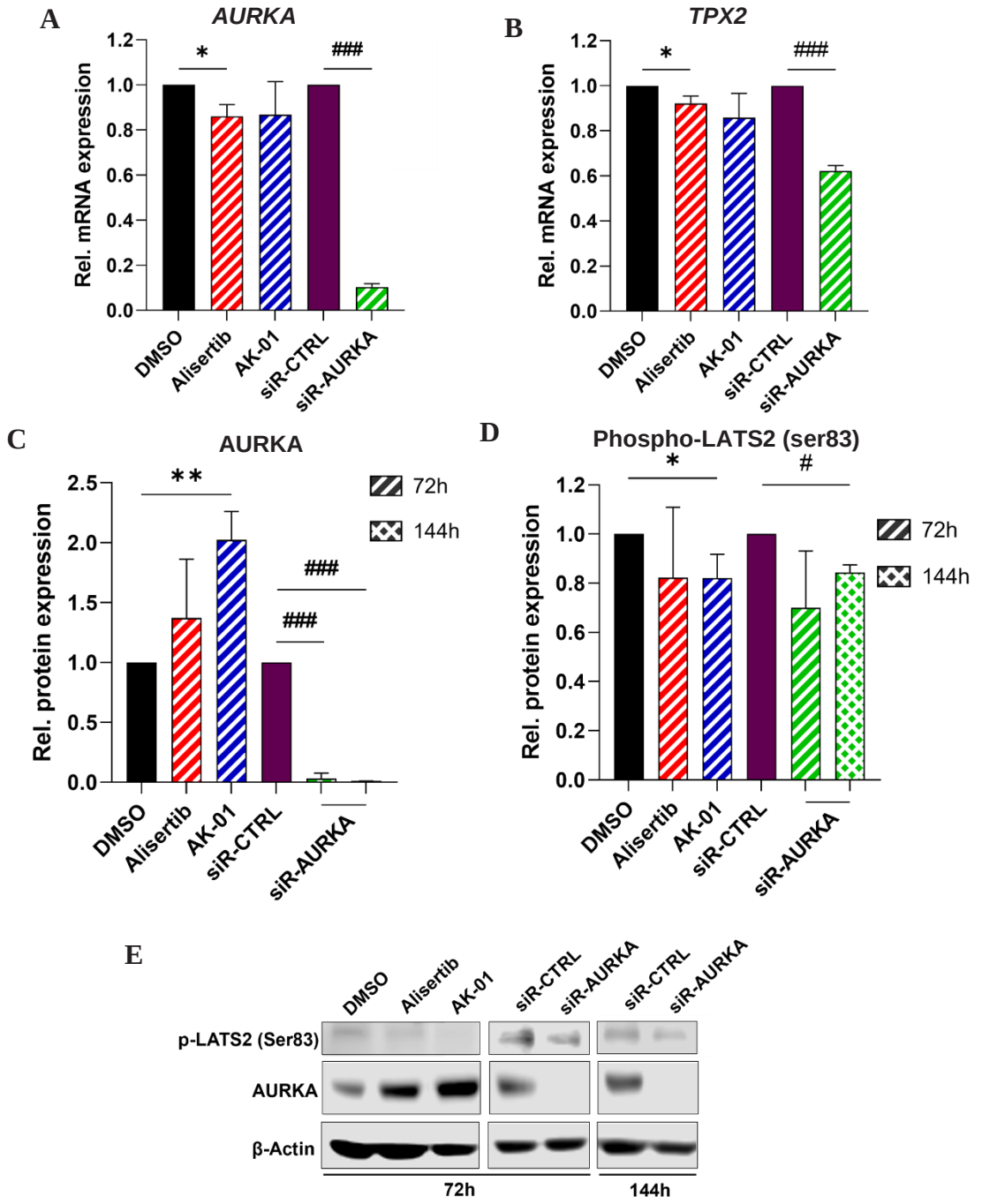

Figure 11. The effects of AURKA inhibition or knockdown on AURKA and *TPX2* expression and AURKA activity in Huh7 cells. (A-B) Relative (A) *AURKA* and (B) *TPX2* mRNA expression at 72h post inhibition or knockdown (n=4). (C-D) Relative expression of (C) AURKA protein and (D) phospho-LATS2 (Ser83) at 72h post inhibition or knockdown and 144h post knockdown (n=3). (E) Representative protein blots of LATS2 (Ser83) phosphorylation, AURKA, and β-Actin post inhibition or knockdown. Statistical significance was calculated using the student's t-test relative to DMSO for AURKA inhibition (* p <0.05, ** p <0.01, *** p <0.001) and siR-CTRL for AURKA knockdown. (# p <0.05, ## p <0.01, ### p <0.001).

4.2.5 AURKA inhibition or knockdown promotes incorrect chromosome segregation and aneuploidy

AURKA plays a crucial role in G2/M transition, spindle assembly, and centrosome maturation, prompting an investigation into mitotic spindle assembly and cell mitosis defects following AURKA inhibition and knockdown. Both AURKA inhibition and knockdown led to an increase in the percentage of cells in the G2/M phase and chromatin accumulation.

Table 12. Cell ploidy after AURKA inhibition or knockdown in JHH6 cells.

Sets of chromosomes	DMSO	Alisertib	AK-01	SiR-CTRL	SiR-AURKA
2n	50.70±4.16	17.97±1.35	24.50±0.20	44.37±1.94	25.63±2.50
4n	23.73±0.38	47.73±2.54	54.27±0.71	32.17±1.19	48.87±3.41
>4n	3.10±0.48	27.20±1.65	14.53±1.36	5.49±0.18	16.00±1.40

Data were reported as cell percentage (mean±SD). 2n: Diploid cells; 4n: Tetraploid cells; >4n: Aneuploid cells with more than 4 sets of chromosomes.

In JHH6 cells, alisertib and AK-01, by blocking the AURKA kinase activity, markedly increased the percentage of tetraploid cells (both $p < 0.001$) and aneuploid cells with more than 4 sets of chromosomes (both $p < 0.001$) compared to the control (Figure 12.A and Table 12). Similar effects were obtained following AURKA knockdown ($p = 0.001$; $p < 0.001$) (Figure 12.A and Table 12). The increase in aneuploid cells treated with alisertib, AK-01, and siR-AURKA was 48% (4n+>4: 24%+24%), 42% (31%+11%), and 28% (17%+11%), respectively.

Table 13. Cell ploidy after AURKA inhibition or knockdown in Huh7 cells.

Sets of chromosomes	DMSO	Alisertib	AK-01	SiR-CTRL	SiR-AURKA
2n	50.70±4.16	17.97±1.35	21.13±3.30	44.10±4.33	27.40±5.05
4n	22.03±0.57	34.60±1.56	39.03±0.83	20.73±1.27	29.37±2.61
>4n	11.00±2.30	22.53±4.11	17.43±3.43	10.46±0.91	20.27±3.56

Data were reported as cell percentage (mean±SD). 2n: Diploid cells; 4n: Tetraploid cells; >4n: Aneuploid cells with more than 4 sets of chromosomes.

In Huh7 cells, Alisertib and AK-01 significantly increased the percentage of tetraploid cells (both $p < 0.001$) and aneuploid cells with more than 4 sets of chromosomes ($p = 0.013$; $p = 0.054$)

compared to the control (Figure 12.B and Table 13). AURKA knockdown led to a modest significant increase compared to the control (p = 0.007; p = 0.010) (Figure 12.B and Table 13). The increase in aneuploid cells with alisertib, AK-01, and siR-AURKA was 26% (4n+>4: 14%+12%), 23% (17%+6%), and 19% (9%+10%), respectively.

JHH6 cells showed a higher percentage of aneuploid cells compared to Huh7 in response to all treatments, and AURKA inhibition induced a greater increase in aneuploid cells compared to AURKA knockdown in both cell lines (Figure 12.A-B).

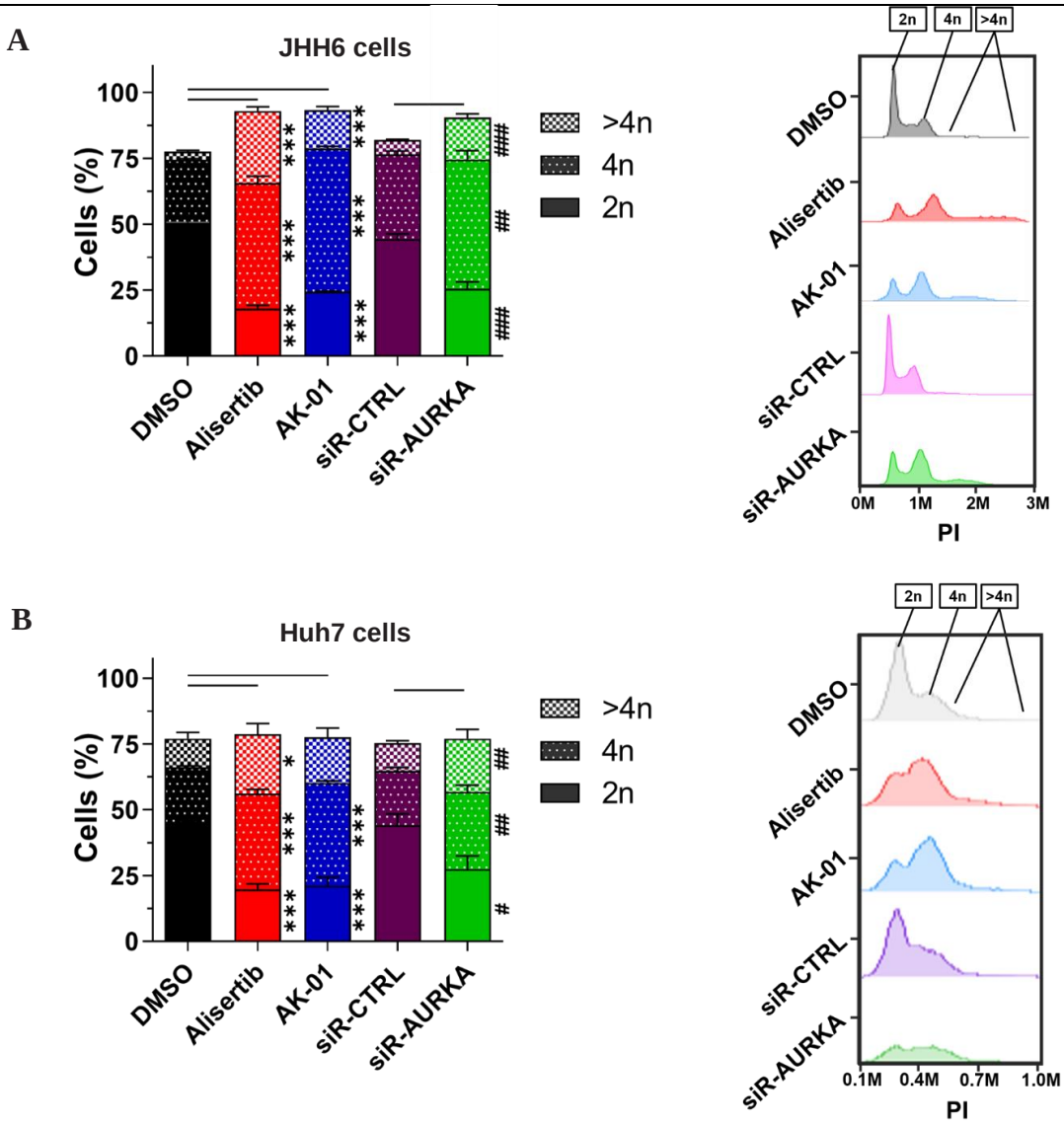

Figure 12. The effects of AURKA inhibition or knockdown on cell chromatin content. (A-B) The percentages of 2n, 4n, and >4n cells at 72h post inhibition or knockdown in (A) JHH6 and (B) Huh7 cells (n=3). Statistical significance was calculated using the student's t-test relative to DMSO for AURKA inhibition (* p <0.05, ** p <0.01, *** p <0.001) and siR-CTRL for AURKA knockdown. (# p <0.05, ## p <0.01, ### p <0.001). 2n: Diploid cells; 4n: Tetraploid cells; >4n: Aneuploid cells with more than 4 sets of chromosomes

An immunofluorescent assay further confirmed changes in cell ploidy and alterations in cell mitosis following AURKA inhibition and knockdown. All treatments resulted in an increased number of cells with multiple nuclei compared to the controls (Figure 13.A).

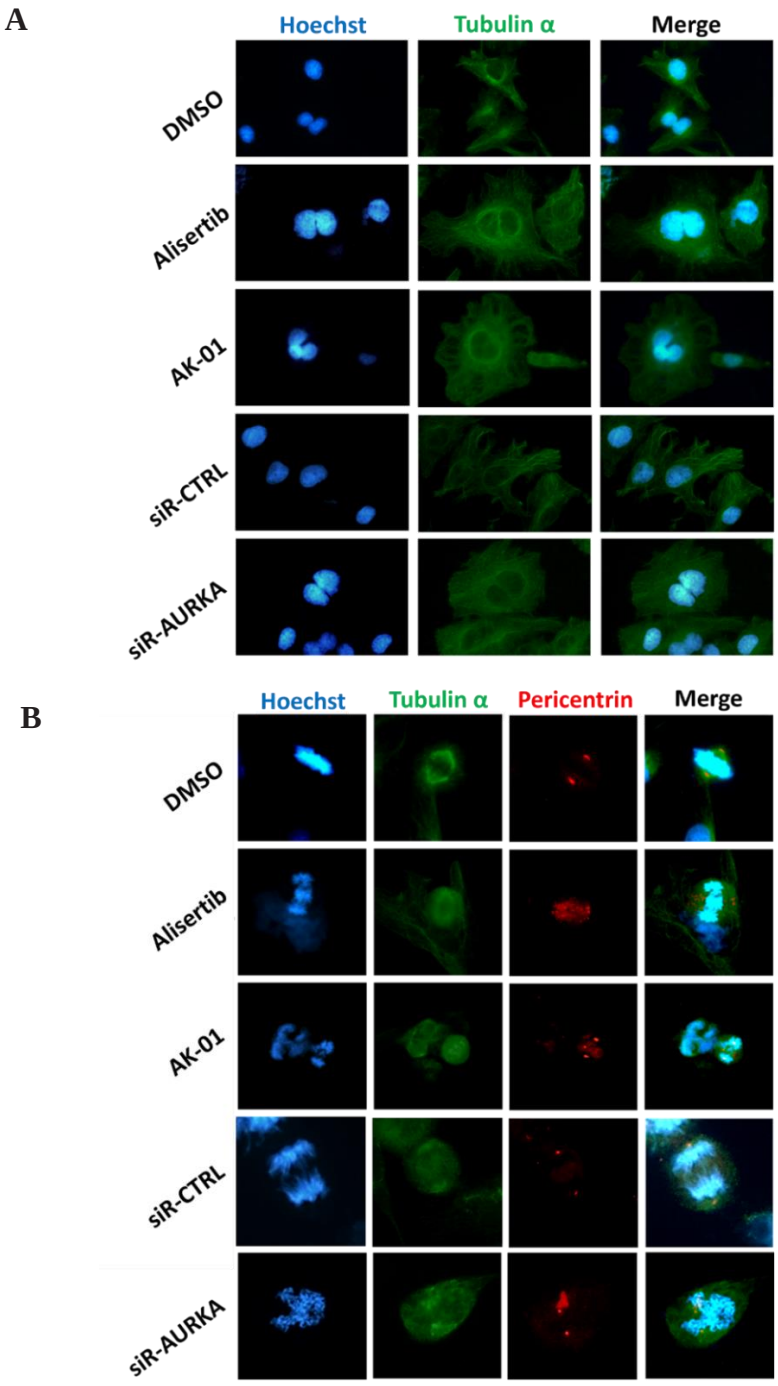

Figure 13. The effects of AURKA inhibition or knockdown on cell ploidy and chromatin organization. (A) Cell ploidy at 72h post inhibition or knockdown in Huh7 cell line. (B) Chromatin and centrosome organization during chromosome segregation at 72h post inhibition or knockdown in JHH6 cells. Blue: Hoechst 33258; Green: Tubulin α; Red: Pericentrin. Magnification: 40X.

Analysis of chromosome segregation during mitosis revealed that control cells exhibited well-organized DNA with a visible metaphase plate in dividing cells, microtubule spindle formation by tubulin α, and correct localization of PCNT (a centrosome marker) at the two opposite sides. AURKA inhibition or knockdown disrupted DNA organization and showed numerous PCNT spots, indicating the presence of multiple unorganized centrosomes (Figure 13.B). These findings underscore the crucial role of AURKA in mitotic processes and the impact of its modulation on cell cycle dynamics and mitotic fidelity.

4.2.6 The multiple effects of AURKA inhibition or knockdown on PD-L1 regulation

The contribution of AURKA to immune checkpoint regulation and cancer immune surveillance remains unclear due to conflicting evidence. This hypothesized mechanism is yet to be explored in HCC. Consequently, we undertook a thorough examination to comprehensively assess the effects of AURKA inhibition or knockdown on PD-L1 expression and regulation.

PD-L1 mRNA expression is generally low in human cell lines, with Huh7 cells exhibiting a lower expression (0.20 TPM) compared to JHH6 cells (18.84 TPM), which represents the second-highest expression in HCC-derived cell lines after SNU423 cells (21.63 TPM) (Figure 14.A). qRT-PCR confirmed the higher abundance of *PD-L1* mRNA expression in JHH6 compared to Huh7 cells (Ct: 27.98±0.21 *vs.* 34.15±0.49, $p < 0.001$) (Figure 14.B).

In JHH6 cells, both alisertib and AK-01 increased *PD-L1* mRNA expression at 24 hours (2.41±1.09, $p = 0.041$; 1.92±0.48, $p = 0.030$) (Figure 14.C). AK-01 treatment demonstrated a sustained elevation in *PD-L1* mRNA expression at 48 hours (2.13±0.65, $p = 0.014$) and 72 hours (5.70±3.61, $p = 0.087$), although the latter was not statistically significant (Figure 14.C). Conversely, AURKA knockdown initially led to a decreased *PD-L1* mRNA expression at 24 hours (0.76±0.12, $p = 0.002$), transitioning into increased expression after 72 hours of treatment (1.71±0.50, $p = 0.030$) (Figure 14.C). In Huh7 cells, AURKA inhibition resulted in an increase of *PD-L1* mRNA expression at 72 hours (Alisertib: 1.34±0.12, $p = 0.008$; AK-01: 1.44±0.26, $p = 0.044$) (Figure 14.D), while knockdown in a reduction (0.80±0.04, $p < 0.001$) (Figure 14.D).

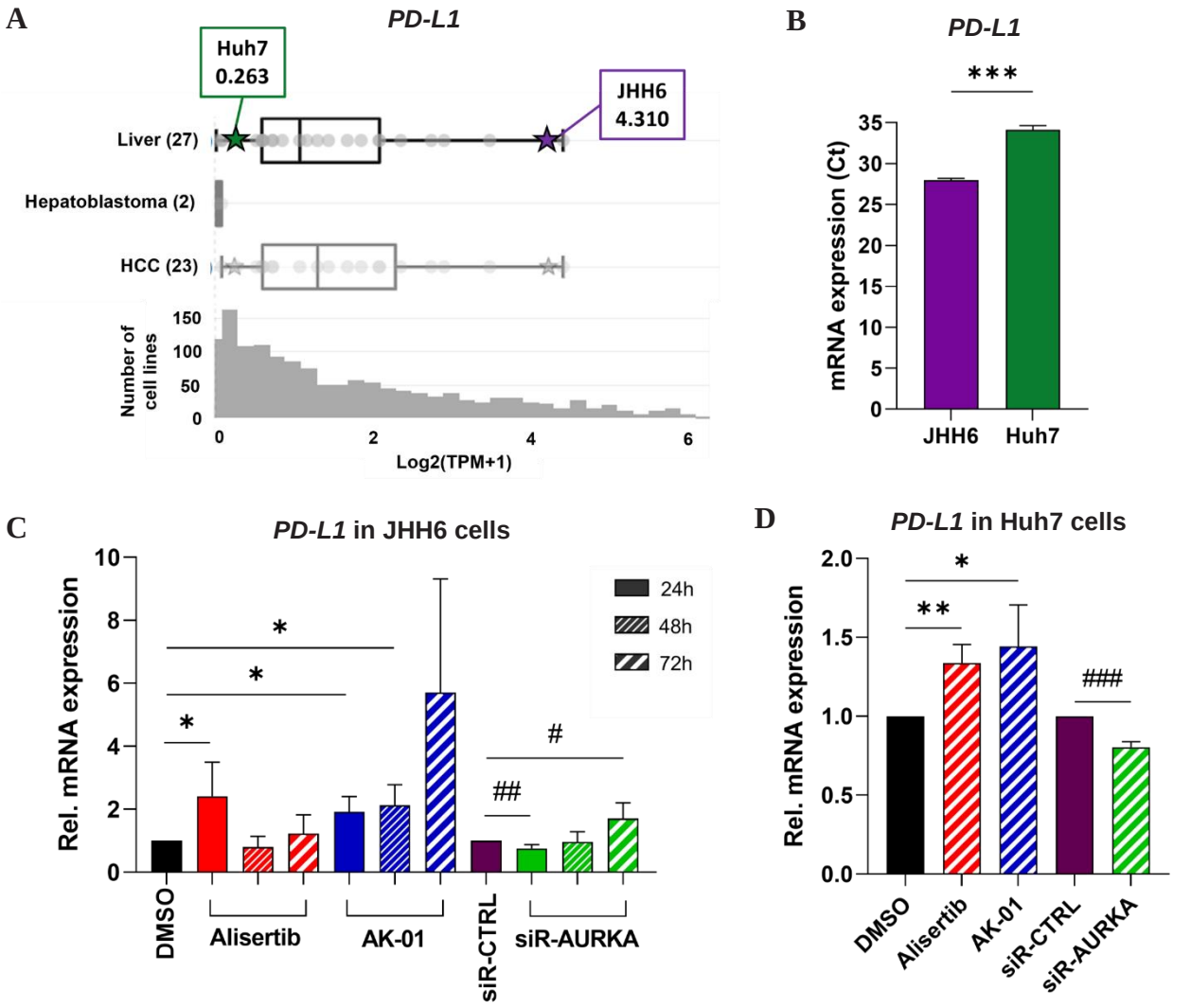

Figure 14. The regulation of *PD-L1* mRNA expression following AURKA inhibition or knockdown. (A) *PD-L1* expression in human cell lines according to the Expression Public 23Q4 dataset from DepMap Portal (https://depmap.org/portal/). (B) *PD-L1* expression in JHH6 and Huh7 cells (n=4). Statistical significance was calculated by using the student's t-test. *** p <0.001. (C) Relative *PD-L1* mRNA expression at 24h, 48h, and 72h post inhibition or knockdown in JHH6 cells (n=4). (D) Relative *PD-L1* mRNA expression at 72h post inhibition or knockdown in Huh7 cells (n=3). Statistical significance was calculated by using the student's t-test relative to DMSO for AURKA inhibition (* p <0.05, ** p <0.01, *** p <0.001) and to siR-CTRL for AURKA knockdown (# p <0.05, ## p <0.01, ### p <0.001).

When analyzing the protein expression a distinct effect resulted from the different treatments, possibly indicating multiple roles of AURKA in PD-L1 regulation. PD-L1 protein expression exhibited multiple bands in WB analysis, with lower bands representing the unglycosylated immature form and upper bands indicating glycosylated mature forms of PD-L1, which are more stable and with membrane localization [130,131]. AK-01 treatment notably decreased the expression of glycosylated PD-L1 in both JHH6 (0.68±0.07, p <0.001) and Huh7 (0.53±0.14, p = 0.005) cells

(Figure 15.A, B, E, and F). AURKA knockdown for 144 hours led to a reduction of unglycosylated non-mature PD-L1 forms in both JHH6 (0.49±0.28, p = 0.040) and Huh7 (0.77±0.06, p = 0.030), and the glycosylated mature forms in JHH6 (0.40±0.21, p = 0.008) (Figure 15.A-F).

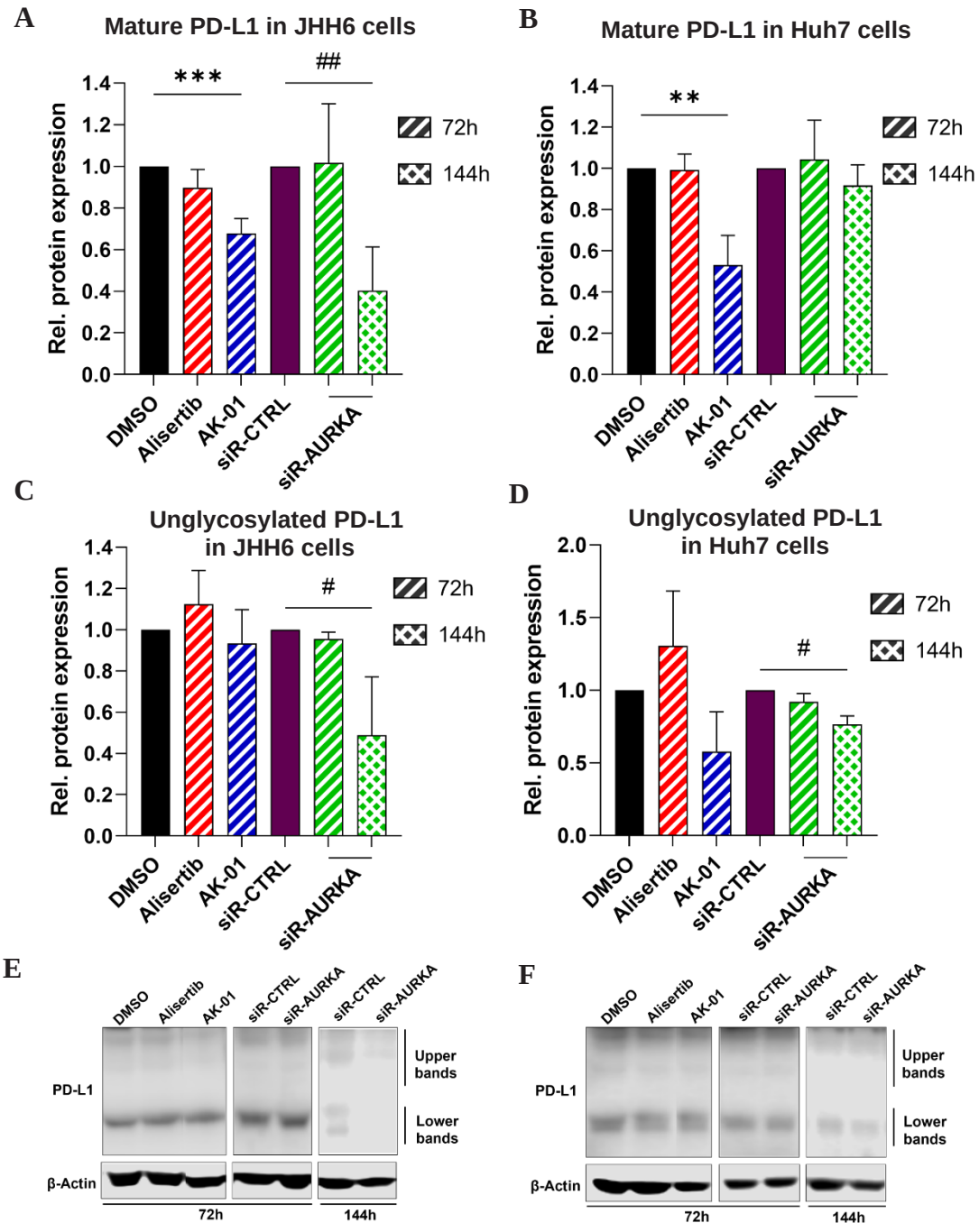

Figure 15. The effects of AURKA inhibition or knockdown on PD-L1 protein expression. (A-B) Relative expression of mature PD-L1, upper bands, at 72h post inhibition or knockdown and 144h post knockdown in (A) JHH6 cells (n=4) and (B) Huh7 cells (n=3). (C-D) Relative expression of unglycosylated PD-L1, lower bands, at 72h post inhibition or knockdown and 144h post knockdown in (C) JHH6 cells (n=4) and (D) Huh7 cells (n=3). (E-F) Representative protein blots of PD-L1 and β-Actin post inhibition or

knockdown in (E) JHH6 cells and (F) Huh7 cells. Statistical significance was calculated using the student's t-test relative to DMSO for AURKA inhibition (* p <0.05, ** p <0.01, *** p <0.001) and to siR-CTRL for AURKA knockdown. (# p <0.05, ## p <0.01, ### p <0.001).

To assess the impact on *PD-L1* mRNA expression, IFN-γ, a recognized inducer of PD-L1, was employed. *PD-L1* showed a concentration-dependent expression at 6 hours (25ng/ml: 1.89±0.39, p = 0.020; 50ng/ml: 2.26±0.36, p = 0.040; 150ng/ml: 2.58±0.27, p <0.001; 300ng/ml: 3.12±1.14, p = 0.030) (Figure 16.A). At 24 hours, a higher and more consistent PD-L1 expression was observed (25ng/ml: 2.97±0.69, p = 0.008; 50ng/ml: 3.15±0.35, p <0.001; 100ng/ml: 3.23±0.94, p = 0.010; 150ng/ml: 3.28±0.67, p <0.001; 300ng/ml: 3.66±0.48, p <0.001) (Figure 16.A). Based on these results, the 25ng/ml concentration was selected for subsequent experiments. Notably, the treatments with IFN-γ did not induce any significant changes in *AURKA* expression (Figure 16.B)

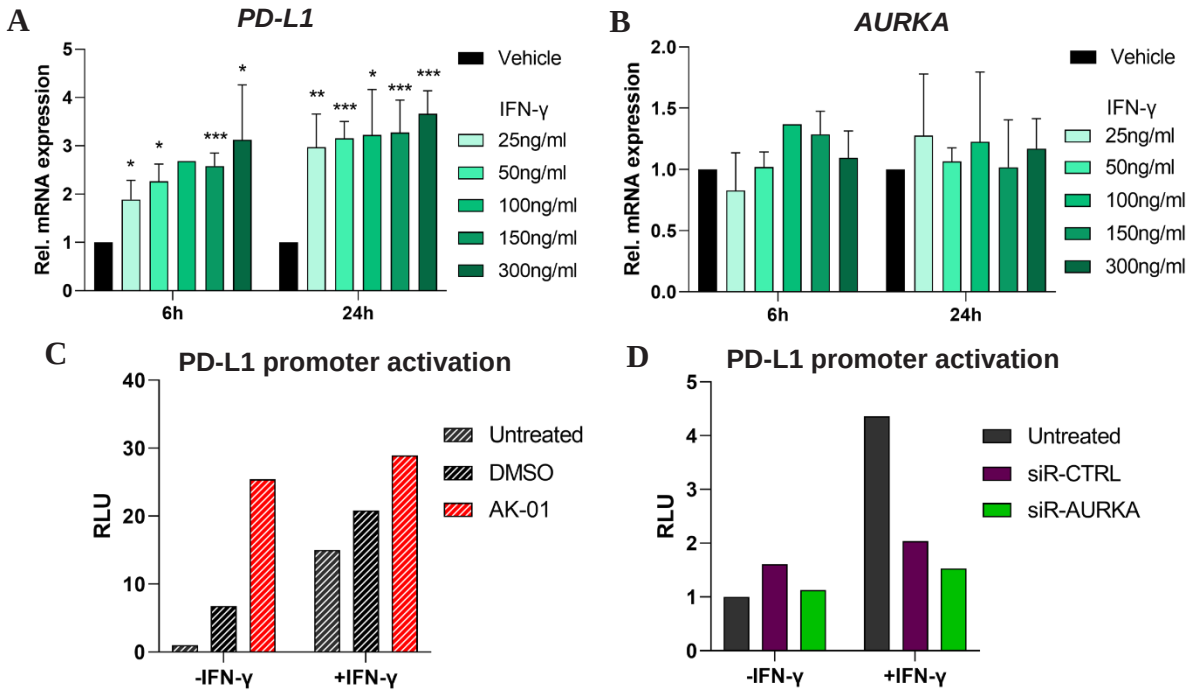

Figure 16. The effects of AURKA inhibition or knockdown on PD-L1 promoter activation. (A-B) Relative (A) *PD-L1* and (B) *AURKA* mRNA expression at 6h (n=2) and 24h (n=3) post-treatment with different concentrations of IFN-γ in JHH6 cells. Statistical analyses were calculated using the student's t-test. * p <0.05, ** p <0.01, *** p <0.001 (C-D) Luciferase reporter assay for *PD-L1* promoter at (C) 48h post-treatment with AK-01 (n=1) or (D) 24h post-treatment with siR-AURKA (n=1) in JHH6 cells.

To gain insights into the mechanism of PD-L1 regulation by AURKA, a preliminary gene reporter assay was performed, in which the luciferase gene was cloned downstream of the *PD-L1* promoter (Figure 6). Concordantly with the mRNA expression data, AK-01 increased the activation of the *PD-*

L1 promoter measured by RLU (25.41) compared to controls (DMSO: 6.79; untreated: 1.00) after 48 hours of treatment (Figure 16.C). The addition of IFN-γ further elevated PD-L1 promoter activation in all tested conditions (AK-01: 28.93; DMSO: 20.82; untreated: 15.03) (Figure 16.C). AURKA knockdown for 24 hours did not affect the *PD-L1* promoter activation (siR-AURKA: 1.13; siR-CTRL: 1.61; untreated: 1.00) (Figure 16.D). However, under IFN-γ stimulation, AURKA knockdown inhibited the *PD-L1* promoter activation (1.53) compared to controls (siR-CTRL: 2.04; untreated: 4.36) (Figure 16.D). Despite the preliminary nature of these findings, they align with the observed results for PD-L1 mRNA regulation, potentially highlighting distinct cellular mechanisms influenced by inhibitors or siRNAs targeting AURKA.

4.2.7 PD-L1 knockdown influences AURKA expression

A research group at the Italian Liver Foundation revealed a diminished *AURKA* mRNA expression in both JHH6 (0.51±0.03, $p = 0.002$) and Huh7 cells (0.24±0.08, $p < 0.001$) following PD-L1 silencing (Figure 17.D). As expected, *PD-L1* mRNA expression was strongly silenced in JHH6 (0.09±0.05, $p = 0.002$) and Huh7 cells (0.24±0.05, $p < 0.001$) (Figure 17.A).

Our preliminary findings in JHH6 cells indicated a reduction in both the mature (0.73) and non-mature forms (0.64) of PD-L1) (Figure 17.B and F), with a concurrent decrease in AURKA protein expression (0.16) (Figure 17.E-F). This observation unveils a potential feedback loop between PD-L1 and AURKA in cancer.

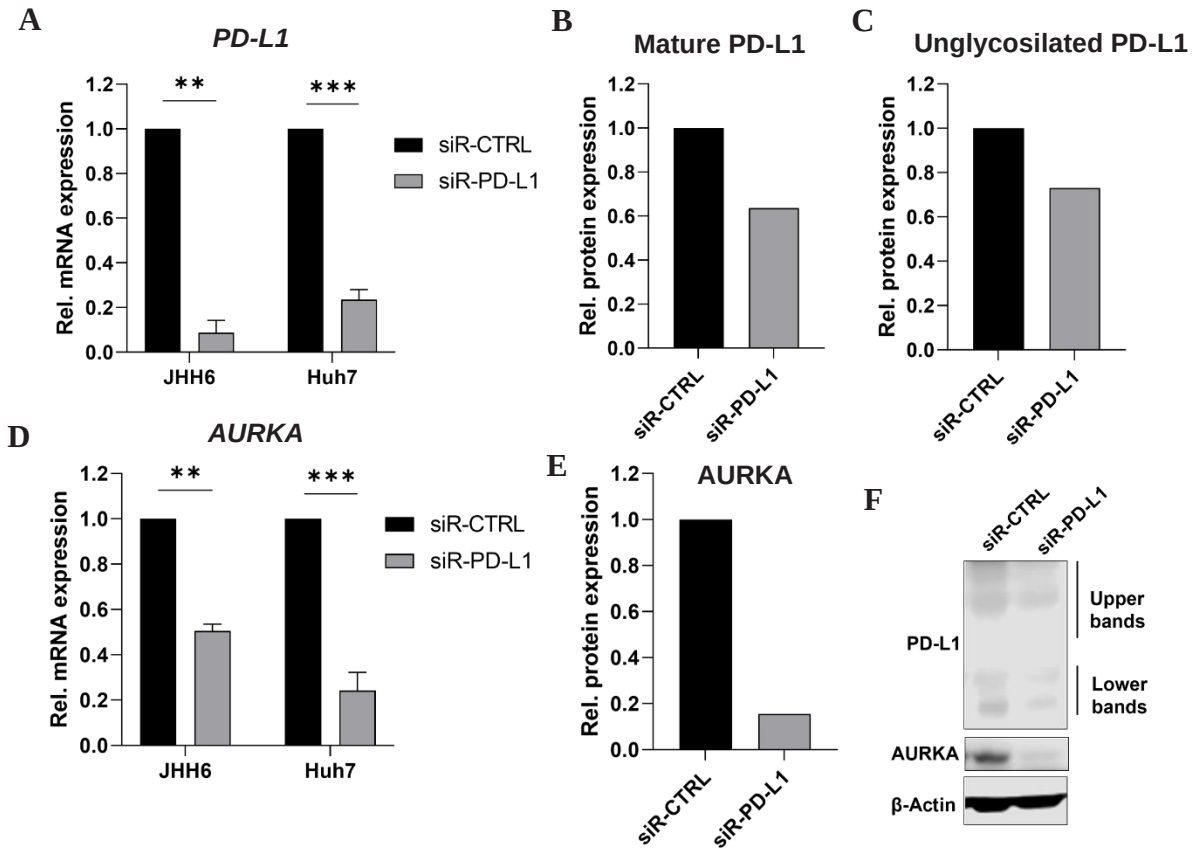

Figure 17. The effects of *PD-L1* knockdown on AURKA expression. (A) Relative *PD-L1* mRNA expression at 48h post-PD-L1 knockdown in JHH6 (n=2) and Huh7 cells (n=3). (B-C) Relative expression of (B) mature PD-L1, upper bands, and (C) unglycosylated PD-L1, lower bands, at 72h post-PD-L1 knockdown in JHH6 (n=1). (D) Relative *AURKA* mRNA expression at 48h post-PD-L1 knockdown in JHH6 (n=2) and Huh7 cells (n=3). (E) Relative expression of AURKA protein at 72h post-PD-L1 knockdown in JHH6 (n=1). (F) Representative protein blots of AURKA, PD-L1 upper and lower bands, and β-Actin at 72h post-PD-L1 knockdown in JHH6 cells. Statistical significance was calculated using the student's t-test. * $p < 0.05$; ** $p < 0.01$; *** $p < 0.001$

4.3 *AURKA* mRNA expression in hepatocarcinogenesis and its correlation with *PD-L1*

The investigation into patient samples was initially conducted to assess AURKA expression in HCC and during hepatocarcinogenesis, encompassing both human and mouse samples. The correlation between *AURKA* and *TPX2*, as well as *AURKA* and *PD-L1*, was examined. Subsequently, the analysis was expanded to include 12 other oncogenes that are potentially implicated in oncogenic pathways alongside AURKA. This comprehensive examination aimed to unravel the complex molecular interactions associated with AURKA in the context of HCC and shed light on potential connections with PD-L1.

4.3.1 The increased AURKA mRNA expression in HCC

Numerous studies [74–86] (Table 1) and data collected from the GEPIA database (Figure 7) consistently demonstrate an overexpression of *AURKA* mRNA in HCC. Our exploration of *AURKA* mRNA expression in HCC liver tissues (n=52) revealed a significant 3.54-fold increase in tumors compared to adjacent non-tumoral tissues (median: 0.097 [IQR: 0.021-0.212] *vs*. 0.028 [0.013-0.078], p <0.001) (Figure 18.A), with 75% of patients (39/52) showing an increase in *AURKA* expression in tumors (Figure 18.B). All the female patients (n=11) showed *AURKA* overexpression in tumors, with a median ratio between tumor and adjacent non-tumoral tissues of 4.78 [2.58-17.54]. *AURKA* expression did not correlate between tumors and adjacent non-tumoral tissues (r: 0.142 [CI95%: -0.313; 0.409], p = 0.320) (Figure 18.C).

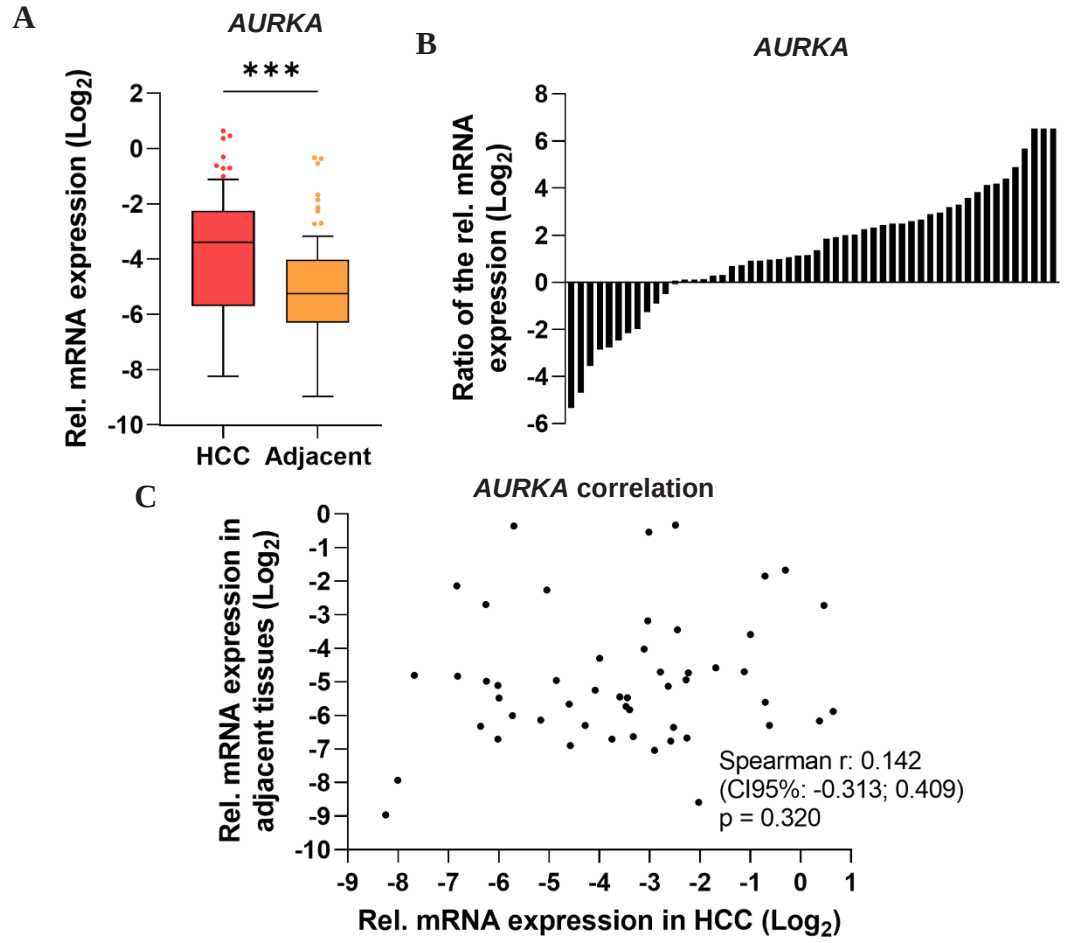

Figure 18. *AURKA* mRNA expression in HCC patients. (A) Relative *AURKA* mRNA expression in tumor and adjacent non-tumoral tissues (n=52). Statistical significance was calculated by using the Wilcoxon signed-rank tests. (B) Ratio of the relative *AURKA* mRNA expression in tumor and adjacent non-tumoral tissues (n=52). (C) Correlation between the relative *AURKA* mRNA expression in tumor and adjacent non-tumoral tissues (n=52). Correlations were calculated using Spearman's rank correlation test. * p <0.05; ** p <0.01; *** p <0.001

Further analysis revealed a positive correlation between *AURKA* expression and direct bilirubin levels in both tumor and adjacent non-tumoral tissues (r: 0.327 [0.293; 0.362], p <0.001; 0.172 [0.154; 0.191], p<0.001) (Table 14). Direct bilirubin, or conjugated bilirubin, represents bilirubin that has undergone conjugation with glucuronic acid within the liver [132].

Table 14. Regression analysis of *AURKA* mRNA relative expression to the clinic-pathological variables.

Variables	Correlation in HCC	P Value	Correlation in Adjacent tissues	P Value
Gender (M/F)	-0.072 (-0.765; 0.621)	0.835	-0.112 (-0.476; 0.252)	0.539
Age	0.003 (-0.026; 0.033)	0.827	-0.001 (-0.016; 0.015)	0.912
Hemoglobin (g/dl)	0.013 (-0.168; 0.194)	0.886	0.019 (-0.077; 0.114)	0.697
Platelet count ($X10^3/mm^3$)	-0.001 (-0.004; 0.002)	0.400	-0.001 (-0.002; 0.001)	0.303
AST (U/l)	0.007 (-0.002; 0.016)	0.144	0.002 (-0.003; 0.007)	0.437
ALT (U/l)	0.002 (-0.006; 0.011)	0.573	0.000 (-0.005; 0.004)	0.951
Pseudocholinesterase (U/l)	0.000 (0.000; 0.000)	0.897	0.000 (0.000; 0.000)	0.827
Total Bilirubin (mg/dl)	0.206 (-0.487; 0.898)	0.553	0.039 (-0.327; 0.405)	0.833
Direct Bilirubin (mg/dl)	0.327 (0.293; 0.362)	<0.001***	0.172 (0.154; 0.191)	<0.001***
Albumin (g/dl)	-0.572 (-1.192; 0.047)	0.069	-0.160 (-0.495; 0.174)	0.340
Creatinine (mg/dl)	-0.553 (-1.900; 0.796)	0.414	-0.265 (-0.976; 0.447)	0.458
INR	-0.099 (-1.329; 1.131)	0.872	0.024 (-0.624; 0.673)	0.940
AFP (ng/ml)	0.000 (0.000; 0.000)	0.805	0.000 (0.000;0.000)	0.894
Etiology (Viral/MASLD or/and ALD)	0.378 (-0.324; 1.081)	0.283	0.222 (-0.153; 0.596)	0.239
Fibrosis Score (F0-F4/F5-F6)	0.349 (-0.274; 0.972)	0.266	0.122 (-0.209; 0.452)	0.463
BCLC classes (0-A/B-C)	-0.071 (-0.666; 0.523)	0.811	-0.113 (-0.425; 0.199)	0.469
Cirrhosis (Y/N)	0.100 (-0.553; 0.754)	0.759	0.084 (-0.260; 0.428)	0.626
Grading (Well-Medium/Poor-Not diff.)	0.156 (-0.487; 0.800)	0.627	0.103 (-0.240; 0.446)	0.549

The correlations were represented using the correlation coefficient (CI95%). α-fetoprotein; ALD, Alcohol-associated liver disease; F, Female; HCC, Hepatocellular Carcinoma; INR, International normalized ratio; M, Male; MASLD, Metabolic dysfunction-associated steatotic liver disease; N, No; Y, Yes. * p <0.05; ** p <0.01; *** p <0.001

The association between *AURKA* expression and both OS and DFS in both tumors and adjacent non-tumoral tissues was investigated (Figure 19.A-D). Patients were divided into high- *vs.* low-*AURKA* expression groups based on the median expression values in tumors (0.097) and adjacent non-tumoral tissues (0.028). No significant differences in either OS or DFS were observed between the two groups when considering AURKA tumoral expression (OS: Hazard ratio (HR): 0.752 [CI95%: 0.313-1.810], p = 0.529; DFS: HR: 0.571 [CI95%: 0.246-1.326], p = 0.192) (Figure 19.A-B) or AURKA expression in adjacent non-tumoral tissues (OS: HR: 1.675 [CI95%: 0.691-4.060], p = 0.253; DFS: HR: 0.725 [CI95%: 0.312-1.685], p = 0.454) (Figure 19.C-D). These results suggest that AURKA expression alone is not a reliable prognostic indicator for OS or DFS in the considered population, at the specified cutoff values.

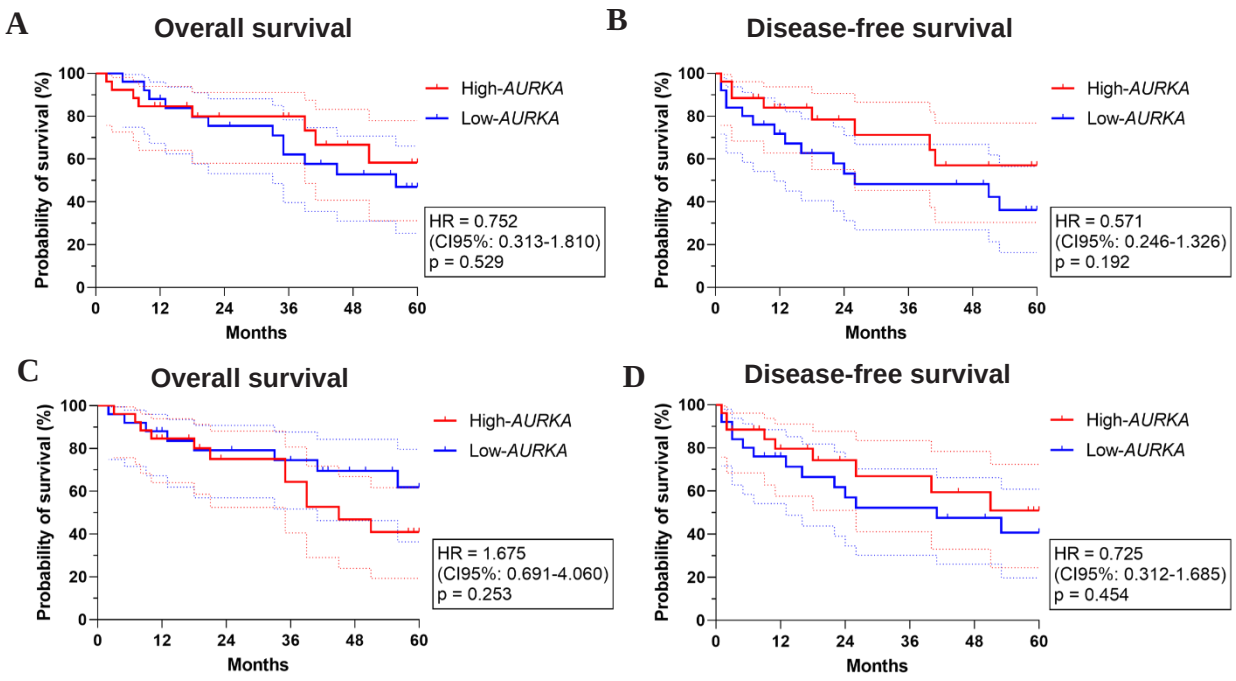

Figure 19. The Kaplan-Meier survival estimates based on *AURKA* mRNA expression. (A) OS and (B) DFS analyses in high-*AURKA* (n=26) *vs.* low-*AURKA* (n=26) patients in tumor tissues. (C) OS and (D) DFS analyses in high-*AURKA* (n=26) *vs.* low-*AURKA* (n=26) patients in adjacent non-tumoral tissues. Median expression of *AURKA* mRNA in tumor and adjacent tissues was used as the cut-off values to divide the population into the two groups. Statistical significance was calculated using the log-rank Mantel-Cox test.

4.3.2 The increase in gene expression during hepatocarcinogenesis in human samples

To comprehensively understand the dynamic changes in *AURKA*, *TPX2*, and *PD-L1* expression throughout hepatocarcinogenesis, different sample groups, including individuals with healthy livers (n=13), subjects with MASLD (n=17), and HCC patients (tumors and adjacent non-tumor tissues, n=52) were analyzed. These groups of samples provided a simplified representation of some pathological stages during hepatocarcinogenesis.

AURKA, *TPX2*, and *PD-L1* exhibited significant differential expression across all the groups (all p <0.001) (Figure 20.A). *AURKA* expression gradually increased from healthy to MASLD tissues (0.003 [0.002-0.005] *vs.* 0.013 [0.007-0.029], p = 0.001), from MASLD to adjacent non-tumoral tissues (0.013 [0.007-0.029] *vs.* 0.028 [0.013-0.078], p = 0.050), and from adjacent non-tumoral tissues to tumors (0.028 [0.013-0.078] *vs.* 0.097 [0.021-0.212], p <0.001) (Figure 20.A).

TPX2 exhibited a significant increase only from healthy to MASLD samples (0.016 [0.008-0.048] *vs.* 0.061 [0.038-0.159], p = 0.008) and from adjacent non-tumoral tissues to tumors (0.095 [0.050-0.228] *vs.* 0.340 [0.148-1.059], p <0.001) (Figure 20.A). *PD-L1* was markedly upregulated from healthy to MASLD samples (0.030 [0.021-0.092] *vs.* 0.128 [0.050-0.194], p = 0.030) and from MASLD to adjacent non-tumoral tissues (0.128 [0.050-0.194] *vs.* 0.248 [0.107-0.821], p = 0.010), while no differences were reported between adjacent non-tumoral tissues and tumors (0.248 [0.107-0.821] *vs.* 0.234 [0.112-0.926], p = 0.500) (Figure 20.A). Both *TPX2* and *PD-L1* expression did not show a significant correlation between tumor and adjacent non-tumoral tissues (r: 0.085 [CI95%: -0.203; 0.360], p = 0.550; r: 0.151 [-0.138; 0.417], p = 0.290) (Figure 20.B-C).

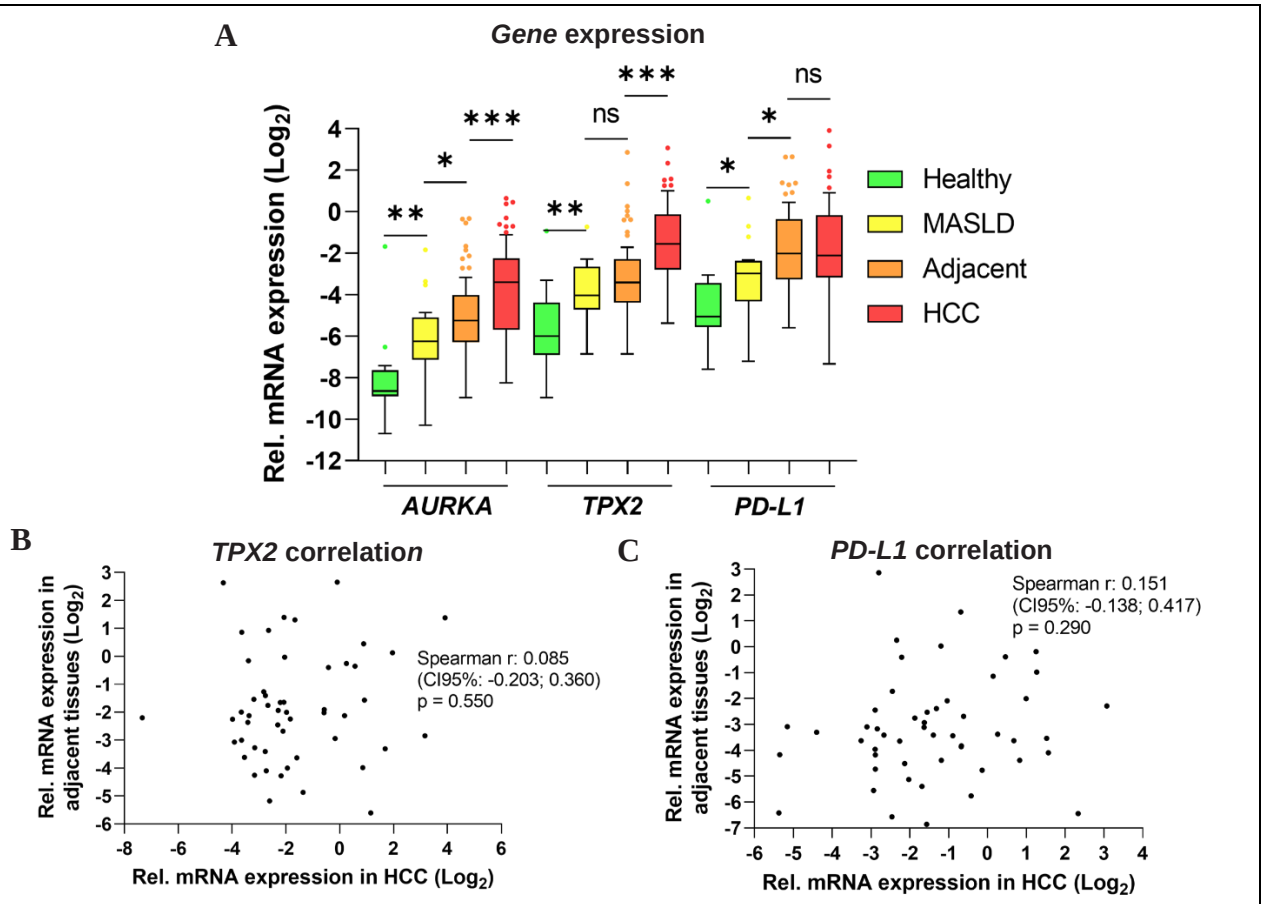

Figure 20. The gene expression in human HCC patients, MASLD individuals, and subjects with healthy livers. (A) Relative *AURKA*, *TPX2*, and *PD-L1* mRNA expression in healthy (n=13), MASLD (n=17), adjacent non-tumor (n=52), and HCC (n=52) liver tissues. Statistical significance was calculated using Kruskal-Wallis tests for multiple group comparison, Wilcoxon signed-rank tests for the paired tissues, and Mann-Whitney U for non-paired tissues. (B-C) Correlations of the relative (B) *TPX2* or (C) *PD-L1* mRNA expression between tumors and adjacent non-tumoral tissues (n=52). Correlation analyses were calculated using Spearman's rank correlation test. * p <0.05; ** p <0.01; *** p <0.001

4.3.3 The diagnostic potential of AURKA

The gradual increase in *AURKA* expression during hepatocarcinogenesis suggests its potential role in discriminating liver diseases. At the considered cutoff (0.040), *AURKA* can distinguish between tumors and adjacent non-tumoral tissues (Area under the curve (AUC): 0.670 [CI95%: 0.564-0.776], p = 0.003) (Figure 21.A), with both sensitivity and specificity corresponding to 0.69. Better performance was obtained when considering the capacity of AURKA in discriminating patients with HCC from those with MASLD or a healthy liver, possibly demonstrating the diagnostic potential of *AURKA* for HCC. *AURKA* showed a good ability in distinguish both HCC tumors (AUC: 0.847 [CI95%: 0.756-0.937], cutoff: 0.019; sensitivity: 0.77, specificity: 0.77, p < 0.001) (Figure 21.B) and HCC-adjacent non-tumoral tissues (AUC: 0.766 [CI95%: 0.652-0.880], cutoff: 0.014; sensitivity: 0.70, specificity: 0.73, p < 0.001) from MASLD and healthy samples (Figure 21.C). Thus, *AURKA* could be useful to diagnose HCC in patients with chronic liver disease.

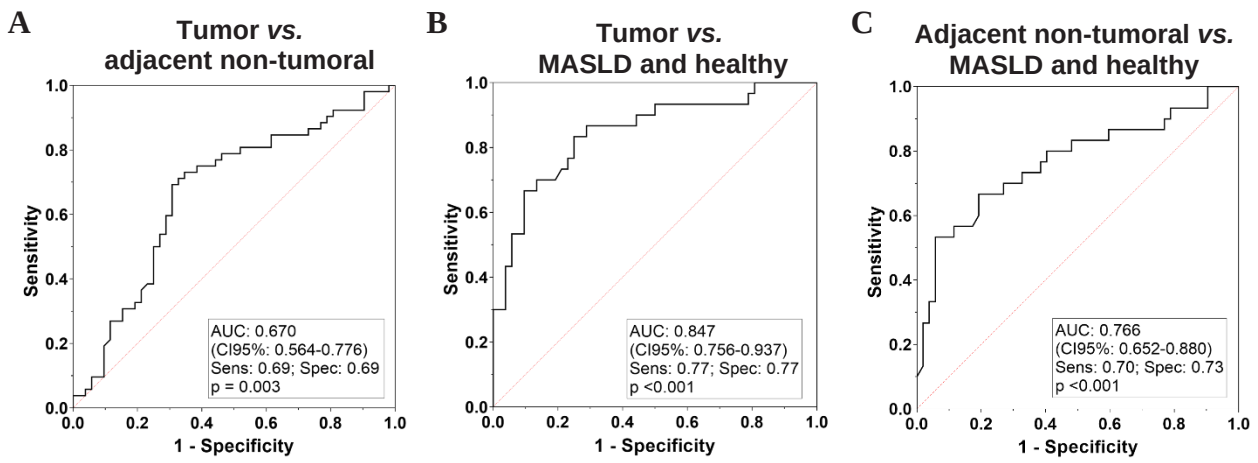

Figure 21. The diagnostic potential of AURKA for HCC. (A-D) Receiver Operating Characteristic (ROC) curve of AURKA ability in discriminating between (A) tumors *vs.* adjacent non-tumor tissues, (B) tumors *vs.* MASLD and healthy samples, (C) HCC-adjacent non-tumoral tissues *vs.* MASLD and healthy samples. Sens, Sensitivity; Spec, Specificity.

4.3.4 The changes in gene expression during hepatocarcinogenesis in mice samples

To further explore the expression of *Aurka*, *Tpx2*, and *Cd274 (Pd-L1)* during hepatocarcinogenesis an HBV-TG mice model developing HCC was used. The genes were studied at 5 different time points (3, 6, 9, 12, and 15 months of age) and exhibited a significant differential expression across all tested conditions (n = 11, all p <0.001) (Figure 22.A-C).

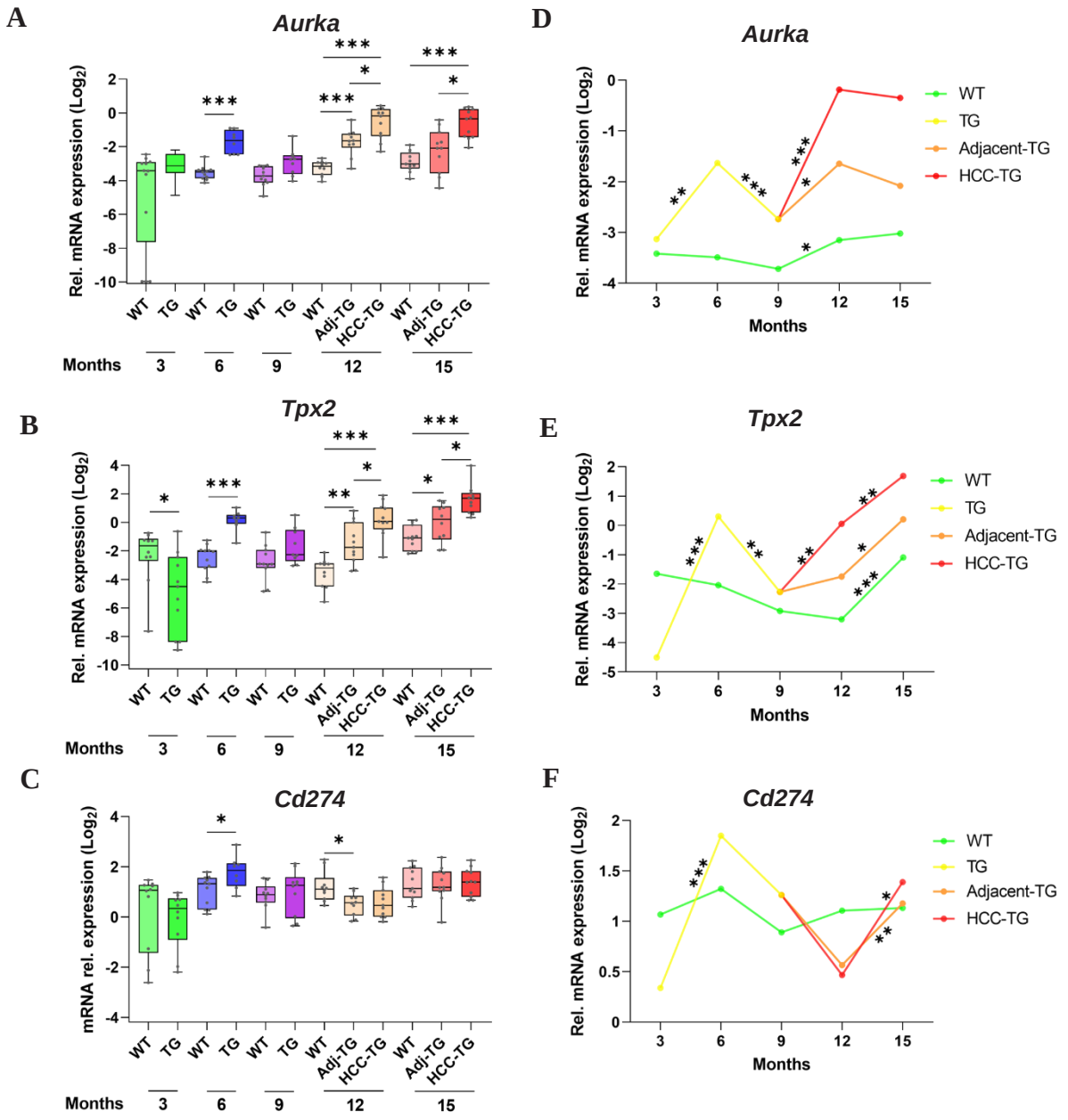

Figure 22. The gene expression analysis in TG and WT mice. (A) Relative *Aurka*, (B) *Tpx2*, and (C) *Cd274* mRNA expression in TG and WT mice at 3m, 6m, 9m, 12m, and 15m of age (per condition, n=11). (D) The *Aurka*, (E) *Tpx2*, and (F) *Cd274* expression trends in TG and WT mice assessed using the median gene expression for each condition. Macroscopic HCC lesions were visible at 12 months of age. Statistical significance was calculated using Kruskal-Wallis tests for multiple groups, Wilcoxon signed-rank tests for the paired tissues, and Mann-Whitney U for non-paired tissues. * p <0.05; ** p <0.01; *** p <0.001

Aurka is overexpressed in TG mice compared to WT with significant differences at 6 months and 12 months (both p <0.001) (Figure 22.A and Table 15). *Aurka* exhibited an increase in the neoplastic

nodule compared to the adjacent-non neoplastic tissues both at 12 months (p = 0.037) and 15 months (p = 0.014) (Figure 22.A and Table 15).

Table 15. *Aurka* expression in TG and WT mice.

Age	WT mice	TG mice	
3 months	0.093 [0.005-0.133]	0.114 [0.085-0.186]	
6 months	0.089 [0.069-0.097]	0.323 [0.183-0.501]	
9 months	0.076 [0.058-0.113]	0.150 [0.082-0.176]	
		Adjacent non-tumoral	**Neoplastic nodules**
12 months	0.113 [0.079-0.132]	0.320 [0.243-0.426]	0.880 [0.389-1.170]
15 months	0.123 [0.102-0.196]	0.236 [0.084-0.456]	0.786 [0.372-1.175]

Gene expression was represented as median [IQR-IIIQR].

Aurka expression showed dynamic changes in TG mice with an increase from 3 to 6 months (p = 0.001), a decrease from 6 to 9 months (p = 0.004), followed by an increase from 9 to 12 months in both adjacent non-neoplastic tissues (p = 0.013) and neoplastic nodules (p <0.001) (Figure 22.D and Table 15). *Aurka* was stable over time in WT mice, with only a slight increase from 9 to 12 months (p = 0.043) (Figure 22.D and Table 15).

In TG mice, the expression pattern of *Tpx2* closely mirrored the trend observed for *Aurka*. However, it also exhibited an increase during the tumor progression both in adjacent non-neoplastic tissues (p = 0.024) and neoplastic nodules (p = 0.005) (Figure 22.B and E and Table 16).

Table 16. *Tpx2* expression in TG and WT mice.

Age	WT mice	TG mice	
3 months	0.320 [0.153-0.450]	0.044 [0.003-0.185]	
6 months	0.243 [0.110-0.258]	1.235 [0.938-1.443]	
9 months	0.132 [0.109-0.261]	0.207 [0.152-0.697]	
		Adjacent non-tumoral	**Neoplastic nodules**
12 months	0.109 [0.045-0.137]	0.298 [0.160-1.011]	1.039 [0.711-2.052]
15 months	0.469 [0.243-0.890]	1.156 [0.434-2.185]	3.221 [1.617-4.149]

Gene expression was represented as median [IQR-IIIQR].

Although there was minimal fluctuation over time, the expression of *Cd274* in WT mice remained constant (Figure 22.C and F and Table 17). In TG mice, *Cd274* reached its maximum increase at 6

months of age (p <0.001). After this age, the expression consistently decreased until the appearance of the tumor at 12 months. Interestingly, an opposite trend was observed for both neoplastic nodules (p = 0.010) and non-neoplastic tissue (p = 0.006) (Figure 22.C and F and Table 17). Importantly, it cannot be excluded that the similar increase of *Cd274* in both tissues was a consequence of the aging process in mice.

Table 17. *Cd274* expression in TG and WT mice.

Age	WT mice	TG mice	
3 months	2.096 [0.370-2.429]	1.265 [0.531-1.671]	
6 months	2.500 [1.226-2.953]	3.602 [2.354-4.399]	
9 months	1.854 [1.484-2.317]	2.396 [0.967-2.996]	
		Adjacent non-tumoral	**Neoplastic nodules**
12 months	2.152 [1.621-2.928]	1.480 [1.040-1.796]	1.383 [1.009-2.090]
15 months	2.193 [1.701-3.896]	2.263 [2.035-3.503]	2.620 [1.744-3.528]

Gene expression was represented as median [IQR-IIIQR].

These results support the observations made in human samples, providing a novel perspective on the roles of *Aurka* and *Cd274* within the context of liver disease and HCC.

4.3.5 The positive correlations between AURKA, TPX2, and PD-L1

The analysis of *AURKA*, *TPX2*, and *PD-L1* expressions in HCC patients revealed significant correlations among these genes. The high-*AURKA* group exhibits elevated *TPX2* and *PD-L1* expressions compared to the low-*AURKA* group in both tumor samples (*TPX2:* 0.910 [0.360-2.191] *vs.* 0.163 [0.127-0.329], p <0.001; *PD-L1:* 0.888 [0.230-1.867] *vs.* 0.147 [0.090-0.233], p <0.001) (Figure 23.A) and adjacent non-tumoral tissues (0.758 [0.248-1.860] *vs.* 0.135 [0.062-0.234], p <0.001; 0.184 [0.095-0.761] *vs.* 0.057 [0.023-0.097], p <0.001) (Figure 23.B).

Positive correlations between *AURKA* and *TPX2* (Figure 23.C) and between *AURKA* and *PD-L1* (Figure 23.D) were observed not only in the tumor (r: 0.818 (CI95%: 0.696; 0.894), p <0.001; r: 0.709 (CI95%: 0.533; 0.826), p <0.001) and adjacent non-tumoral tissues (r: 0.813 (CI95%: 0.688; 0.891), p <0.001; r: 0.748 (CI95%: 0.589; 0.851), p <0.001) but also in MASLD subjects (r: 0.746 (CI95%: 0.365; 0.913), p = 0.002; r: 0.811 (CI95%: 0.531-0.932), p <0.001) (Figure 23.C-D). *AURKA* and *TPX2* positively correlated in healthy livers (r: 0.825 (CI95%: 0.489; 0.948), p <0.001), but not *AURKA* and *PD-L1* (Figure 23.C-D).

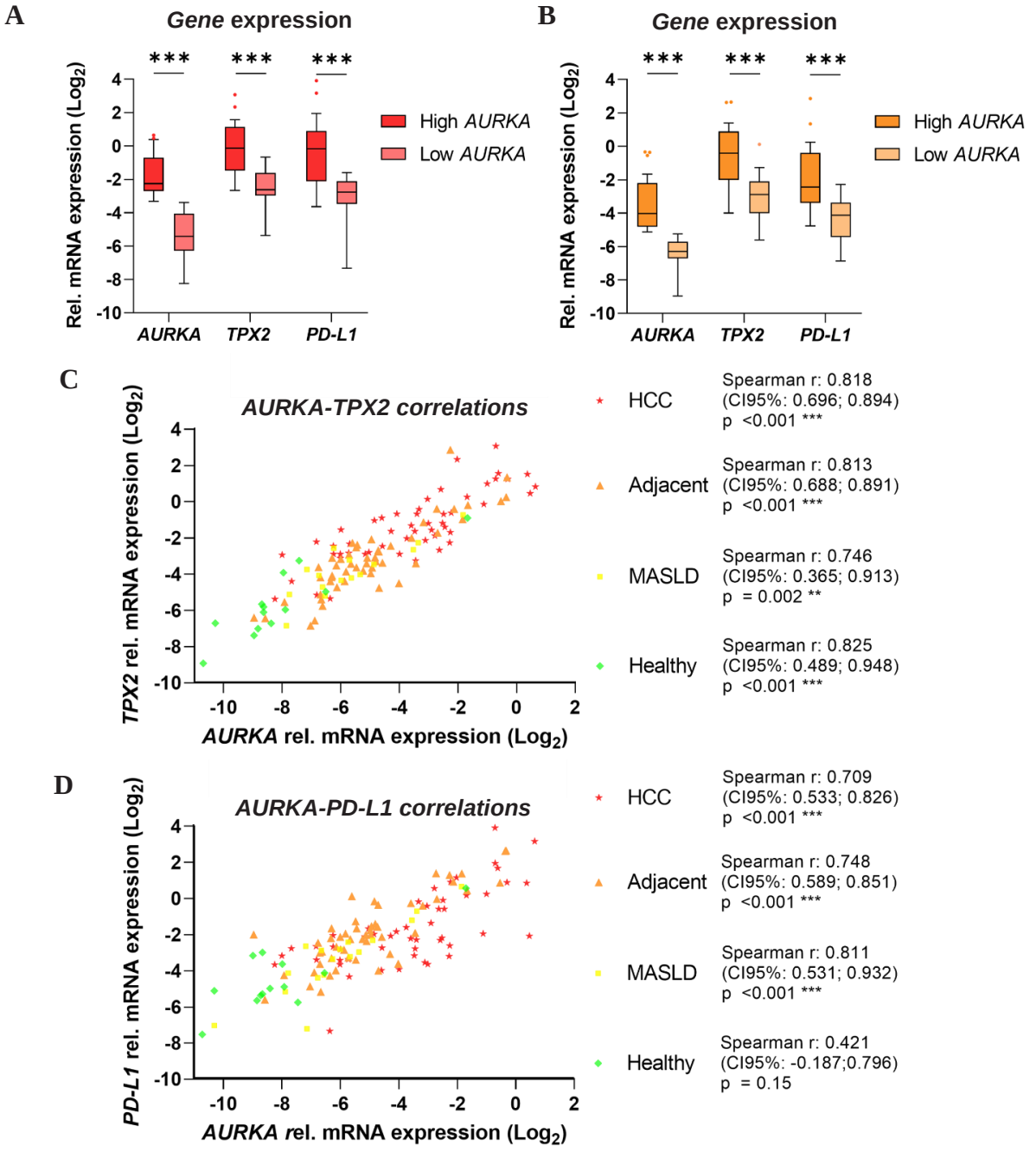

Figure 23. The correlations between *AURKA*, *TPX2*, and *PD-L1* mRNA expression. (A-B) Relative *AURKA*, *TPX2*, and *PD-L1* mRNA expression in high-*AURKA* (n=26) *vs.* low-*AURKA* (n=26) in (A) HCC tumors and (B) adjacent non-tumoral tissues. Median expression of *AURKA* mRNA in tumor and adjacent tissues was used as the cut-off values to divide the population into the two groups. Statistical significance was calculated using the Mann-Whitney U tests. (C-D) Correlation between the relative mRNA expression of *AURKA* and (C) *TPX2* or (D) *PD-L1* in HCC (n=52), adjacent non-tumor (n=52), MASLD (n=17), and healthy (n=13) liver tissues. Correlations were calculated using Spearman's rank correlation test. * p <0.05; ** p <0.01; *** p <0.001

AURKA expression in adjacent non-tumoral tissues showed a positive association with total bilirubin and the International Normalized Ratio (INR) (Table 18 and Table 19). The high-*AURKA*

group showed higher levels of total bilirubin and INR compared to the low-*AURKA* group (0.90 [0.74-1.29] *vs.* 0.70 [0.52-0.96], p = 0.010; 1.12 [1.06-1.15] *vs.* 1.07 [0.98-1.12] (Table 19). Bilirubin is a pigment generated through the breakdown of various heme-containing proteins, particularly from hemoglobin catabolism. Elevated levels of total bilirubin are commonly linked to liver lesions [133]. INR serves as a blood clotting test, assessing an individual's response to anticoagulation therapy with a vitamin-K antagonist. A standard INR value is 1.0, and any increase signifies a diminished clotting ability, often associated with liver disease and cirrhosis [134].

Table 18. The association between demographic, clinical, and pathological variables and high-*AURKA* *vs.* low-*AURKA* groups in HCC tumors.

Variables	Total patients (HCC = 52)	High-*AURKA* group (HCC = 26)	Low-*AURKA* group (HCC = 26)	P-value
***AURKA* mRNA**	0.097 [0.021-0.212]	0.221 [0.157-0.624]	0.024 [0.013-0.060]	<0.001***
Gender (M/F)	41/11	18/8	23/3	0.173
Age	69.90 [62.33-73.65]	69.90 [62.25-73.28]	69.25 [62.68-75.43]	0.750
Hemoglobin (g/dl)	14.15 [13.60-15.43]	13.95 [12.78-15.05]	14.30 [13.95-15.80]	0.090
Platelet Count ($X10^3/mm^3$)	171 [111-223]	171 [106-232]	172 [112-222]	0.820
AST (U/l)	30.00 [24.00-51.00]	35.00 [25.75-61.00]	27.50 [22.00-48.75]	0.350
ALT (U/l)	29.50 [19.00-52.75]	28.00 [19.00-54.25]	29.50 [18.50-53.50]	0.790
Pseudocholinesterase (U/l)	6651 [5447-7384]	6790 [5086-7286]	6597 [5499-7484]	0.930
Total Bilirubin (mg/dl)	0.82 [0.57-1.01]	0.86 [0.66-1.19]	0.74 [0.57-0.98]	0.270
Direct Bilirubin (mg/dl)	0.19 [0.13-0.25]	0.19 [0.14-0.30]	0.19 [0.13-0.22]	0.500
Albumin (g/dl)	4.10 [3.88-4.40]	4.12 [3.81-4.43]	4.10 [3.99-4.38]	0.870
Creatinine (mg/dl)	0.82 [0.73-0.96]	0.81 [0.73-0.96]	0.87 [0.73-0.95]	0.920
INR	1.08 [1.03-1.14]	1.08 [1.05-1.14]	1.09 [1.03-1.14]	0.920
AFP (ng/ml)	9.65 [3.63-111.03]	10.10[4.25-133.00]	5.20 [3.60-11.03]	0.420
Etiology (Viral/SLD)	22/19	13/10	9/9	0.758
Fibrosis Score (F0-F4/F5-F6)	16/34	6/19	10/15	0.364
BCLC Classes (0-A/B-C)	34/18	15/11	19/7	0.382
Cirrhosis (Y/N)	39/13	19/7	20/6	1.000
Grading (Well/ Medium-Poor-Not diff.)	15/34	7/16	8/18	1.000
Vascular invasion (Y/N)	12/35	6/17	6/18	1.000

Categorical variables were represented by the number of patients and the differences were calculated using Fisher's exact test. Continuous variables were represented as median [IQR-IIIQR] and the differences were calculated using the Mann-Whitney U test. AFP, α-fetoprotein; F, Female; HCC, Hepatocellular carcinoma; INR, International normalized ratio; M, Male; N, No; SLD, Steatotic liver disease; Y, Yes. * p <0.05; ** p <0.01; *** p <0.001

Table 19. The association between clinic-pathological variables and high-*AURKA vs.* low-*AURKA* groups in adjacent non-tumoral tissues.

Variables	Total patients (HCC = 52)	High-*AURKA* group (HCC = 26)	Low-*AURKA* group (HCC = 26)	P-value
***AURKA* mRNA**	0.028 [0.013-0.078]	0.073 [0.036-0.240]	0.013 [0.010-0.019]	<0.001***
Gender (M/F)	41/11	22/4	19/7	0.499
Age	69.90 [62.33-73.65]	69.20 [62.38-73.03]	70.15 [61.65-75.25]	0.800
Hemoglobin (g/dl)	14.15 [13.60-15.43]	14.40 [13.55-15.73]	14.00 [13.53-15.05]	0.380
Platelet Count ($X10^3/mm^3$)	171 [111-223]	165 [112-225]	178 [110-225]	0.910
AST (U/l)	30.00 [24.00-51.00]	39.50 [24.75-61.00]	26.50 [22.00-48.75]	0.170
ALT (U/l)	29.50 [19.00-52.75]	38.50 [19.00-52.25]	25.50 [18.50-58.00]	0.650
Pseudocholinesterase (U/l)	6651 [5447-7384]	6704 [5344-7260]	6597 [5395-7837]	0.570
Total Bilirubin (mg/dl)	0.82 [0.57-1.01]	0.90 [0.74-1.29]	0.70 [0.52-0.96]	0.010*
Direct Bilirubin (mg/dl)	0.19 [0.13-0.25]	0.20 [0.16-0.40]	0.16 [0.13-0.22]	0.060
Albumin (g/dl)	4.10 [3.88-4.40]	4.09 [3.79-4.29]	4.13 [3.98-4.46]	0.250
Creatinine (mg/dl)	0.82 [0.73-0.96]	0.89 [0.74-0.96]	0.80 [0.72-0.98]	0.330
INR	1.08 [1.03-1.14]	1.12 [1.06-1.15]	1.07 [0.98-1.12]	0.030*
AFP (ng/ml)	9.65 [3.63-111.03]	10.85 [5.45-133.50]	5.05 [3.23-16.30]	0.060
Etiology (Viral/SLD)	22/19	11/11	11/8	0.756
Fibrosis Score (F0-F4/F5-F6)	16/34	7/19	9/15	0.547
BCLC Classes (0-A/B-C)	34/18	18/8	16/10	0.771
Cirrhosis (Y/N)	39/13	21/5	18/8	0.523
Grading (Well/ Medium-Poor-Not diff.)	15/34	7/16	8/18	1.000
Vascular invasion (Y/N)	12/35	6/16	6/19	1.000

Categorical variables were represented by the number of patients and the differences were calculated using Fisher's exact test. Continuous variables were represented as median [IQR-IIIQR] and the differences were calculated using the Mann-Whitney U test. AFP, α-fetoprotein; F, Female; HCC, Hepatocellular carcinoma; INR, International normalized ratio; M, Male; N, No; SLD, Steatotic liver disease; Y, Yes. * p <0.05; ** p <0.01; *** p <0.001

Despite the strong correlation between *AURKA, TPX2,* and *PD-L1* in HCC, the combination of *AURKA, TPX2,* and *PD-L1* expression lacks prognostic significance for OS and DFS. As an example, Cox proportional-hazards regression analysis combining *AURKA* expression (Exp(b): 0.845 (CI95%: 0.173; 4.141), p = 0.836) and *PD-L1* expression (Exp(b): 0.843 (CI95%: 0.534; 1.333), p = 0.466) did not provide significant results for OS (p = 0.241) (Table 20, Table 21, and Table 22).

Table 20. The overall model fit of the Cox proportional-hazards regression analysis assessing overall survival using the combined *AURKA* and *PD-L1* mRNA expression in HCC.

Null model -2 Log Likelihood	151.672
Full model -2 Log Likelihood	148.823
Chi-squared 2	2.849
P-value	0.241

Table 21. Coefficients and standard errors of the Cox proportional-hazards regression analysis assessing overall survival using the combined *AURKA* and *PD-L1* mRNA expression in HCC.

Values	***AURKA***	***PD-L1***
b±SE	-0.168±0.811	-0.171±0.234
Wald	0.043	0.533
P-value	0.836	0.466
Exp(b)	0.845 (CI95%: 0.173; 4.141)	0.843 (CI95%: 0.534; 1.333)

Table 22. Baseline cumulative hazard function of the Cox proportional-hazards regression analysis assessing overall survival using the combined *AURKA* and *PD-L1* mRNA expression in HCC.

Time (Months)	**Baseline Cumulative Hazard**	**At the mean of Covariates Cumulative Hazard**	**At the mean of Covariates Survival**
1	0.070	0.035	0.965
2	0.120	0.061	0.941
3	0.173	0.087	0.917
5	0.201	0.101	0.904
7	0.230	0.116	0.891
9	0.260	0.131	0.877
11	0.293	0.147	0.863
13	0.331	0.167	0.847
16	0.370	0.186	0.830
18	0.413	0.208	0.812
22	0.463	0.234	0.792
24	0.519	0.261	0.770
26	0.632	0.318	0.727
40	0.697	0.351	0.704
41	0.765	0.385	0.680
51	0.855	0.431	0.650
53	0.953	0.480	0.619

While the gene association may not be significant as a prognostic tool, *AURKA* demonstrates a robust correlation with *TPX2* and *PD-L1* in hepatocarcinogenesis. This connection holds potential clinical relevance, as indicated by associations with liver function parameters.

4.3.6 The positive correlations between AURKA expression and other oncogenes

A comprehensive analysis was conducted to investigate the correlation between *AURKA* and a selected set of oncogenes known to be associated with pathways in which AURKA is involved [95,135–144]. The expression levels of *AKT Serine/Threonine Kinase 1 (AKT1), ATPase Na+/K+ Transporting Subunit α1 (ATP1A1), B-Raf Proto-Oncogene, Serine/Threonine Kinase (BRAF), C-MYC, Epidermal Growth Factor Receptor (EGFR), Glycogen Synthase Kinase 3β (GSK3B), HRas Proto-Oncogene, GTPase (HRAS), KRAS Proto-Oncogene, GTPase (KRAS), RELA Proto-Oncogene, NF-kB Subunit (NFKB3), NFKBIA, PD-L1, PTEN, TPX2, Yes1 Associated Transcriptional Regulator (YAP1)* were examined using the GEPIA database (Figure 24.A). *ATP1A1* (136.19 TPM), *NFKBIA* (77.79), and *AKT1* (38.40) exhibited the highest expression, while *PD-L1* (0.52), *BRAF* (3.59), and *KRAS* (3.92) showed the lowest expression levels (Figure 24.A).

The correlation between *AURKA* and these genes was investigated in 39 HCC-paired tissues divided into high- *vs.* low-*AURKA* groups according to the median *AURKA* expression in tumor tissues (0.059) and adjacent non-tumoral tissues (0.026). For each gene, the mean rank difference was calculated, and the adjusted p-value was determined. The graphical representation (Figure 24.B-C) illustrates the mean rank differences (X-axis) and $\log_{10}$ (adjusted P-values) (Y-axis) for the correlations of each gene with *AURKA* expression in HCC patients.

The upper-right quadrant (Figure 24.B-C) indicates genes with a significantly positive difference in mean ranks between high-*AURKA* and low-*AURKA* groups, and the lower-right quadrant (Figure 24.B-C) represents genes with a non-significant positive difference. Conversely, the lower-left quadrant (Figure 24.B-C) contains genes with a non-significant negative difference, and the upper-left quadrant (Figure 24.B-C) shows genes with a significantly negative difference. *PD-L1*, *TPX2*, and *KRAS* exhibited the highest and most significant differences in both tumor tissues (PD-L1: mean rank difference: 16.93, $p < 0.001$; TPX2: 14.88, $p < 0.001$; KRAS: 12.96, $p < 0.001$) and adjacent non-tumoral tissues (PD-L1: 14.37, $p < 0.001$; TPX2: 14.88, $p < 0.001$; KRAS: 13.13, $p < 0.001$) (Figure 24.B-D).

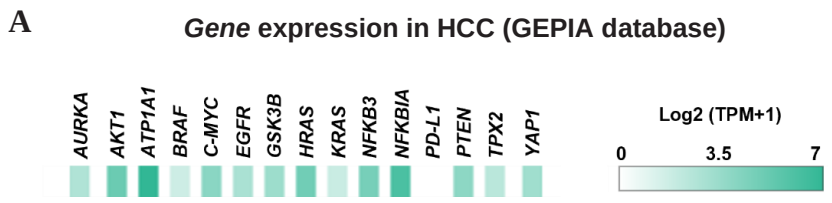

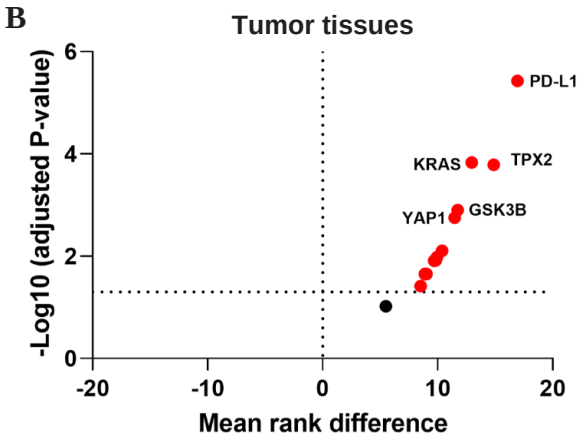

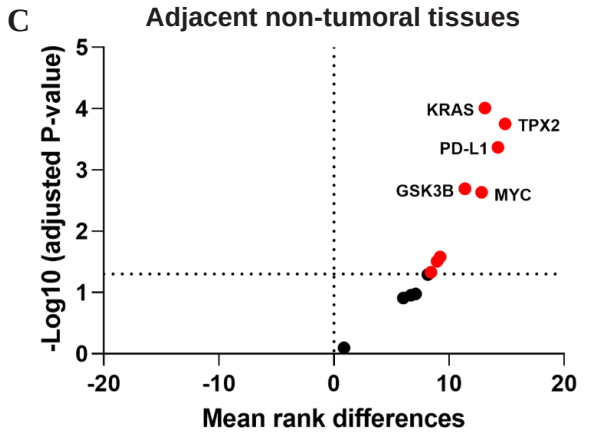

D

Adjusted p-values

Genes	P-value (HCC)	P-value (Adjacent tissues)
AKT1	0.022 *	0.051
ATP1A1	0.008 **	0.031 *
BRAF	0.012 *	0.123
C-MYC	0.038 *	0.002 **
EGFR	0.010 *	0.802
GSK3B	0.001 **	0.002 **
HRAS	0.022 *	0.111
KRAS	<0.001 ***	<0.001 ***
NFKB3	0.012 *	0.026 *
NFKBIA	0.022 *	0.047 *
PD-L1	<0.001 ***	<0.001 ***
PTEN	0.095	0.106
TPX2	<0.001 ***	<0.001 ***
YAP1	0.002 **	0.002 **

Figure 24. The correlations between *AURKA* expression and 14 oncogenes in HCC. (A) The mRNA expression of *AURKA, AKT1, ATP1A1, BRAF, C-MYC, EGFR, GSK3B, HRAS, KRAS, NFKB3, NFKBIA, PD-L1, PTEN, TPX2,* and *YAP1* from GEPIA database (http://gepia.cancer-pku.cn/). (B-C) The correlations between the expression of *AURKA* and the 14 oncogenes in (B) tumor (n=39) and (C) adjacent non-tumoral (n=39) tissues. The statistical significance was calculated using the Mann-Whitney U tests. (D) The adjusted p-values of the associations between the relative mRNA expression of *AURKA* and the oncogenes in tumors and adjacent non-tumoral tissues. * p <0.05; ** p <0.01; *** p <0.001. *AKT1, AKT Serine/Threonine Kinase 1; ATP1A1, ATPase Na+/K+ Transporting Subunit α1; BRAF, B-Raf Proto-Oncogene, Serine/Threonine Kinase; C-MYC, MYC Proto-Oncogene, BHLH Transcription Factor; EGFR, Epidermal Growth Factor Receptor; GSK3B, Glycogen Synthase Kinase 3β; HRAS, HRas Proto-Oncogene, GTPase; KRAS, KRAS Proto-Oncogene, GTPase; NFKB3, RELA Proto-Oncogene, NF-kB Subunit; NFKBIA, NFKB Inhibitor α; PTEN, Phosphatase And Tensin Homolog; YAP1, Yes1 Associated Transcriptional Regulator.*

Despite *PD-L1* being the least expressed oncogene among the analyzed group in HCC, it showed the most robust association with *AURKA* expression. These findings not only reinforce previous observations regarding *AURKA*'s correlation with *PD-L1* and *TPX2* but also spotlight *KRAS* as a potential key player in *AURKA*-related signaling pathways.

4.4 AURKA protein expression in human and mice samples

4.4.1 The decrease in AURKA protein expression in HCC

In contrast to prior reports suggesting AURKA protein overexpression in tumors (Table 1) [87–90], the analysis, utilizing two distinct antibodies targeting different AURKA domains (sc-398814 from Santa Cruz Biotechnology targeting amino acids 1-130 (N-terminal) and ab52973 from Abcam targeting amino acids 350-450 (C-terminal)), revealed a significant decrease in AURKA expression in HCC tumor tissues (Figure 25.A-D).

AURKA showed a 2.66-fold decrease in tumors compared to adjacent non-tumoral tissues (n=54) (0.276 [0.094-0.478] *vs.* 0.733 [0.393-0.971], p <0.001) (Figure 25.A and C), with only the 17% of patients showing an AURKA overexpression in tumors (Figure 25.E). Among patients overexpressing AURKA in tumors, 56% (5/9) had HCV infection, while 33% (3/9) and 11% (1/9) were associated with steatotic liver disease (SLD) and HBV, respectively.

These results were further confirmed by testing a subset of samples (12 out of 54 patients) with the ab52973 antibody, revealing a robust decrease in AURKA expression in tumor samples (0.027 [0.005-0.177] *vs.* 0.170 [0.098-0.317], p = 0.052) (Figure 25.B and D). Once again, only 17% of the samples exhibited AURKA overexpression in tumors.

There was no observable correlation in AURKA expression between the tumors and adjacent non-tumoral tissues (r: 0.266 [CI95%: -0.015; 0.509], p = 0.056) (Figure 25.F). Additionally, no correlation was observed between *AURKA* mRNA and AURKA protein expression in tumor tissues (r: 0.127 [CI95%: -0.169; 0.401], p = 0.386) (Figure 25.G) and adjacent non-tumoral tissues (r: -0.098 [CI95%: -0.383; 0.203], p = 0.510) (Figure 25.H).

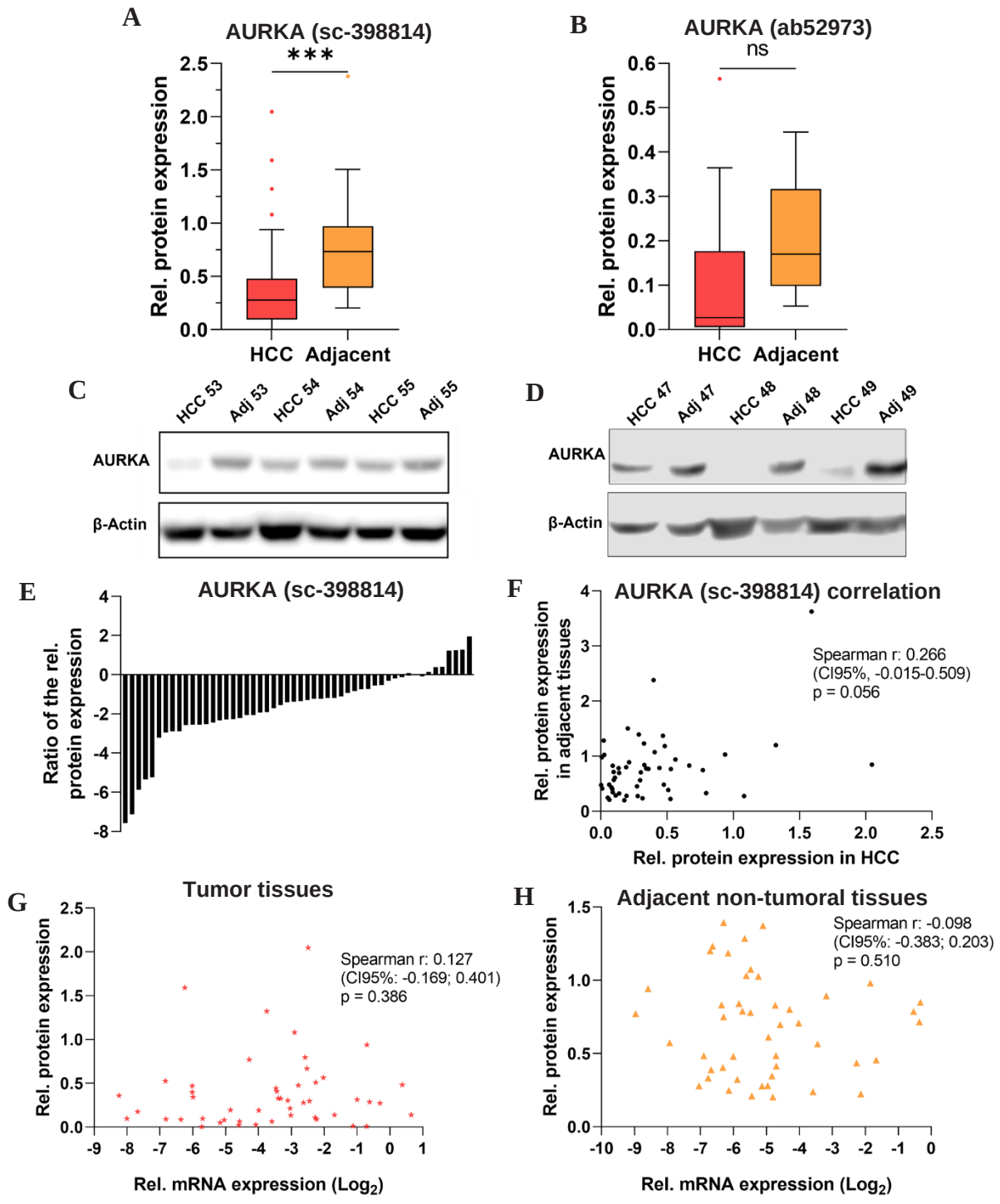

Figure 25. AURKA protein expression in HCC patients. (A-B) Relative AURKA protein expression in tumor and adjacent non-tumoral tissues using the antibody (A) sc-398814, from Santa Cruz Biotechnology (n=54), or (B) ab52973, from Abcam (n=12). Statistical significance was calculated using the Wilcoxon signed-rank test. (C-D) Representative protein blots of AURKA and β-Actin in tumor and adjacent non-tumoral tissues with the antibody (C) sc-398814 or (D) ab52973. (E) Ratio of the relative AURKA protein expression between tumors and adjacent non-tumoral tissues (n=52). (F) Correlation between the relative AURKA protein expression in the tumor and adjacent non-tumoral tissues (n=52). (G-

H) Correlation between the relative *AURKA* mRNA and AURKA protein expression in (G) tumor or (H) adjacent non-tumoral tissues (n=49). Correlations were calculated using Spearman's rank correlation test. * p <0.05; ** p <0.01; *** p <0.001

4.4.2 The phosphorylation of AURKA on Thr288 residue in HCC

To evaluate the activation status of AURKA in human HCC tissues (n=12), we examined AURKA phosphorylation on Thr288 in both tumor and adjacent non-tumoral tissues. This particular

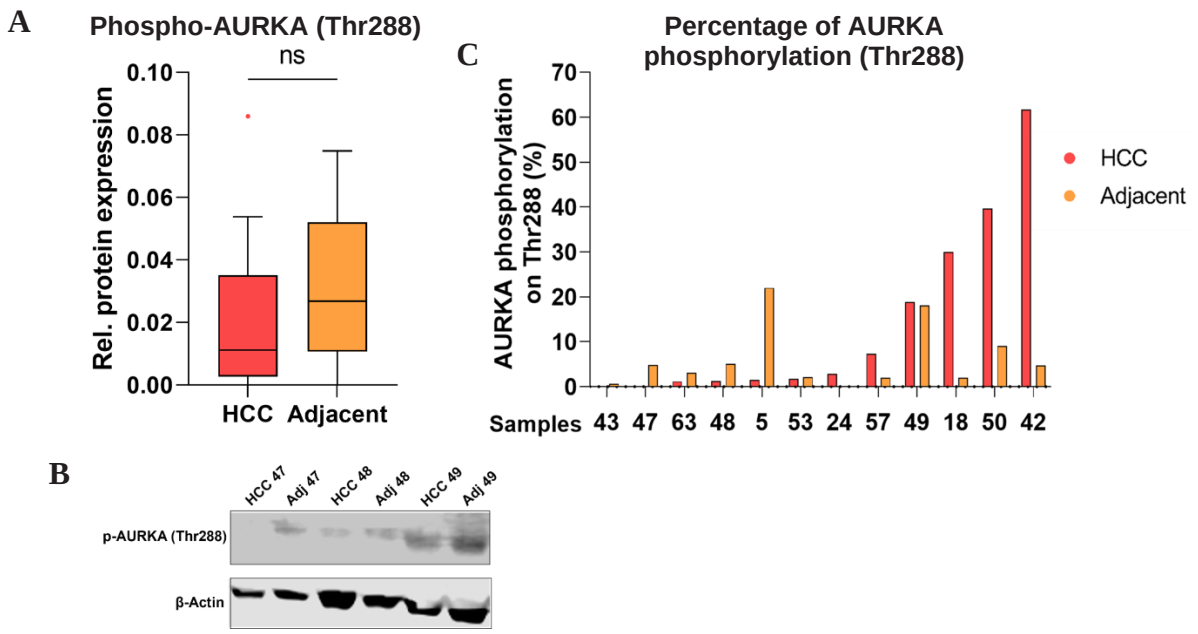

Figure 26. The phosphorylation of AURKA on Thr288 in HCC patients. (A) Relative expression of phosphor-AURKA (Thr288) in tumor and adjacent non-tumoral tissues (n=12). Statistical significance was calculated using the Wilcoxon signed-rank tests. Ns, Non-significant. (B) Representative protein blots of phospho-AURKA (Thr288) and β-Actin in tumor and adjacent non-tumoral tissues. (C) Percentage of phosphor-AURKA (Thr288) relative to the total AURKA protein expression in both tumor and adjacent non-tumoral tissues for each patient (n=12).

phosphorylation site is commonly associated with the enzymatic activation of AURKA [145,146].

A low signal of phosphorylated AURKA (Thr288) was detected in both tissues, with no significant differences between tumors and adjacent tissues (0.011 [0.003-0.035] *vs*. 0.027 [0.011-0.052], p = 0.380) (Figure 26.A-B). Interestingly, in 50% of the patients (6/12), the expression of phospho-AURA (Thr288) was higher in tumors compared to the adjacent non-tumoral tissues (Figure 26.C). The mean percentage of activated AURKA was higher in tumors compared to adjacent non-tumoral tissues (13.84% *vs.* 6.14%) (Figure 26.C). Thus, although expressing lower levels of

AURKA, tumors showed a higher amount of activated AURKA. However, until now, no experimental explanation can be provided regarding the implications of this activation in tumors.

Given the higher percentage of AURKA phosphorylation (Thr288) in tumors, AURKA might play a significant role in cell mitosis and replication. The phosphorylation of AURKA on Thr288 promotes a conformational change to an opened state, enhancing the kinase activity of the protein and facilitating the phosphorylation of its co-factors and substrates. These alterations are crucial in the mitotic process, where the correct activation of AURKA is pivotal for the G2/M transition and the organization of the mitotic spindle [27].

However, immunohistochemical assays conducted in 8 HCC patients not only confirmed the generally low abundance of AURKA in tumors but also revealed limited Ki67 positivity, a marker of cell proliferation. Although with slight positivity, Ki67 staining was higher in 37% of the tumor tissues (3/8), while the remaining patients exhibited a very low signal (0-2% positivity to the marker) in both tumor and adjacent non-tumoral tissues. Despite the increased AURKA phosphorylation (Thr288) in tumor components, it does not appear to significantly affect cell proliferation. However, considering the diverse range of functions associated with active AURKA and total AURKA, further analyses are warranted to unravel the potentially distinct roles of this protein in both tumor and adjacent non-tumoral tissues.

A representative case (Figure 27) illustrated weak positivity for the AURKA antibody in the tumor tissue compared to the contiguous non-cirrhotic non-tumoral hepatic parenchyma, showing intense positivity (Figure 27, left panels). Conversely, Ki-67 antibody positivity was evident only in the tumor component (Figure 27, right panels).

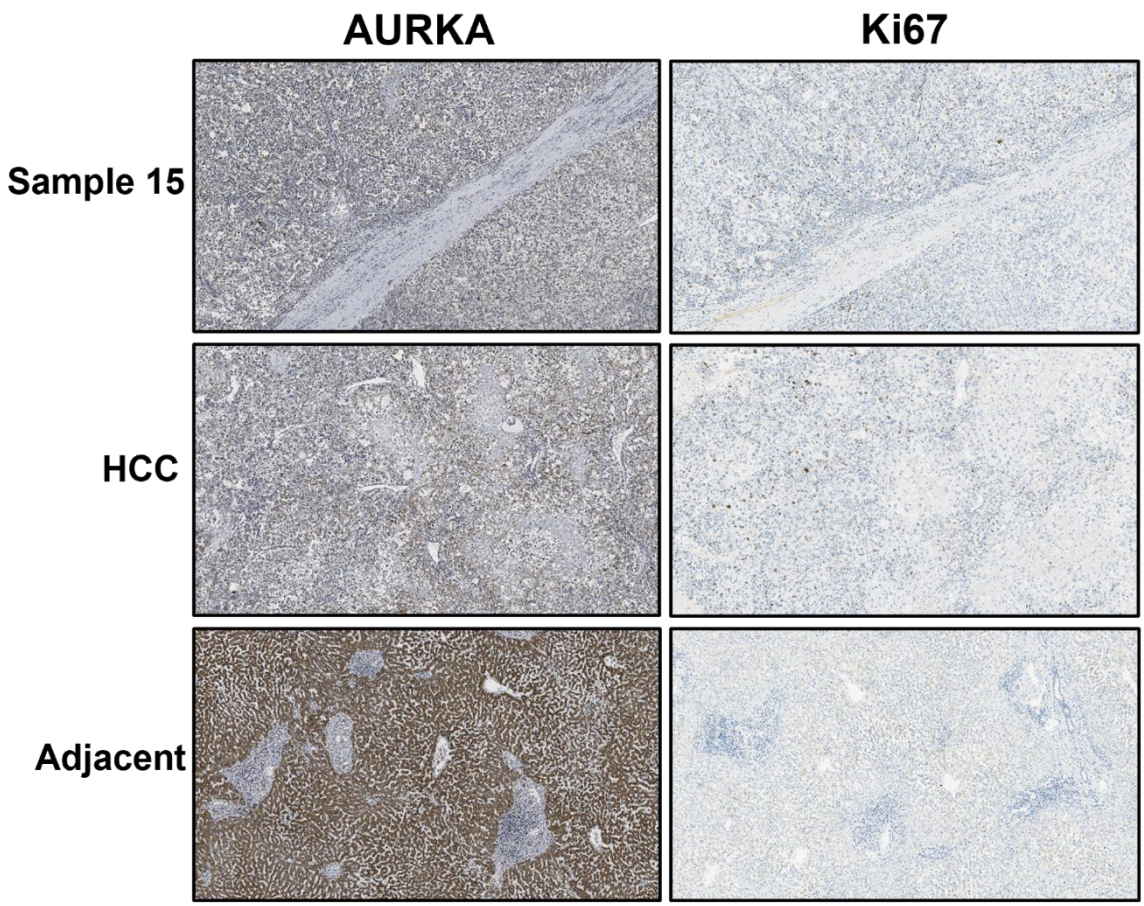

Figure 27. Immunohistochemical staining of AURKA and Ki67 in a representative HCC patient (sample 15). The top panels show the transition area between the tumor and adjacent non-tumoral tissues, the middle panels the tumor component, and the bottom panels the adjacent non-tumoral component. Ki67: a marker of cell proliferation. Magnification:10X.

In another case (Figure 28), both tumor and adjacent non-tumoral components showed moderate AURKA positivity (Figure 28, left panels), and Ki-67 expression remained consistent between the tissues (Figure 28, right panels).

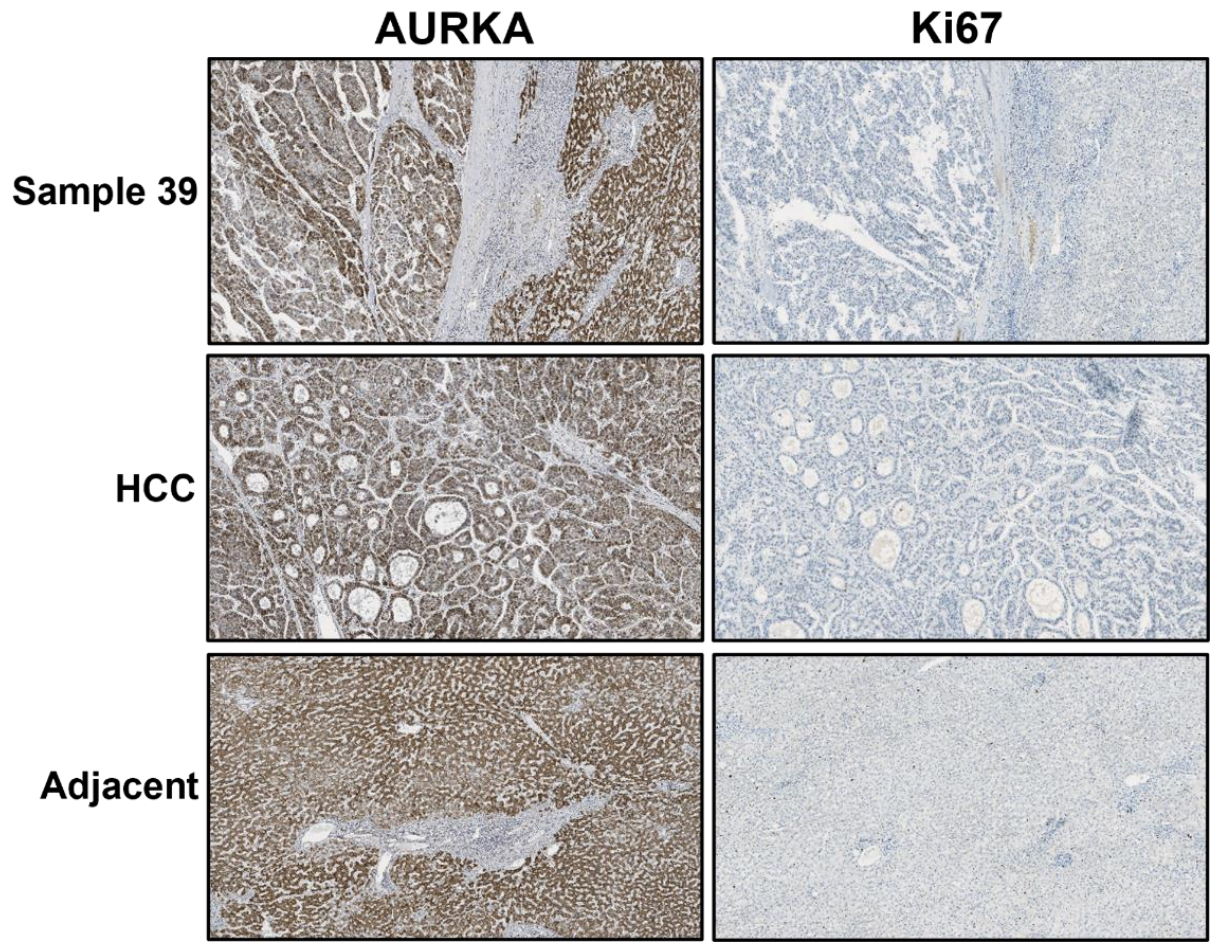

Figure 28. Immunohistochemical staining of AURKA and Ki67 in a representative HCC patient (sample 39). The top panels show the transition area between the tumor and adjacent non-tumoral tissues, the middle panels the tumor component, and the bottom panels the adjacent non-tumoral component. Ki67: a marker of cell proliferation. Magnification:10X

4.4.3 The changes in AURKA protein expression during hepatocarcinogenesis

In response to the unexpected findings regarding AURKA expression in HCC, our investigation expanded to include individuals with MASLD and subjects with healthy livers. AURKA exhibited significant ($p < 0.001$) differential expression across healthy (0.945 [0.563-1.470]), MASLD (1.945 [0.455-2.423]), adjacent non-tumor (0.733 [0.393-0.971]), and tumor samples (0.276 [0.094-0.478]). AURKA was overexpressed in both healthy and MASLD samples compared to tumors (both $p < 0.001$) (Figure 29.A-B) and in MASLD samples compared to adjacent non-tumoral tissues ($p = 0.031$) (Figure 29.A-B).

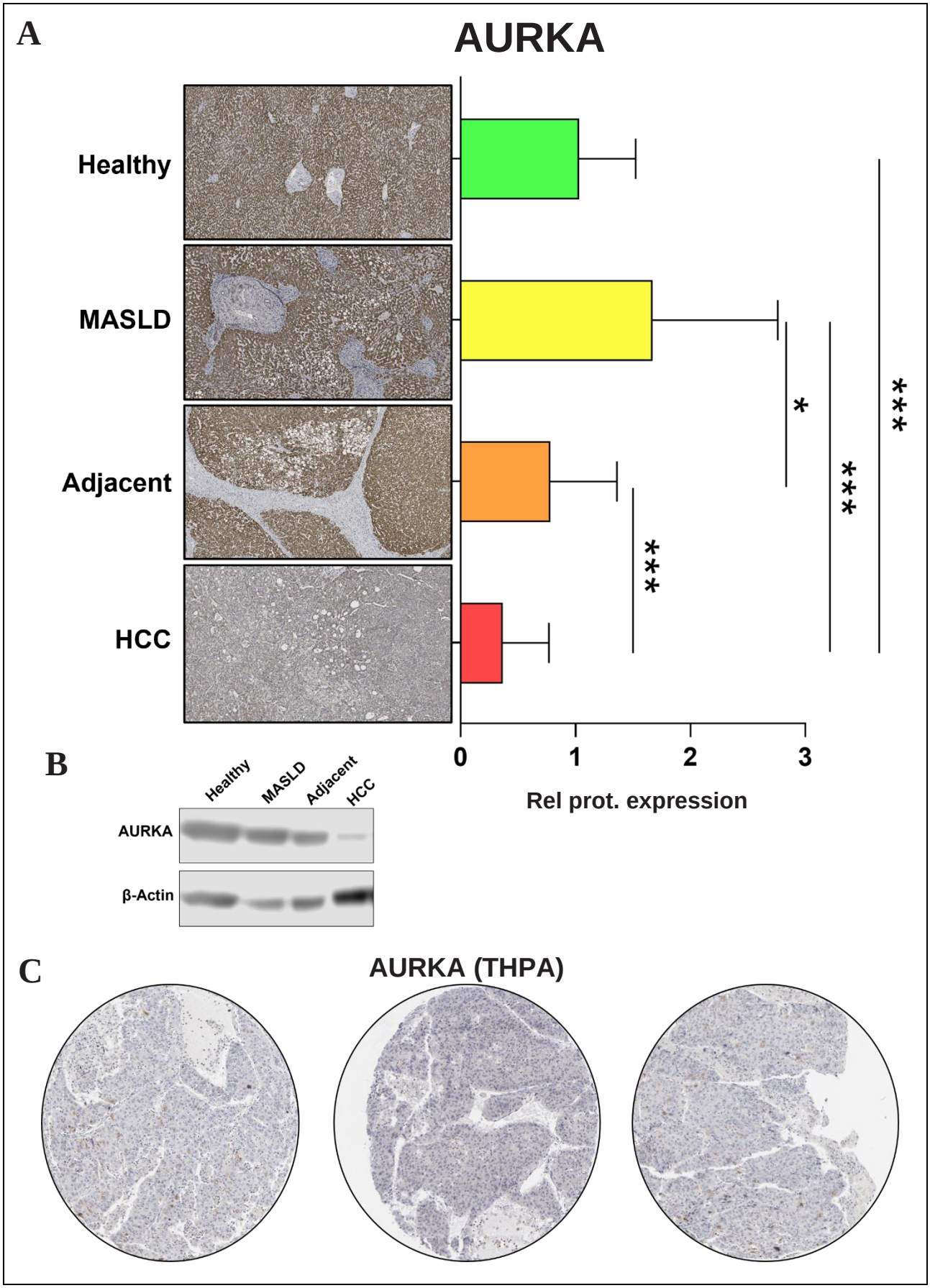
A
AURKA
Healthy
MASLD
Adjacent
HCC
0
1
2
3
Rel prot. expression
*
***
****
****
B
Healthy
MASLD
Adjacent
HCC
AURKA
β-Actin
C
AURKA (THPA)

Figure 29. The protein expression of AURKA in human HCC patients, MASLD individuals, and subjects with healthy liver. (A) Relative AURKA protein expression by Western Blot in HCC (n=54), adjacent non-tumor (n=52), MASLD (n=10), and healthy (n=10) liver tissues and immunohistochemical staining of AURKA performed on tissue samples from one representative subject per each condition. Statistical significance was calculated using Kruskal-Wallis tests for multiple groups, Wilcoxon signed-rank tests for the paired tissues, and Mann-Whitney U for non-paired tissues. * $p < 0.05$; ** $p < 0.01$; *** $p < 0.001$ (B) Representative protein blots of AURKA and β-Actin in the tumor, adjacent non-tumoral, MASLD, and healthy liver tissues. (C) Immunohistochemical staining of AURKA performed on tissue samples from three representative patients from the THPA database (https://www.proteinatlas.org/).

Immunohistochemical staining revealed widespread and intense positivity for the AURKA antibody in the epithelial elements of hepatocytes, with sparing of the stromal component in healthy, MASLD, and adjacent non-tumoral samples (Figure 29.A). In contrast, the tumor sample displayed weak positivity with a heterogeneous distribution (Figure 29.A), aligning with the results available from the THPA database obtained using CAB001454 (Novocastra Antibodies) or HPA002636 (Sigma-Aldrich) antibodies (Figure 29.C). The first and third representative cases exhibited focal weak positivity for the antibody, while the second tissue sample was completely negative (Figure 29.C).

The analysis of AURKA protein expression in the mouse model revealed significant differential expression across all tested conditions ($p = 0.001$) (Figure 30.A-B). A stable expression was observed in WT mice, while AURKA expression increased in TG mice from 3 to 9 months, with a significant difference between 6 and 9 months (0.559 [0.336-0.683] *vs.* 0.783 [0.500-0.853], $p = 0.033$) (Figure 30.C). After the neoplastic formation, AURKA expression was decreased in neoplastic nodules compared to adjacent non-neoplastic tissues, although not significantly (0.655 [0.520-0.780] *vs.* 0.765 [0.634-0.924], $p = 0.084$) (Figure 30.A-B), aligning with the observations in human samples.

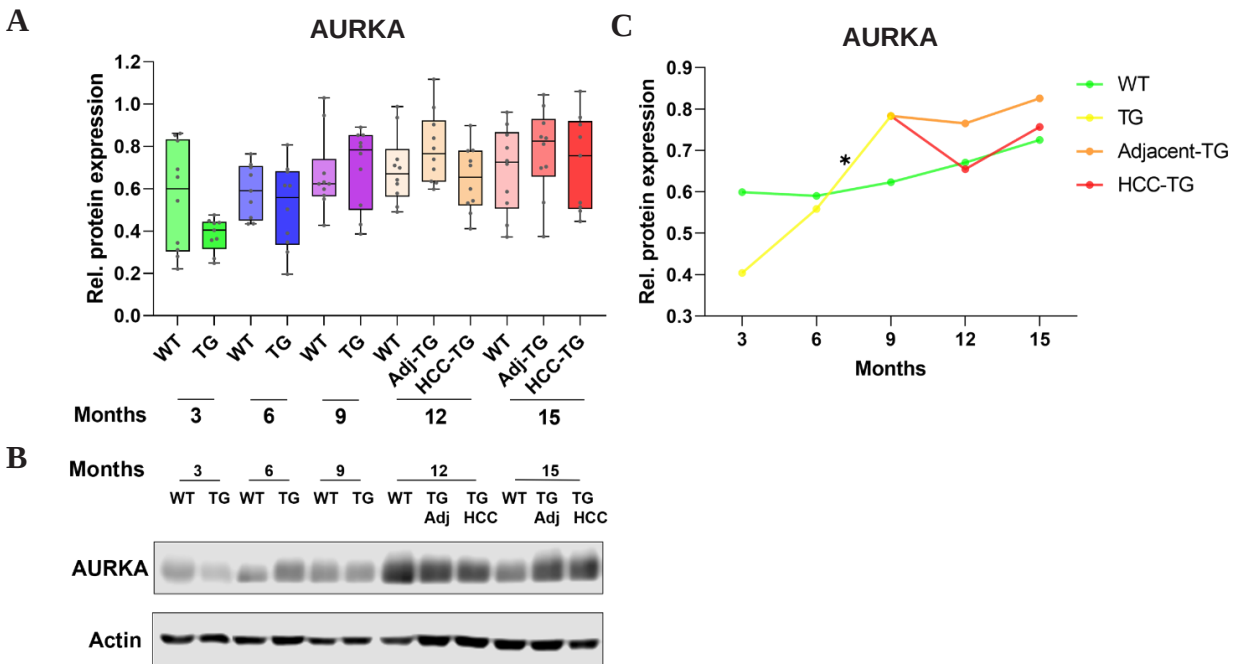

Figure 30. The protein expression of AURKA in TG and WT mice at different ages. (A) Relative AURKA protein expression in TG and WT mice at 3m, 6m, 9m, 12m, and 15m of age (per condition, n=10). (B) Representative protein blots of AURKA and Actin in mice liver tissues from all the different twelve conditions. (C) The AURKA expression trend in TG and WT mice assessed using the median AURKA expression for each condition. Macroscopic HCC lesions were visible at 12 months of age. Statistical significance was calculated using Kruskal-Wallis tests for multiple groups, Wilcoxon signed-rank tests for the paired tissues, and Mann-Whitney U for non-paired tissues. * p <0.05; ** p <0.01; *** p <0.001

Together, these findings suggest a dynamic pattern of AURKA expression, increasing during chronic liver disease and the pre-neoplastic stage, followed by a decrease in tumors.

4.5 PD-L1 protein expression in HCC: A possible correlation with AURKA

After establishing correlations at the mRNA levels and identifying potential mechanisms linking AURKA and PD-L1 *in vitro*, a subsequent investigation was conducted in human HCC samples to validate and strengthen the evidence related to PD-L1.

4.5.1 PD-L1 protein expression in HCC

In the analyzed 54 HCC samples, total PD-L1 protein exhibited an overall increased expression in tumor tissues compared to adjacent non-tumoral tissues (0.607 [0.354-0.834] *vs.* 0.447 [0.305-0.599], p = 0.029) (Figure 31.A and E), with 59% of patients demonstrating PD-L1 overexpression in tumors (Figure 31.B). Upon more detailed analysis, this difference was primarily attributed to unglycosylated non-mature forms (lower bands) of PD-L1 (tumor: 0.219 [0.102-0.326] *vs*. adjacent non-tumoral: 0.168 [0.108-0.253], p = 0.135) (Figure 31.C and E). No differences in glycosylated mature forms of PD-L1 were observed (upper bands) (0.168 [0.101-0.267] *vs*. adjacent 0.139 [0.054-0.239], p = 0.023 (Figure 31.D-E).

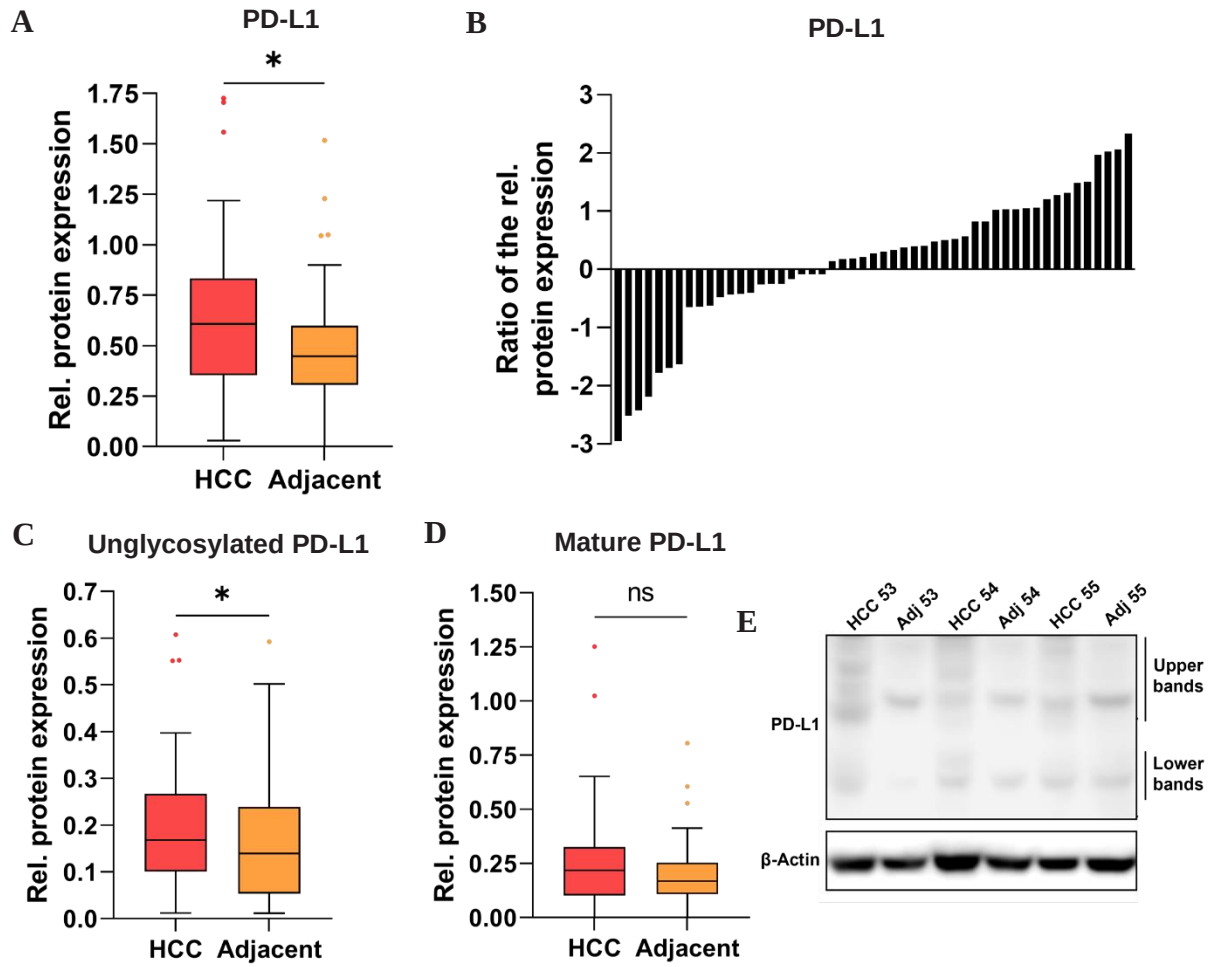

Figure 31. PD-L1 protein expression in HCC patients. (A) Relative total PD-L1 protein expression in tumor and adjacent non-tumoral tissues (n=54). (B) Ratio of the relative PD-L1 protein expression between tumor and adjacent non-tumoral tissues (n=51). (C-D) Relative expression of (C) immature unglycosylated (lower bands) and (D) mature glycosylated (upper bands) PD-L1 in tumor and adjacent non-tumoral tissues (n=54). (E) Representative protein blots of total PD-L1 and β-Actin in tumor and adjacent non-tumoral tissues. Statistical significance was calculated using the Wilcoxon signed-rank tests. * p <0.05; ** p <0.01; *** p <0.001

Upon categorizing the population into two groups based on the median expression (0.607) in tumors, PD-L1 was found to be overexpressed in tumors compared to adjacent non-tumoral tissues in 35% (9/26) of the samples in the low-PD-L1 group (Figure 32.A), while in 85% (22/26) in the high-PD-L1 group (Figure 32.A). Further analysis revealed a positive correlation in total PD-L1 expression between tumor and adjacent non-tumoral tissues (r: 0.385 [CI95%: 0.117; 0.601], p = 0.005) (Figure 32.B). Additionally, we observed a positive correlation between *PD-L1* mRNA and PD-L1 protein expression (n=49) only in tumor tissues (r: 0.322 [CI95%: 0.036; 0.559], p = 0.024) (Figure 32.C). No correlation was observed in adjacent non-tumoral tissues (r: -0.023 [CI95%: -0.310; 0.267], p = 0.873) (Figure 32.D).

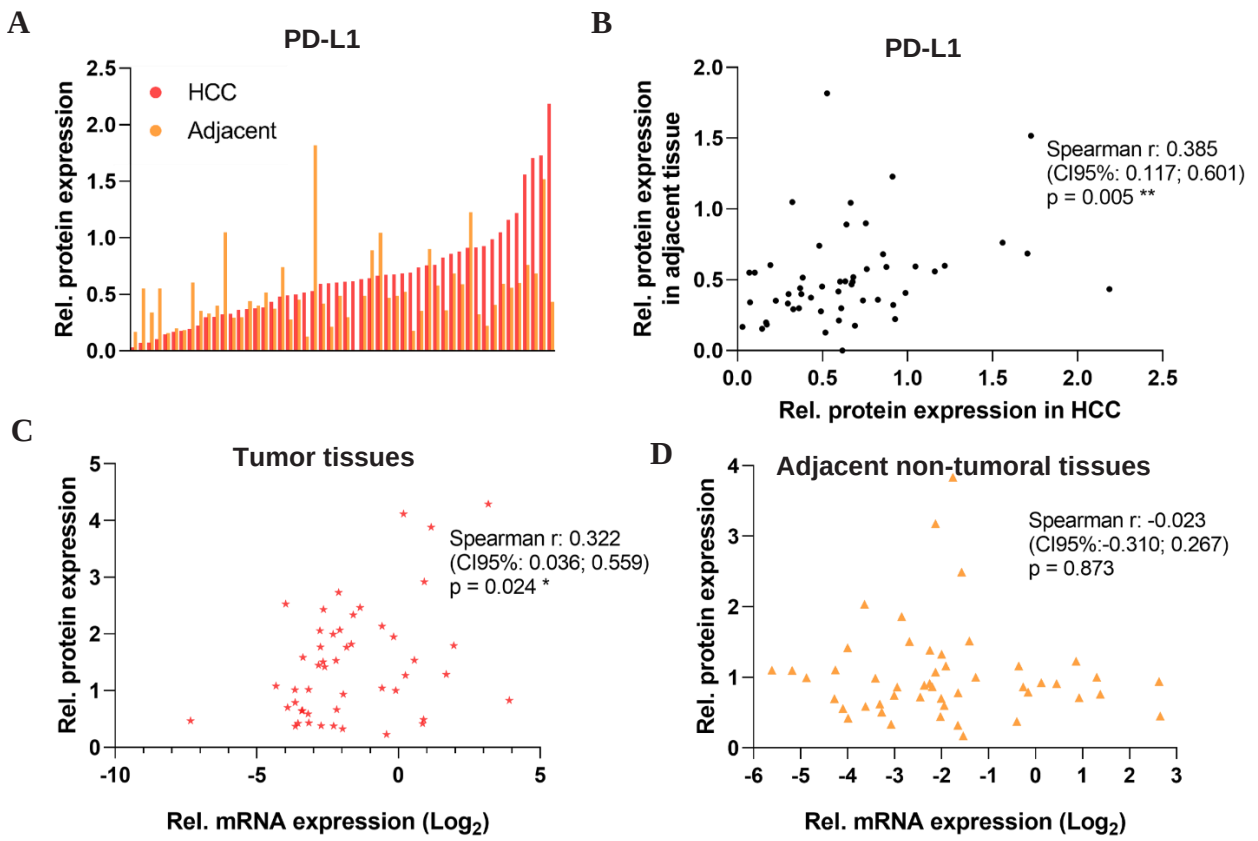

Figure 32. PD-L1 correlation in HCC patients. (A) Relative PD-L1 protein expression in each tumor tissue, flanked by its adjacent non-tumoral tissue (n=52). Samples were ordered according to PD-L1 expression in the tumor. (B) Correlation between the relative PD-L1 protein expression in tumor and adjacent non-tumoral tissues (n=52). (C-D) Correlation between the relative *PD-L1* mRNA and PD-L1 protein expression in (C) tumor and (D) adjacent non-tumoral tissues (n=49). Correlations were calculated using Spearman's rank correlation test. * p <0.05; ** p <0.01; *** p <0.001

4.5.2 PD-L1 and AURKA protein expression in HCC

Despite the previous analysis uncovered a correlation between *AURKA* and *PD-L1* mRNA expression (Figure 20.C), no correlation was observed between the protein expressions of AURKA and PD-L1 in tumor tissues (r: -0.005 [CI95%: -0.280; 0.271], p = 0.972) (Figure 33.A) or adjacent non-tumoral tissues (r: 0.186 [CI95%: -0.100; 0.443], p = 0.188) (Figure 33.B).

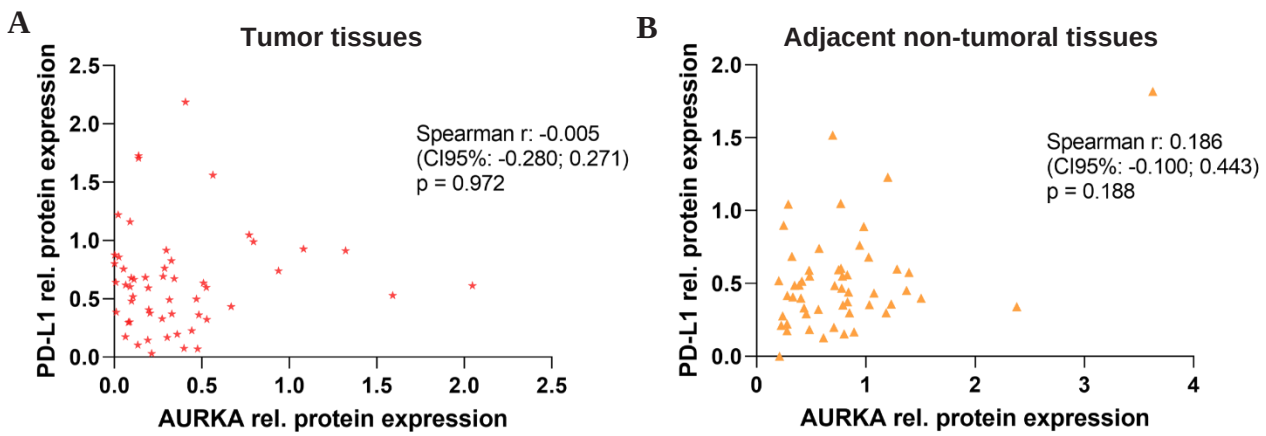

Figure 33. The correlation between AURKA and PD-L1 protein expression. (A-B) Correlation between the relative protein expression of AURKA and total PD-L1 in (A) HCC (n=54) or (B) adjacent non-tumor tissues (n=52). Correlations were calculated using Spearman's rank correlation test. * p <0.05; ** p <0.01; *** p <0.001

The immunohistochemical staining for PD-L1 in 8 HCC patients consistently revealed low expression (0-1%) in both tumor and adjacent non-tumoral tissues. A representative case (Figure 34) illustrated focal intense positivity for the AURKA antibody in the tumor tissue and diffuse positivity at the epithelial level in the non-tumoral cirrhotic tissue counterpart (Figure 34, left panels). Only macrophage elements displayed positivity for the PD-L1 antibody (Figure 34, right panels), implying that the higher positivity in the tumor component may be indicative of increased inflammation in this tissue.

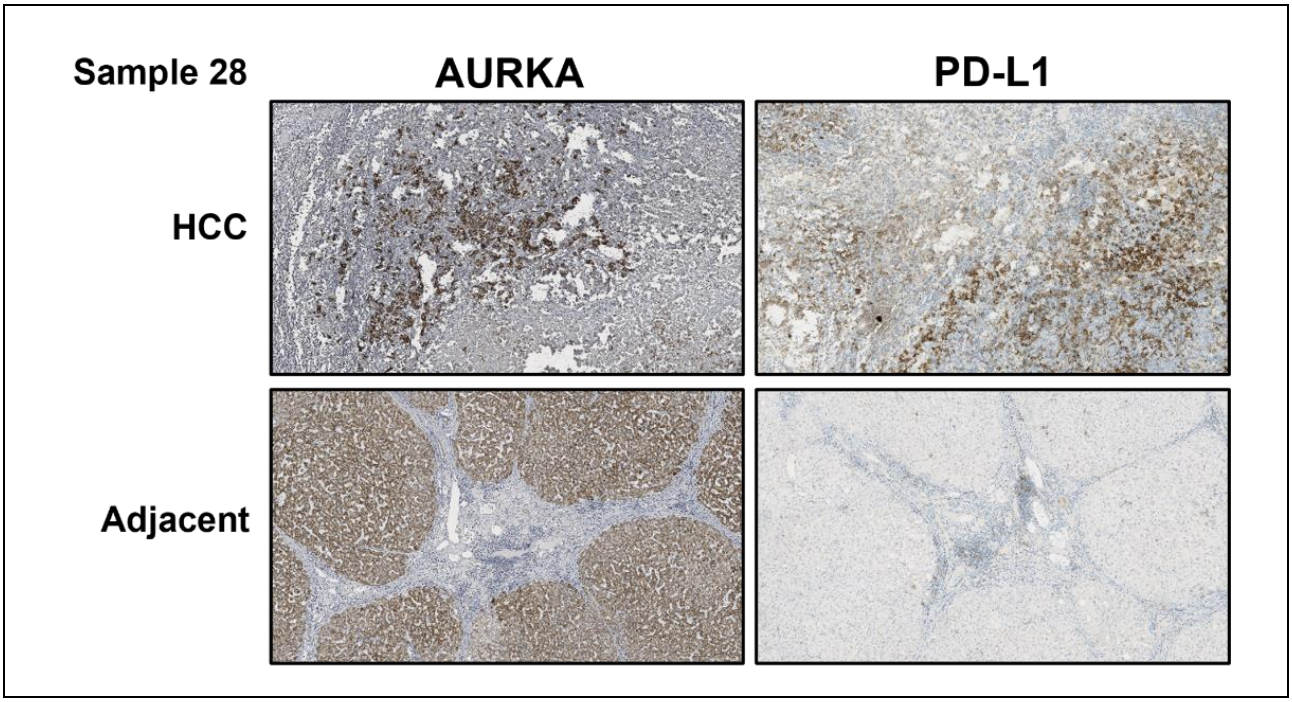

Figure 34. Immunohistochemical staining of AURKA and PD-L1 in a representative HCC patient (sample 28). The top panels show the tumor component and the bottom panels the adjacent non-tumoral component. Magnification:10X.

In another case (Figure 35), both tumor and adjacent non-tumoral components exhibited moderate AURKA positivity (Figure 35, left panels), while PD-L1 was not expressed (Figure 35, right panels).

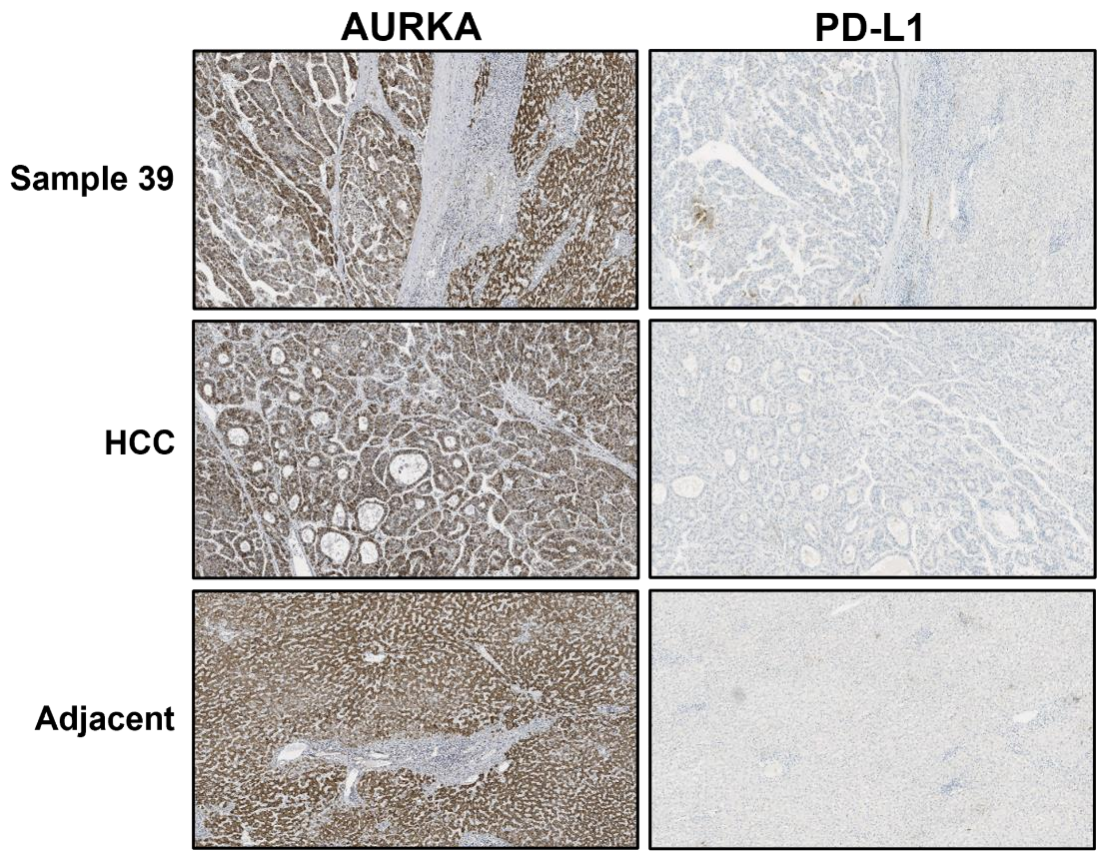

Figure 35. Immunohistochemical staining of AURKA and PD-L1 in a representative HCC patient (sample 39). The top panels show the transition area between the tumor and adjacent non-tumoral tissues, the middle panels the tumor component, and the bottom panels the adjacent non-tumoral component. Magnification:10X.

These results were consistent with the immunohistochemical staining for PD-L1 (CAB076385 antibody, Cell Signaling Technology) in HCC tissues from the THPA database (Figure 36). The first case exhibited focal positivity in some elements likely of macrophage origin, while the second and third tissue samples showed complete negativity.

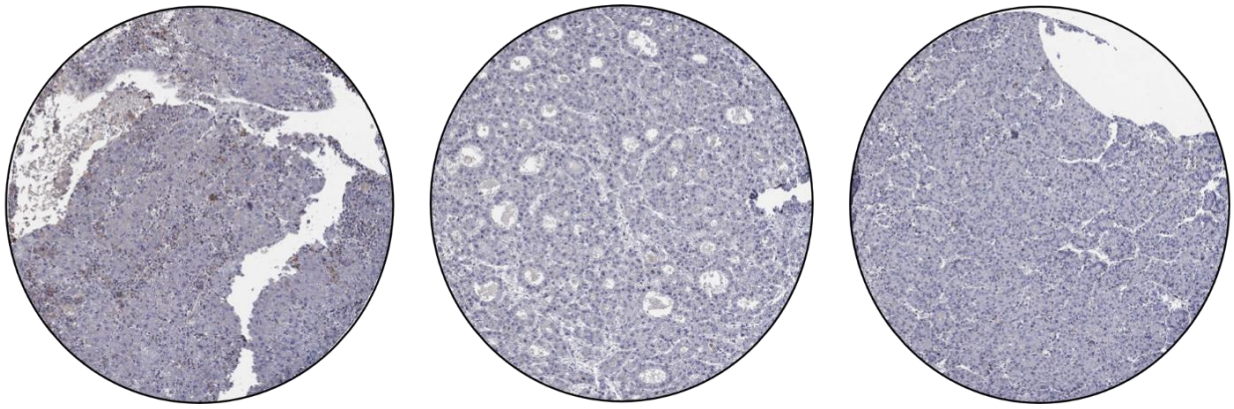

Figure 36. Immunohistochemical staining of PD-L1 in HCC patients from The Human Protein Atlas (https://www.proteinatlas.org/). The staining was performed on tissue samples from three representative patients, distinct from those used for AURKA staining.

The immunohistochemical staining unveiled a lower expression of PD-L1 protein compared to the WB results. This variance can be attributed to the use of a different antibody, validated for clinical practice in various tumors (though not specifically in HCC).

Chapter 5 - Discussion

HCC is a significant global health concern, ranking as the fourth leading cause of cancer-related deaths [1], with both the incidence and mortality expected to increase in the coming years [2]. The persistently high mortality associated with HCC is mainly attributed to late-stage diagnoses and limited therapeutic options.

Diagnoses at advanced stages limit access to curative treatment options, impacting overall prognosis. LT and hepatic resection, which offer improved survival and lower recurrence rates, are restricted to patients with single nodules or a maximum of three small lesions [1,19]. For patients diagnosed with advanced-stage HCC, systemic therapies give limited prospects for long-term survival. The recent introduction of combinatorial treatments, specifically the combination of targeted therapy and immunotherapy, has improved outcomes in advanced-stage patients [147]. This combination treatment can optimize treatment efficacy and long-term effectiveness through its dual impact on both tumor cells and immune modulation [23]. Thus, recent clinical trials have focused on the development of targeted therapies, immune checkpoint inhibitors, and synergistic treatments [147]. The generation of a comprehensive panel of therapeutic targets and immune checkpoint inhibitors can offer a more personalized and efficient treatment approach for patients.

During the last two decades, studies exploring the genomic landscape of HCC have identified several key genes crucial in carcinogenesis. Among these, AURKA, a member of the Aurora serine/threonine kinase family [10], plays a crucial role in regulating the mitotic process, particularly in G2/M transition, centrosome maturation, mitosis entry, and formation of the mitotic spindle [27,35]. *AURKA* overexpression has been reported in various tumor types, where it can drive cancer cell proliferation. Our study revealed a significant 3.54-fold increase in *AURKA* mRNA expression in 75% of tumor tissues compared to adjacent non-tumoral tissues in a population of 52 HCC patients who underwent hepatic resection. This finding is consistent with data from the TCGA database and aligns with numerous studies investigating *AURKA* expression in HCC across diverse gene expression datasets [74–86] and patient cohorts from local hospitals [69,77,81,90].

According to the TCGA database, *AURKA* expression in the liver is a potential prognostic biomarker. Patients exhibiting high *AURKA* expression demonstrated a twofold increase in the likelihood of shorter OS and a 1.6 times higher risk of earlier recurrence. However, our study did not confirm these findings, potentially due to variations in the population characteristics. Notably, the

TCGA database comprises a substantial proportion (43%) of Asian individuals [148]. Asian HCC patients are predominantly affected by chronic HBV infection [1,149]. Among the patients enrolled in the INSIGHT study, HBV was the predominant risk factor for HCC in numerous Asian countries, including China (91.3%), Taiwan (62.2%), South Korea (64.4%), Hong Kong (82.8%), Thailand (48.0%), and Singapore (46.0%) [150]. In contrast, our HCC population exhibited HBV as the etiology of malignancy in only 11% of patients. No significant associations were observed in our population between *AURKA* expression and etiology or other pathological features, such as tumor grades. Notably, the limited number of cases available for analysis in our study may contribute to the absence of observed associations.

Intriguingly, *AURKA* expression positively correlated with the quantity of direct bilirubin, and the high-*AURKA* group of patients displayed elevated levels of total bilirubin. Increased total bilirubin levels are commonly associated with hepatic damage [133], suggesting a possible association between *AURKA* expression and liver dysfunction. This hypothesis highlights the potential multiple mechanisms of action and roles of the kinase during the progression of the disease. While AURKA is traditionally associated with mitosis, its role expands to other functions linked to liver dysfunction during disease progression. Notably, AURKA can play a crucial role in promoting liver fibrosis and is involved in various oncogenic pathways beyond cell replication. In hepatic stellate cells, the increased stability of AURKA is associated with a reduction in cellular senescence, contributing to alcohol-related liver fibrosis [151]. Additionally, AURKA is implicated in resistance to apoptosis by dysregulating the NF-κB signaling pathway [99] and promoting stemness by regulating the PI3K/AKT pathway [90].

This initial evidence prompted an extension of the research to include precancerous conditions, encompassing human MASLD and healthy liver samples, along with an HBV-TG mouse, a model of chronic liver disease leading to HCC. The analysis revealed a gradual increase in *AURKA* expression during the progression of liver disease, from a healthy state to tumor development, with elevated levels observed in the presence of hepatic damage, irrespective of its etiology, whether metabolic or viral. To our knowledge, this study [152] represents the first investigation evaluating *AURKA* expression throughout hepatocarcinogenesis, offering new insights into the role and significance of *AURKA*, even in precancerous conditions. The observed increase in *AURKA* expression in the presence of liver disease suggests non-canonical functions of AURKA in the context of hepatic damage. Notably, AURKA's potential involvement in liver fibrosis and steatosis, and its association

with HBV-HCC susceptibility and viral replication highlights the multifaceted role of this kinase in various aspects of liver pathology.

In zebrafish, AURKA overexpression promoted the expression of lipogenic factors and enzymes. In AURKA-TG fish, stably overexpressing AURKA, the expression of *peroxisome proliferator-activated receptor γ (pparγ), sterol regulatory element-binding protein 1 (srebp1), carbohydrate-responsive element-binding protein (chrebp)* were upregulated, suggesting a potential role of AURKA in steatosis [72]. AURKA has been implicated in enhancing HBV replication and expression independently of its kinase activity. In HepG2 cells transfected with recombinant Adeno-associated virus-hepatitis B virus (HBV1.3), AURKA knockdown significantly inhibited viral replication and expression. Intriguingly, the kinase-dead mutant K162R, incapable of binding ATP at the catalytic site, and the non-phosphorylatable mutant T288A exhibited a marked increase in viral DNA [153]. Furthermore, a specific *AURKA* polymorphism (Ile31Phe) has been associated with mediating susceptibility to HBV-related HCC in a Chinese population [154].

The progressive increase of *AURKA* expression observed during hepatocarcinogenesis suggests its potential utility as a promising biomarker for diagnosing the progression of chronic liver disease toward HCC. This becomes particularly significant when considering the transition from MASLD to more severe pathological conditions. However, the practical use of this biomarker in real-world applications is constrained by the reliance on tissue specimens since liver biopsy is an invasive and risk-prone procedure [155], and the lack of studies demonstrating superior performance of tissue biomarkers compared to current imaging-based methods.

The analysis of AURKA protein expression in human and mouse tissues revealed unexpected results compared to prior studies, which showed a general upregulation of AURKA in HCC [87–89] (Table 1). However, it is essential to consider that these study populations were predominantly composed of Asian patients. Conversely, our study revealed a noteworthy decrease (2.66-fold) in AURKA protein expression in 83% of tumors compared to adjacent non-tumoral tissues. This disparity between mRNA and protein expression may be attributed to differential post-transcriptional regulation in tumoral and normal contexts, resulting in multiple isoforms of *AURKA* mRNA with distinct translation efficiencies.

Sixteen high-scoring transcript isoforms resulting from alternative splicing have been annotated until 2022 in the National Center for Biotechnology Information (NCBI) and Ensemble databases,

primarily involving 5′UTR splicing variants. Given that the splicing process is tightly coupled to transcription, and considering the cell cycle periodicity of *AURKA* transcription, it is not surprising that *AURKA* is among the genes undergoing periodic alternative splicing during the cell cycle [30]. A study identified three 5′UTR splicing isoforms in a breast cancer cell line, while only one isoform lacking exon II was found in a non-cancerous cell line, suggesting that exon II might be implicated in tumorigenesis. However, all three alternative splicing isoforms supported equal AURKA protein translation, excluding exon II as the sole determinant for AURKA protein overexpression in breast cancers [156]. Conversely, in colorectal cancers, an exon II-dependent mechanism of AURKA translational activation was proposed. The two exon II-containing transcripts were the most expressed AURKA splicing isoforms in colorectal cancer. Exon II enabled *AURKA* mRNA to respond to the Epidermal Growth Factor (EGF) stimulus, leading to translational up-regulation [157], possibly explaining why exon II-dependent AURKA overexpression could not be detected using *in vitro* assays.

Moreover, *AURKA* mRNA also exhibited short and long 3'UTR isoforms in breast cancer due to alternative polyadenylation. The short isoform was prevalent in TNBC, correlating with faster relapse times. It demonstrated higher translational efficiency resulting in increased proliferation and migration rates of cells *in vitro* since the translation and decay rates of the long isoform were regulated by hsa-let-7a tumor-suppressor miRNA [158]. Additionally, a recent study revealed the existence of AURKAPS1, a long non-coding RNA (lncRNA) and AURKA pseudo-gene. This lncRNA showed higher expression in HCC tumor tissues, mainly associated with tumor size and tumor, node, and metastases (TNM) stage. *In vitro*, AURKAPS1 promoted cell migration, and invasion, increasing the protein expression of Rac Family Small GTPase 1 (RAC1), activating Mitogen-Activated Protein Kinase (ERK), and enhancing membrane ruffle formation by competitively binding with miR-182, miR-155, and miR-142 [159].

The complexities of post-transcriptional regulation, context-dependent isoform with different translation efficiencies, and the presence of the non-protein-coding AURKAPS1 may contribute to the observed disparities between AURKA mRNA and protein expression. Ongoing investigations by our group aim to explore potential differences in mRNA isoforms between HCC tissues and adjacent non-tumoral tissues, as well as inter-patient variations.

The analysis of precancerous conditions showed a higher AURKA protein expression in MASLD subjects compared to HCC patients, suggesting a potential role of AURKA in chronic liver diseases. Interestingly, various studies showed AURKA's potential role in promoting fibroblast proliferation and fibrosis in different organs. Indeed, the selective AURKA inhibitor MK-5108 alleviated renal fibrosis in mouse samples, possibly by inhibiting fibroblast proliferation and activation and suppressing the phenotypic transition of renal cells. *In vitro*, MK-5108 inhibited the pro-fibrotic response in renal cells induced by TGF-β1 [160]. In lung fibrosis, MK-5108 led to a consequential reduction in the expression of profibrotic genes through YAP phosphorylation and cytoplasmic retention independently of the Hippo pathway [161]. Possibly some of those mechanisms are responsible for the fibrotic process in the liver, although our immunohistochemical assays did not reveal the presence of AURKA in fibrogenic cells. In addition, AURKA expression was markedly increased in patients with liver fibrosis and a history of alcohol consumption, as well as in acetaldehyde-stimulated hepatic stellate cells (HSC-T6 and LX-2 cells). The overexpression of 5'-Nucleotidase Ecto (NT5E) in hepatic stellate cells protected AURKA from ubiquitination, promoting its stability, and resulting in a reduction of cellular senescence. AURKA inhibition by alisertib attenuated high levels of *Actin α2, Smooth Muscle (α-SMA)*, and *Collagen Type I α1 Chain (COL1A1)* induced by acetaldehyde, while increasing Senescence-Associated β-galactosidase (SA-β-gal) staining, a marker of cellular senescence. Thus, the authors hypothesized that AURKA inhibition may attenuate acetaldehyde-stimulated fibrosis by promoting hepatic stellate cell senescence, implying a potential positive role of AURKA in aggravating alcohol-related liver fibrosis [151]. However, the limited data related to the role of AURKA in the pathogenesis of chronic liver disease, combined with the results of the present study highlight the importance of further research exploring the still unknown functions of this kinase in the progression of liver disease.

Interestingly, the AURKA co-activator and interactor, *TPX2,* follows the *AURKA*'s expression trend in hepatocarcinogenesis, exhibiting a gradual increase from healthy individuals to those with hepatic steatosis and a further overexpression in HCC. In the mouse model of HCC progression, *Tpx2* demonstrates a marked increase from early-stage to advanced neoplasia. Multiple studies showed overexpression of *TPX2* mRNA or TPX2 protein in HCC tissues compared to adjacent normal liver tissues [162–164]. The positive correlation between *AURKA* and *TPX2* expression underscores a persistent association throughout the progression of the disease. Beyond being activated and stabilized by TPX2 during mitosis [10,165], AURKA exhibited a positive feedback loop with TPX2. *In vitro,* AURKA phosphorylated TPX2 on two residues (Ser121 and Ser125), a process crucial for

maintaining the normal length of the mitotic spindle [166,167]. This intricate interplay between AURKA and TPX2 suggests a coordinated regulation that contributes to the dynamics of HCC development and progression.

Moreover, several genes that are either regulated by AURKA or involved in common pathways with AURKA [95,135–144] exhibited co-expression in the human HCC samples of the present study. Among all, *KRAS*, an oncogene encoding a small GTPase transductor protein, plays a crucial role in regulating cell division by relaying external signals to the cell nucleus [168,169]. In pancreatic ductal adenocarcinomas (PDAC), the high expression of *AURKA* and *TPX2* was associated with shorter patient survival and the presence of oncogenic *KRAS* mutations. KRAS knockdown in *KRAS*-mutant PDAC cells reduced AURKA and TPX2 mRNA and protein expression [170]. AURKA or AURKB knockdown, as well as the dual inhibition of AURKA and AURKB, resulted in decreased growth, viability, proliferation, transformation, and increased apoptosis in KRAS-positive lung cancer cell lines. AURKA knockdown in non-small cell lung cancer (NSCLC) cells (A549 cell line) determined a reduction in tumor growth *in vivo* [171]. In activated-KRAS gastrointestinal cancer cell lines, AURKA plays a pivotal role in the phosphorylation of Ribosomal Protein S6 Kinase B1 (RPS6KB1) on Thr389, thereby facilitating cell proliferation, survival, and the growth of xenograft tumors in mice. *In vivo*, the administration of alisertib resulted in reducing tumor growth, diminishing the phosphorylation of RPS6KB1, suppressing cell proliferation, and concurrently enhancing apoptosis [138]. The emerging correlation between *AURKA* and *KRAS* in cancer underscores a potential interplay that necessitates further investigation, particularly in the context of therapeutic strategies for HCC.

AURKA phosphorylation on Thr288 is a post-translational modification that induces a conformational change, transitioning the protein to an opened state. This modification enhances the kinase activity of the protein, facilitating the phosphorylation of its co-factors and substrates [146]. Despite the analysis being conducted only on 12 patients, the percentage of phosphorylated AURKA (Thr288) on the total AURKA protein was higher in tumor samples compared to adjacent non-tumoral tissues. This finding suggests an enhanced kinase activity in the tumor microenvironment.

AURKA's kinase activity is pivotal for proper mitotic progression, and the phosphorylation of Thr288 is associated with its role in the cell cycle. In mitosis, the kinase activity of AURKA is tightly regulated through the phosphorylation of the Thr288 residue by various co-factors, including AJUBA,

TPX2, BORA, and Transforming Acidic Coiled-Coil Containing Protein 3 (TACC3) [10,27]. Despite heightened phosphorylation on Thr288 in HCC, the kinase activity of AURKA did not result in promoting cell proliferation. No correlation was evidenced with Ki67, a marker of cell proliferation, in human specimens.

In the literature, the phosphorylation of the Thr288 residue was not exclusively associated with the cell cycle process, indicating diverse roles in other cellular processes. AURKA's kinase activity is implicated in DNA transcription [57,58], primary cilium remodeling [59,60], neuromorphogenesis [66–68], mitochondrial fission [64,65], and regulation of epigenetic factors [61–63]. The increased AURKA phosphorylation in the HCC nodules may be linked to its potential localization within mitochondria, where it controls organelle dynamics and energy production. The presence of AURKA enzymatic activity within mitochondria was demonstrated using a FRET biosensor, which tracked AURKA activation through autophosphorylation at Thr288 using the FRET/FLIM system. The AURKA inhibitor alisertib counteracted AURKA activation in mitochondria [146].

In vitro studies with breast cancer cell lines have further elucidated the impact of AURKA on mitochondrial function. When expressed at physiological levels, AURKA maintained mitochondrial fission, while its overexpression actively enhanced ATP production by promoting mitochondrial interconnectivity. Mitochondria with high metabolic capacity could escape turnover through fusion mechanisms, sustaining the high metabolic needs of cancer cells and potentially providing a selective advantage for cancer progression [64]. Moreover, AURKA directly interacted with the Complex V core subunits ATP synthase F1 subunit α (ATP5F1A) and β (ATP5F1B). Altering AURKA, ATP5F1A, or ATP5F1B levels induced dramatic metabolic changes affecting both the mitochondrial respiratory chain and glycolysis rates. The G1-phase arrest observed upon AURKA, ATP5F1A, or ATP5F1B downregulation was specific to oxidative cell lines expressing high levels of AURKA (MCF7 and T47D cells). Conversely, no impact on the cell cycle was observed in cells expressing low levels of AURKA and relying more on glycolysis (Hs 578T). In this model, AURKA, ATP5F1A, or ATP5F1B downregulation triggered cell death, possibly implying that the cellular metabolic state played a crucial role in determining cell fate [172]. Thus, determining the cells and the sub-cellular localization of the enzymatically active AURKA inside HCC tissues would provide valuable insights into its functional roles within the tumor microenvironment. This can contribute to a comprehensive understanding of AURKA's activity and its potential implications for HCC development and progression.

The findings from human and mouse samples prompted an investigation into the effects of two AURKA inhibitors, alisertib and AK-01, on *in vitro* models of HCC (JHH6 and Huh7 cells). The aim was to elucidate the role of the kinase in tumors and provide evidence supporting the hypothesis that AURKA is involved in the regulation of PD-L1, a key player in immune tumor surveillance and a target of current anticancer therapies.

The two selected cellular model exhibited high *AURKA* expression and strong dependency on *AURKA* for their growth. The chosen concentrations of 0.25µM for alisertib and 1.00µM for AK-01 were selected to efficiently inhibit AURKA, considering their significant impact on cell viability in Huh7 cells and their proximity to the LC50 in JHH6 cells at 72 hours. Importantly, these concentrations were chosen to minimize potential off-target effects of the drugs, as higher concentrations were shown to impact AURKB [115].

Both AURKA inhibitors demonstrated efficacy in reducing AURKA enzymatic activity, with AK-01 exhibiting superior AURKA inhibition in both cell lines. The higher effectiveness of AURKA inhibition treatments in JHH6 cells, belonging to the S1/TGFβ-Wnt activated subtype [126], suggested that differences in response could be attributed to the distinct HCC subtypes of the two cell lines, supporting the importance of tumor heterogeneity when considering eligible therapies. The differences in the response to drug treatments according to the cell subtypes have been observed in other contexts, such as for sorafenib, being effective in down-regulating targets in the S2/progenitor subtype, to which Huh7 cells belong [173].

As expected, the inhibition of AURKA resulted in the disruption of cell mitosis, causing centrosomal disorganization, defective mitotic spindle assembly, chromosome misalignments, impaired chromosome separation, and incomplete cytokinesis. These disruptions led to a delay in mitotic progression [115,174,175], promoting cellular stress and a gradual reduction in cell viability over time. Cancer cells, characterized by resistance to apoptosis and the accumulation of aberrations, demonstrated the ability to progress through anaphase and telophase but were incapable of completing cytokinesis accurately. This led to the accumulation of multiple chromosomes and the formation of aneuploid cells, especially pronounced in JHH6 cells. However, the accumulation of multiple aberrations contributed to a progressive increase in cell death.

In JHH6 cells, the inhibition of AURKA resulted in an elevation of both *AURKA* mRNA and AURKA protein expression, concomitant with the overexpression of *TPX2*. This observation implies

the activation of a compensatory mechanism in response to the inhibition of phosphorylated AURKA, aiming to generate new enzymatically active AURKA proteins. However, the presence of the drugs inhibited the activity of these newly generated proteins. Similar results have been observed in various cell lines, including neuroblastoma, HCC (HepG2 cells), glioma, and colorectal adenocarcinoma cell lines following 48 hours of AURKA inhibition by alisertib [109,176]. In Huh7 cells, alisertib decreased *AURKA* and *TPX2* mRNA expression, while AK-01 increased AURKA protein expression, highlighting the subtype-specific nature of the response to each AURKA inhibitor. However, additional analysis is necessary to fully understand the disparities between AURKA mRNA and protein expression in Huh7 cells.

AURKA silencing significantly reduced both AURKA mRNA and protein expression in the two cell lines, leading to alterations in *TPX2* expression that varied based on the specific cell line. Consistent with chemical inhibition, AURKA knockdown disrupted cell mitosis, resulting in an increased population of aneuploid cells, particularly prominent in JHH6 cells, and a reduction in cell viability over time. These results emphasize the essential role of both the kinase activity and the presence of the AURKA protein itself in maintaining a correct cell cycle process.

The role of AURKA in immune checkpoint regulation and tumor immune response is complex and context-dependent, with conflicting evidence in different cancer types [117–120]. In TNBC, AURKA has been associated with enhancing PD-L1 levels, contributing to the immune escape of tumor cells [117,118]. AURKA showed a positive correlation with tumor growth *in vivo* and a negative correlation with the enrichment and activity of tumor-infiltrating CD8+ T cells. [117]. The treatment with alisertib reduced CD44 levels and PD-L1 expression, promoting the infiltration of CD8+ T cells [118]. Contrastingly, recent studies proposed a significant role of AURKA in negatively regulating PD-L1 expression in tumors through the cGAS/STING/NF-κB pathway or the phosphorylation of STAT3, leading to enhanced immune cell infiltration and improved immune responses [119,120]. Alisertib treatment in 4T1-breast tumor xenograft models decreased CD3+ and CD8+ T cell infiltration [119]. These results indicate the presence of multiple regulatory layers and potentially a context- (cell-, tissue-, and disease-) dependent role of AURKA in immune regulation, necessitating further in-depth investigations.

In the *in vitro* models employed in our study, *PD-L1* expression was higher in JHH6 cells compared to Huh7 cells. The results after AURKA knockdown or inhibition in terms of PD-L1

mRNA and protein expression, as well as promoter activation, implied the existence of diverse mechanisms through which AURKA regulates PD-L1.

One potential mechanism involves the kinase activity of AURKA. The treatment with the AURKA inhibitor AK-01 resulted in a decrease in mature glycosylated PD-L1 in both cell lines, suggesting a potential role in stabilizing PD-L1. The reduction in stable forms of the protein could trigger a compensatory mechanism, leading to increased transcription of *PD-L1* mRNA to restore physiological conditions, which became particularly pronounced over time in JHH6 cells. Supporting this finding, initial observations revealed increased *PD-L1* promoter activation at 48 hours following AK-01 treatment. However, this enhanced gene transcription did not result in a corresponding increase in protein translation, possibly requiring longer experiment durations to observe. AURKA inhibition did not impact the expression of non-mature PD-L1 forms, emphasizing the need for extended experiments to confirm these hypotheses.

To further verify the involvement of AURKA in PD-L1 regulation independently of its kinase activity, silencing experiments were conducted. AURKA knockdown results suggest the existence of a regulatory mechanism that requires AURKA. In JHH6 cells, AURKA knockdown for 24 hours led to decreased *PD-L1* mRNA expression, confirmed by preliminary results indicating reduced *PD-L1* promoter activation following AURKA knockdown for the same time duration. However, since PD-L1 transcription is regulated by numerous transcriptional factors [177], other mechanisms may contribute to the increased *PD-L1* mRNA following AURKA knockdown for 72 hours. In Huh7 cells, AURKA silencing for 72 hours resulted in a slight decrease in *PD-L1* expression, potentially reflecting differences in the response to treatment attributed to distinct HCC subtypes. At the protein level, 72-hour knockdown did not impact PD-L1 protein expression in both cell lines, while extending the treatment duration to 144 hours significantly reduced unglycosylated forms. This can be attributed to the temporal requirements for the effective silencing of AURKA, coupled with our preliminary experimental findings indicating that the half-life of PD-L1 is estimated to be approximately 72 hours. Thus, an extended timeframe is necessary to observe the effects of *PD-L1* transcription dysregulation at the translational level. Furthermore, the reduction in unglycosylated forms was more pronounced in JHH6 cells, suggesting greater efficacy of the silencing treatment on PD-L1 expression in this cell line. Additionally, knockdown led to a decrease in glycosylated forms, with significant differences in JHH6 cells. We hypothesized that the glycosylated protein is degraded over time, and its replacement by newly translated protein is limited due to the overall reduction in gene translation, resulting in reduced protein synthesis.

Our preliminary findings, along with the results obtained by Cabral and collaborators [173], collectively observed the downregulation of AURKA mRNA and protein following PD-L1 silencing. These results, coupled with the roles of AURKA in PD-L1 regulation, reveal a potential positive feedback loop between AURKA and PD-L1. To our knowledge, this represents the first evidence of PD-L1 regulation on AURKA. Further analyses are necessary to unravel the complexities of this intricate interplay and understand the regulatory mechanisms governing the mutual interaction between AURKA and PD-L1 in HCC. Despite the need for deeper clarification, these preliminary results open an important and new perspective in anticancer treatments.

To better clarify the possible association between AURKA and PD-L1 *in vivo*, both human and mouse tissue were analyzed. *PD-L1* mRNA increased from healthy to MASLD individuals and was further elevated in HCC patients. Interestingly, *PD-L1* exhibited comparable expression levels between tumor and adjacent non-tumoral liver tissues. In the mouse model, the gene also displayed a significant increase during neoplastic progression from early-stage to advanced neoplasia. Data from the GEPIA database revealed a positive correlation between *AURKA* and *PD-L1* in both HCC-paired normal tissues and tumoral samples. In our samples, the positive correlation expression persisted throughout the hepatocarcinogenesis. These findings align with evidence indicating that elevated expression of a gene cluster containing *AURKA* was associated with increased expression of immune checkpoints, including *PD-L1*, in HCC [74]. This underscores the potential role of AURKA in the immune regulatory landscape during hepatocarcinogenesis, presenting opportunities for further exploration in therapeutic interventions targeting immune checkpoint pathways in HCC.

The analysis of PD-L1 protein expression in HCC revealed potential roles of the oncogene that extend beyond the traditional immunological context. Total PD-L1 protein was overexpressed in 59% of HCC tumor tissues compared to adjacent non-tumoral tissues, consistent with existing literature [178], with a positive expression correlation between the two tissues. Further exploration of PD-L1 indicated that the distinct expression between tumors and adjacent non-tumoral tissues can be attributed to the unglycosylated non-mature forms. This observation suggests potential additional functions for the protein beyond its established immunological roles. Various studies have underscored PD-L1's participation in non-immunological, pro-oncogenic processes, including but not limited to EMT, cellular metabolism, maintenance of stemness, and regulation of autophagy [179,180]. Nevertheless, even with these intriguing findings, a notable gap persists in our

understanding. Currently, there is no evidence confirming that the PD-L1 forms analyzed in these studies are indeed the unglycosylated ones.

The promotion of EMT by PD-L1 varies across tumor types, engaging different cellular pathways. In renal tumors, PD-L1 induced EMT through the regulation of Sterol Regulatory Element-Binding Transcription Factor 1 (SREBF1), a key factor in cancer-cell migration [181]. In hypopharyngeal squamous-cell carcinoma, the PI3K/AKT pathway was implicated [182], while in glioblastoma multiforme, the Ras/MEK/ERK pathway was involved [183]. Additionally, PD-L1 demonstrated diverse roles in regulating glycolysis and influencing embryonic stem-cell transcription factors. In sarcoma, PD-L1 knockdown resulted in the downregulation of glycolysis through inhibition of the AKT/ mTOR pathway [184]. Similarly, in NSCLC, PD-L1 influenced glycolysis through the PI3K/AKT and ERK pathways [185]. RNAi-based studies also revealed PD-L1's direct regulation of embryonic stem-cell transcription factors, including Octamer-binding protein 4 (OCT4), Nanog Homeobox (NANOG), and the stemness factor BMI1 Proto-Oncogene Polycomb Ring Finger (BMI1) [186,187]. The involvement of PD-L1 in autophagy remains controversial. In glioblastoma multiforme, elevated PD-L1 suppressed autophagy by facilitating AKT translocation to the plasma membrane [188], while in ovarian cancer, PD-L1 enhanced autophagy by upregulating Beclin 1 (BECN1) [189]. The multifaceted roles of PD-L1 and its involvement in intricate pathways across numerous cancer types underscore the need for further investigation to fully understand the potential non-immunological pro-oncogenic functions of PD-L1 in HCC.

An alternative interpretation suggests that the increase in unglycosylated forms of PD-L1 in HCC can represent an initial step for the subsequent PD-L1 maturation and membrane localization during advanced stages when further dysregulations may occur. The membrane localization of PD-L1 and its interaction with PD-1 plays a pivotal role in tumor immunosuppression by inhibiting T lymphocyte activation and enhancing immune tolerance, ultimately facilitating tumor immune escape [190]. Notably, a significant portion (68%) of the patients in our study were classified as BCLC 0/A, suggesting that they might not have yet localized the mature PD-L1 forms on the cell membrane.

The use of immune checkpoint inhibitors, particularly those targeting PD-L1, has become a common first-line treatment for patients with advanced HCC [1,19,191]. However, recent insights from the IMbrav050 trial have provided a new perspective on the application of immune checkpoint inhibitors in HCC. In the study, a total of 668 patients who underwent liver resection or ablation were enrolled. They were then divided into two groups: One received treatment with a combination of

atezolizumab and bevacizumab, while the other group underwent active surveillance. Notably, the study demonstrated the unprecedented efficacy of the atezolizumab and bevacizumab combination as a recurrence-suppressing therapy (recurrence of 32.9% and 39.8% for atezolizumab/bevacizumab and active surveillance, respectively) following curative therapy by resection or ablation, with an HR for DFS at the primary endpoint of 0.72 (CI95%: 0.56–0.93, p = 0.012) [192]. The obtained results indicate that immune checkpoint inhibitors may exhibit efficacy even in the early stages of the disease, despite the current absence of evidence elucidating the underlying molecular mechanisms.

Immunohistochemical assays utilizing a clinically approved antibody for tumor diagnosis across various cancer types (not HCC) showed a generally low PD-L1 expression in both HCC nodules and adjacent non-tumoral samples. The limited positivity observed in certain tissues was attributed to macrophage elements. This low detection is consistent with results from the THPA database, highlighting the crucial importance of using specific antibodies for accurate diagnostic assessments.

The disparity between immunohistochemical and western blot results in the present study may be attributed to the utilization of different antibodies designed to recognize distinct epitopes [193] (https://www.thermofisher.com). It is essential to highlight that false negatives in IHC assessments can occur, as evidenced in previous research, particularly due to extensive PD-L1 glycosylation. This glycosylation phenomenon has been estimated to impact approximately 50% of the samples, leading to the underestimation of PD-L1 levels [194].

A comprehensive immunohistochemical analysis involving a cohort of 453 HCC patients who underwent resection provided additional insights into the intricate patterns of PD-L1 expression. Notably, PD-L1 was absent in both tumor cells and macrophages in most patients (70.2%), with only 15.2% exhibiting PD-L1 expression in macrophages and 19.2% in tumor cells [195]. These findings highlight significant heterogeneity in PD-L1 expression within the patient population, questioning the efficacy of current anticancer treatments. Conflicting reports in the literature, indicating increased PD-L1 signals in HCC tumor samples compared to peritumoral normal tissues [196] or adjacent non-tumoral tissues [178], emphasize the necessity for expanded immunohistochemical assays across a broader spectrum of HCC cases.

Exploring the possible co-localization of PD-L1 and phosphorylated form (Thr288) of AURKA associated with the kinase activity is crucial, given the potential interplay between these molecules. Thus, comprehensive investigations are essential to unravel the multifaceted roles of PD-L1 in HCC and to elucidate its potential interactions with AURKA.

In this study, the analysis of *AURKA* expression in HCC and pre-tumor conditions revealed a gradual increase in mRNA expression as the disease progressed. *AURKA* expression positively correlated with several oncogenes, including *TPX2*, *PD-L1*, and *KRAS* in HCC patients. The correlation with *TPX2* and *PD-L1* persisted from precancerous conditions to malignancy, with both genes increasing with the progression of the disease.

Interestingly, AURKA protein levels were reduced in HCC tumor tissues, with the highest expression observed in steatotic tissues. However, within the tumor, the AURKA phosphorylated form (Thr288) was augmented, indicating increased kinase activity. At the protein level, the study found an increase in unglycosylated immature PD-L1 forms in tumor tissues. This suggests potential non-immunological pro-oncogenic functions of PD-L1 in HCC or can represent the initial step for subsequent membrane localization of PD-L1, promoting the immune escape of tumor cells. In HCC-derived JHH6 and Huh7 cell lines, AURKA was shown to regulate PD-L1 through multiple mechanisms. The kinase-mediated activity of AURKA on PD-L1 involves protein stabilization, while the presence of the AURKA protein, independently from its kinase activity, influenced PD-L1 transcription. Treatment with AK-01 decreased PD-L1 glycosylated mature forms, triggering a compensatory mechanism that promoted new AURKA transcription. Conversely, AURKA knockdown led to a decrease in *PD-L1* promoter activation, *PD-L1* mRNA, and newly translated PD-L1 forms.

Moreover, AURKA was found to play a crucial role in proper mitotic progression and cell division. As expected, *in vitro* the inhibition of AURKA with alisertib and AK-01, as well as AURKA silencing, resulted in centrosomal disorganization, defective mitotic spindle assembly, chromosome misalignments, impaired chromosome separation, and incomplete cytokinesis, leading to cell aneuploidy. However, the accumulation of multiple aberrations contributed to a progressive increase in cell death.

The findings from this study represent a significant advancement in our understanding of AURKA's role in HCC. The identified interplay between PD-L1 and AURKA not only deepens our comprehension of their interaction in HCC but also holds great promise for the development of more precise and effective therapeutic strategies. This approach, characterized by the concurrent targeting of multiple pathways implicated in HCC, has the potential to significantly improve treatment outcomes for patients affected by this challenging cancer.

Chapter 6 - Conclusions and future perspectives

HCC is a global health burden, with incidence and mortality rates projected to worsen over the years. Late-stage diagnoses and limited therapeutic options contribute to the complexity of managing this cancer, emphasizing the need for innovative approaches. While the recent advancements in combination treatments integrating oncogene-targeted therapies and immune checkpoint inhibitors are promising, the unique challenges of HCC warrant intensified translational research efforts.

This study represents a novelty in this field by focusing on AURKA, a pivotal kinase in mitosis, and deciphering its mRNA and protein expression dynamics during liver disease progression. We explored correlations with *TPX2*, an AURKA interactor, and the immune checkpoint *PD-L1*. Novel evidence uncovered opposing roles of AURKA in PD-L1 regulation, dependent on tumor type, underscoring the need for further investigation in HCC. Thus, we investigated the effects of AURKA inhibition and knockdown on mitosis and PD-L1 regulation, seeking potential therapeutic approaches.

Our findings revealed a gradual increase in *AURKA* mRNA during disease progression, suggesting its potential as a tissue biomarker for HCC diagnosis. AURKA protein expression displayed a different trend, peaking in pre-tumoral conditions, indicating a plausible role in fibrogenesis. Despite its lack of direct involvement in cell proliferation, the heightened AURKA kinase activity in tumors underscores its significance in HCC. This suggests the need for further analysis to comprehend the diverse roles of the kinase in the progression of the disease.

The AURKA inhibitor AK-01 exhibited superior efficacy over alisertib in reducing AURKA enzymatic activity *in vitro*, with cell subtype-specific responses. AURKA inhibition and silencing induced mitotic dysregulation, resulting in aneuploidy and increased cell mortality. Intriguingly, our study unveiled multiple regulation mechanisms of AURKA on PD-L1, possibly acting at transcriptional and post-translation levels, emphasizing the need for further exploration.

Consistent positive correlations between *AURKA* and *TPX2* or *PD-L1* throughout hepatocarcinogenesis pointed to potential interplays independently of disease progression. The additional correlations between *AURKA* and *KRAS* in HCC tissues hinted at additional complexities requiring in-depth exploration for therapeutic strategies.

Based on our findings and the emerging landscape of combination therapy in HCC management, it would be relevant to explore the combination of AURKA-targeted therapy with immune checkpoint

inhibitors like atezolizumab. This approach holds promise for enhanced therapeutic benefits by concurrently targeting multiple pathways implicated in HCC progression. This strategy can provide a more effective and personalized treatment approach, especially considering the existence of a possible feedback loop involving AURKA and PD-L1.

The assessment of combined treatments involving AK-01 and atezolizumab *in vitro* is a pivotal step in unraveling their impact on HCC progression. Our comprehensive plan aims to delve into the effects on tumor cell mortality and the modulation of immune effector molecules, specifically Perforin 1 (PRF-1) and Interleukin 2 (IL2), released by CD8+ T cells.

Atezolizumab, a monoclonal antibody targeting PD-L1, enhances T-cell activity against HCC cells by disrupting the PD-L1/PD-1 interaction. To simulate a physiological environment, our strategy involves establishing co-cultures encompassing various ratios of HCC-derived cells (JHH6 or Huh7) and peripheral blood mononuclear cells (PBMCs), including CD8+ T cells. These immune cells are recognized for their cytotoxic role in promoting apoptosis in target cells, mirroring the complex interplay within the immune microenvironment.

In our preliminary experiments, HCC-derived cells were exposed to atezolizumab in monocultures, employing a range of concentrations (25ng/ml to 400ng/ml) chosen based on prior experiments conducted with HCC-derived cell lines [197]. The observations made at 24 and 48 hours indicated no significant impact of atezolizumab on tumor cells (Figure 37.A-B). This initial assessment established the treatment conditions for further co-culture experiments designed to evaluate the efficacy of the combined treatments.

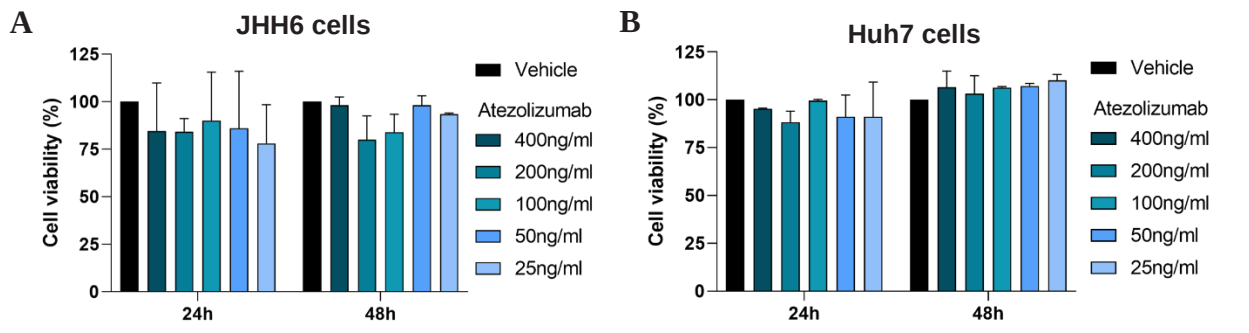

Figure 37. The effects of atezolizumab on cell viability *in vitro*. (A-B) Relative cell viability at 24h and 48h post-treatment with different concentrations of atezolizumab in (A) JHH6 and (B) Huh7 cells (n=2).

The upcoming co-culture experiments will offer a more comprehensive understanding of the dynamic interactions between AK-01 and atezolizumab, providing insights into their potential synergistic effects on tumor cells.

In conclusion, our study revealed the multifaceted roles of AURKA in the HCC progression, uncovering its potential as both a biomarker and a therapeutic target. The investigation into combination therapy with immune checkpoint inhibitors aligns with evolving trends in HCC management, offering a more effective and personalized approach for this challenging cancer. Future studies should delve deeper into the intricate molecular mechanisms and roles of AURKA in hepatocarcinogenesis, paving the way for innovative advancements in HCC treatment.

References

1 Llovet JM, Kelley RK, Villanueva A, Singal AG, Pikarsky E, Roayaie S, et al. Hepatocellular carcinoma. Nat Rev Dis Primers. 2021 Jan;7(1):1–28.

2 Rumgay H, Arnold M, Ferlay J, Lesi O, Cabasag CJ, Vignat J, et al. Global burden of primary liver cancer in 2020 and predictions to 2040. Journal of Hepatology. 2022 Dec;77(6):1598–606.

3 Mu X, Español-Suñer R, Mederacke I, Affò S, Manco R, Sempoux C, et al. Hepatocellular carcinoma originates from hepatocytes and not from the progenitor/biliary compartment. The Journal of Clinical Investigation. 2015 Oct;125(10):3891.

4 Yang JD, Hainaut P, Gores GJ, Amadou A, Plymoth A, Roberts LR. A global view of hepatocellular carcinoma: trends, risk, prevention and management. Nat Rev Gastroenterol Hepatol. 2019 Oct;16(10):589–604.

5 Gomez-Quiroz LE, Roman S. Influence of genetic and environmental risk factors in the development of hepatocellular carcinoma in Mexico. Ann Hepatol. 2022 Jan;27 Suppl 1:100649.

6 Eslam M, Sanyal AJ, George J, Sanyal A, Neuschwander-Tetri B, Tiribelli C, et al. MAFLD: A Consensus-Driven Proposed Nomenclature for Metabolic Associated Fatty Liver Disease. Gastroenterology. 2020 May;158(7):1999-2014.e1.

7 Rinella ME, Lazarus JV, Ratziu V, Francque SM, Sanyal AJ, Kanwal F, et al. A multisociety Delphi consensus statement on new fatty liver disease nomenclature. Hepatology. 2023;10.1097/HEP.0000000000000520.

8 McGlynn KA, Petrick JL, El-Serag HB. Epidemiology of Hepatocellular Carcinoma. Hepatology. 2021 Jan;73(Suppl 1):4–13.

9 Craig AJ, von Felden J, Garcia-Lezana T, Sarcognato S, Villanueva A. Tumour evolution in hepatocellular carcinoma. Nat Rev Gastroenterol Hepatol. 2020 Mar;17(3):139–52.

10 Du R, Huang C, Liu K, Li X, Dong Z. Targeting AURKA in Cancer: molecular mechanisms and opportunities for Cancer therapy. Molecular Cancer. 2021 Jan;20(1):15.

11 Giraud J, Chalopin D, Blanc J-F, Saleh M. Hepatocellular Carcinoma Immune Landscape and the Potential of Immunotherapies. Frontiers in Immunology. 2021 [cited 2023 Jan 5]. ;12. Available from: https://www.frontiersin.org/articles/10.3389/fimmu.2021.655697

12 Wu B, Sodji QH, Oyelere AK. Inflammation, Fibrosis and Cancer: Mechanisms, Therapeutic Options and Challenges. Cancers. 2022 Jan;14(3):552.

13 Baglieri J, Brenner DA, Kisseleva T. The Role of Fibrosis and Liver-Associated Fibroblasts in the Pathogenesis of Hepatocellular Carcinoma. Int J Mol Sci. 2019 Apr;20(7):1723.

14 Yang JD, Heimbach JK. New advances in the diagnosis and management of hepatocellular carcinoma. BMJ. 2020 Oct;371:m3544.

15 Yang JD, Addissie BD, Mara KC, Harmsen WS, Dai J, Zhang N, et al. GALAD Score for Hepatocellular Carcinoma Detection in Comparison to Liver Ultrasound and Proposal of GALADUS Score. Cancer Epidemiol Biomarkers Prev. 2019 Mar;28(3):531–8.

16 Guan M-C, Zhang S-Y, Ding Q, Li N, Fu T-T, Zhang G-X, et al. The Performance of GALAD Score for Diagnosing Hepatocellular Carcinoma in Patients with Chronic Liver Diseases: A Systematic Review and Meta-Analysis. J Clin Med. 2023 Jan;12(3):949.

17 Piñero F, Silva M, Iavarone M. Sequencing of systemic treatment for hepatocellular carcinoma: Second line competitors. World J Gastroenterol. 2020 Apr;26(16):1888–900.

18 Galle PR, Forner A, Llovet JM, Mazzaferro V, Piscaglia F, Raoul J-L, et al. EASL Clinical Practice Guidelines: Management of hepatocellular carcinoma. Journal of Hepatology. 2018 Jul;69(1):182–236.

19 Reig M, Forner A, Rimola J, Ferrer-Fàbrega J, Burrel M, Garcia-Criado Á, et al. BCLC strategy for prognosis prediction and treatment recommendation: The 2022 update. Journal of Hepatology. 2022 Mar;76(3):681–93.

20 Kudo M, Finn RS, Galle PR, Zhu AX, Ducreux M, Cheng A-L, et al. IMbrave150: Efficacy and Safety of Atezolizumab plus Bevacizumab versus Sorafenib in Patients with Barcelona Clinic Liver Cancer Stage B Unresectable Hepatocellular Carcinoma: An Exploratory Analysis of the Phase III Study. Liver Cancer. 2022 Nov;12(3):238–50.

21 Ando Y, Kawaoka T, Kosaka M, Shirane Y, Johira Y, Miura R, et al. Early Tumor Response and Safety of Atezolizumab Plus Bevacizumab for Patients with Unresectable Hepatocellular Carcinoma in Real-World Practice. Cancers (Basel). 2021 Aug;13(16):3958.

22 Daassi D, Mahoney KM, Freeman GJ. The importance of exosomal PDL1 in tumour immune evasion. Nat Rev Immunol. 2020 Apr;20(4):209–15.

23 Bergholz JS, Wang Q, Kabraji S, Zhao JJ. Integrating immunotherapy and targeted therapy in cancer treatment: mechanistic insights and clinical implications. Clin Cancer Res. 2020 Nov;26(21):5557–66.

24 Abou-Alfa GK, Lau G, Kudo M, Chan SL, Kelley RK, Furuse J, et al. Tremelimumab plus Durvalumab in Unresectable Hepatocellular Carcinoma. NEJM Evidence. 2022 Jul;1(8):EVIDoa2100070.

25 Mou PK, Yang EJ, Shi C, Ren G, Tao S, Shim JS. Aurora kinase A, a synthetic lethal target for precision cancer medicine. Exp Mol Med. 2021 May;53(5):835–47.

26 Machado CB, Da Silva EL, Dias Nogueira BM, Da Silva JBS, De Moraes Filho MO, Montenegro RC, et al. The Relevance of Aurora Kinase Inhibition in Hematological Malignancies. Cancer Diagn Progn. 2021 Jul;1(3):111–26.

27 Willems E, Dedobbeleer M, Digregorio M, Lombard A, Lumapat PN, Rogister B. The functional diversity of Aurora kinases: a comprehensive review. Cell Division. 2018 Sep;13(1):7.

28 Ma HT, Poon RYC. Aurora kinases and DNA damage response. Mutation Research/Fundamental and Molecular Mechanisms of Mutagenesis. 2020 May;821:111716.

29 Tang A, Gao K, Chu L, Zhang R, Yang J, Zheng J. Aurora kinases: novel therapy targets in cancers. Oncotarget. 2017 Jan;8(14):23937–54.

30 Cacioppo R, Lindon C. Regulating the regulator: a survey of mechanisms from transcription to translation controlling expression of mammalian cell cycle kinase Aurora A. Open Biology. 2022 Sep;12(9):220134.

31 Littlepage LE, Wu H, Andresson T, Deanehan JK, Amundadottir LT, Ruderman JV. Identification of phosphorylated residues that affect the activity of the mitotic kinase Aurora-A. Proc Natl Acad Sci U S A. 2002 Nov;99(24):15440–5.

32 Walter AO, Seghezzi W, Korver W, Sheung J, Lees E. The mitotic serine/threonine kinase Aurora2/AIK is regulated by phosphorylation and degradation. Oncogene. 2000 Oct;19(42):4906–16.

33 Gustafson WC, Meyerowitz JG, Nekritz EA, Chen J, Benes C, Charron E, et al. Drugging MYCN through an Allosteric Transition in Aurora Kinase A. Cancer Cell. 2014 Sep;26(3):414–27.

34 Janeček M, Rossmann M, Sharma P, Emery A, Huggins DJ, Stockwell SR, et al. Allosteric modulation of AURKA kinase activity by a small-molecule inhibitor of its protein-protein interaction with TPX2. Sci Rep. 2016 Jun;6(1):28528.

35 Yan M, Wang C, He B, Yang M, Tong M, Long Z, et al. Aurora-A Kinase: A Potent Oncogene and Target for Cancer Therapy. Medicinal Research Reviews. 2016;36(6):1036–79.

36 Tanaka M, Ueda A, Kanamori H, Ideguchi H, Yang J, Kitajima S, et al. Cell-cycle-dependent Regulation of Human aurora A Transcription Is Mediated by Periodic Repression of E4TF1 *. Journal of Biological Chemistry. 2002 Mar;277(12):10719–26.

37 Marumoto T, Hirota T, Morisaki T, Kunitoku N, Zhang D, Ichikawa Y, et al. Roles of aurora-A kinase in mitotic entry and G2 checkpoint in mammalian cells. Genes to Cells. 2002;7(11):1173–82.

38 Müller GA, Wintsche A, Stangner K, Prohaska SJ, Stadler PF, Engeland K. The CHR site: definition and genome-wide identification of a cell cycle transcriptional element. Nucleic Acids Research. 2014 Sep;42(16):10331–50.

39 Hirota T, Kunitoku N, Sasayama T, Marumoto T, Zhang D, Nitta M, et al. Aurora-A and an Interacting Activator, the LIM Protein Ajuba, Are Required for Mitotic Commitment in Human Cells. Cell. 2003 Sep;114(5):585–98.

40 Kufer TA, Silljé HHW, Körner R, Gruss OJ, Meraldi P, Nigg EA. Human TPX2 is required for targeting Aurora-A kinase to the spindle. The Journal of Cell Biology. 2002 Aug;158(4):617.

41 Hutterer A, Berdnik D, Wirtz-Peitz F, Žigman M, Schleiffer A, Knoblich JA. Mitotic Activation of the Kinase Aurora-A Requires Its Binding Partner Bora. Developmental Cell. 2006 Aug;11(2):147–57.

42 Liu Q, Ruderman JV. Aurora A, mitotic entry, and spindle bipolarity. Proceedings of the National Academy of Sciences. 2006 Apr;103(15):5811–6.

43 Zheng F, Yue C, Li G, He B, Cheng W, Wang X, et al. Nuclear AURKA acquires kinase-independent transactivating function to enhance breast cancer stem cell phenotype. Nat Commun. 2016 Jan;7(1):10180.

44 Wang G, Jiang Q, Zhang C. The role of mitotic kinases in coupling the centrosome cycle with the assembly of the mitotic spindle. Journal of Cell Science. 2014 Oct;127(19):4111–22.

45 Brodie KM, Henderson BR. Characterization of BRCA1 Protein Targeting, Dynamics, and Function at the Centrosome. J Biol Chem. 2012 Mar;287(10):7701–16.

46 Terada Y, Uetake Y, Kuriyama R. Interaction of Aurora-A and centrosomin at the microtubule-nucleating site in Drosophila and mammalian cells. J Cell Biol. 2003 Sep;162(5):757–64.

47 Hsu L-C, White RL. BRCA1 is associated with the centrosome during mitosis. Proc Natl Acad Sci U S A. 1998 Oct;95(22):12983–8.

48 Floyd S, Pines J, Lindon C. APC/CCdh1 Targets Aurora Kinase to Control Reorganization of the Mitotic Spindle at Anaphase. Current Biology. 2008 Nov;18(21):1649–58.

49 Abdelbaki A, Akman HB, Poteau M, Grant R, Gavet O, Guarguaglini G, et al. AURKA destruction is decoupled from its activity at mitotic exit but is essential to suppress interphase activity. J Cell Sci. 2020 Jun;133(12):jcs243071.

50 Castro A, Arlot-Bonnemains Y, Vigneron S, Labbé J-C, Prigent C, Lorca T. APC/Fizzy-Related targets Aurora-A kinase for proteolysis. EMBO Rep. 2002 May;3(5):457–62.

51 Lindon C, Grant R, Min M. Ubiquitin-Mediated Degradation of Aurora Kinases. Frontiers in Oncology. 2016 [cited 2023 Jul 13]. ;5. Available from: https://www.frontiersin.org/articles/10.3389/fonc.2015.00307

52 Matsumoto ML, Wickliffe KE, Dong KC, Yu C, Bosanac I, Bustos D, et al. K11-Linked Polyubiquitination in Cell Cycle Control Revealed by a K11 Linkage-Specific Antibody. Molecular Cell. 2010 Aug;39(3):477–84.

53 Castro A, Vigneron S, Bernis C, Labbé J-C, Prigent C, Lorca T. The D-Box-activating domain (DAD) is a new proteolysis signal that stimulates the silent D-Box sequence of Aurora-A. EMBO Rep. 2002 Dec;3(12):1209–14.

54 Bertolin G, Tramier M. Insights into the non-mitotic functions of Aurora kinase A: more than just cell division. Cell Mol Life Sci. 2020 Mar;77(6):1031–47.

55 Naso FD, Boi D, Ascanelli C, Pamfil G, Lindon C, Paiardini A, et al. Nuclear localisation of Aurora-A: its regulation and significance for Aurora-A functions in cancer. Oncogene. 2021;40(23):3917–28.

56 Kitajima S, Kudo Y, Ogawa I, Tatsuka M, Kawai H, Pagano M, et al. Constitutive Phosphorylation of Aurora-A on Ser51 Induces Its Stabilization and Consequent Overexpression in Cancer. PLOS ONE. 2007 set;2(9):e944.

57 Ballabeni A, Melixetian M, Zamponi R, Masiero L, Marinoni F, Helin K. Human Geminin promotes pre-RC formation and DNA replication by stabilizing CDT1 in mitosis. The EMBO Journal. 2004 Aug;23(15):3122–32.

58 Tsunematsu T, Takihara Y, Ishimaru N, Pagano M, Takata T, Kudo Y. Aurora-A controls pre-replicative complex assembly and DNA replication by stabilizing geminin in mitosis. Nat Commun. 2013 May;4(1):1885.

59 Pugacheva EN, Jablonski SA, Hartman TR, Henske EP, Golemis EA. HEF1-Dependent Aurora A Activation Induces Disassembly of the Primary Cilium. Cell. 2007 Jun;129(7):1351–63.

60 Sánchez I, Dynlacht BD. Cilium assembly and disassembly. Nat Cell Biol. 2016 Jun;18(7):711–7.

61 Grzenda A, Leonard P, Seo S, Mathison AJ, Urrutia G, Calvo E, et al. Functional impact of Aurora A-mediated phosphorylation of HP1γ at serine 83 during cell cycle progression. Epigenetics & Chromatin. 2013 Jul;6(1):21.

62 Wike CL, Graves HK, Hawkins R, Gibson MD, Ferdinand MB, Zhang T, et al. Aurora-A mediated histone H3 phosphorylation of threonine 118 controls condensin I and cohesin occupancy in mitosis. Elife. 2016 Feb;5:e11402.

63 Kim S-R, Kim K-B, Chae Y-C, Park JW, Seo S-B. H3S10 phosphorylation-mediated transcriptional regulation by Aurora kinase A. Biochem Biophys Res Commun. 2016 Jan;469(1):22–8.

64 Bertolin G, Bulteau A-L, Alves-Guerra M-C, Burel A, Lavault M-T, Gavard O, et al. Aurora kinase A localises to mitochondria to control organelle dynamics and energy production. Elife. 2018 Aug;7:e38111.

65 Kashatus DF, Lim K-H, Brady DC, Pershing NLK, Cox AD, Counter CM. RALA and RALBP1 regulate mitochondrial fission at mitosis. Nat Cell Biol. 2011 Sep;13(9):1108–15.

66 Nikonova AS, Astsaturov I, Serebriiskii IG, Dunbrack RL, Golemis EA. Aurora-A kinase (AURKA) in normal and pathological cell growth. Cell Mol Life Sci. 2013 Feb;70(4):661–87.

67 Mori D, Yamada M, Mimori-Kiyosue Y, Shirai Y, Suzuki A, Ohno S, et al. An essential role of the aPKC–Aurora A–NDEL1 pathway in neurite elongation by modulation of microtubule dynamics. Nat Cell Biol. 2009 Sep;11(9):1057–68.

68 Lefkowitz GK, Gleeson JG. Aurora A moonlights in neurite extension. Nat Cell Biol. 2009 Sep;11(9):1053–4.

69 Jeng Y-M, Peng S-Y, Lin C-Y, Hsu H-C. Overexpression and Amplification of Aurora-A in Hepatocellular Carcinoma. Clinical Cancer Research. 2004 Mar;10(6):2065–71.

70 Wang B, Hsu C-J, Chou C-H, Lee H-L, Chiang W-L, Su C-M, et al. Variations in the AURKA Gene: Biomarkers for the Development and Progression of Hepatocellular Carcinoma. Int J Med Sci. 2018 Jan;15(2):170–5.

71 Huang C-H, Chen C-J, Chen P-N, Wang S-S, Chou Y-E, Hung S-C, et al. Impacts of AURKA Genetic Polymorphism on Urothelial Cell Carcinoma Development. J Cancer. 2019 Feb;10(6):1370–4.

72 Su Z-L, Su C-W, Huang Y-L, Yang W-Y, Sampurna BP, Ouchi T, et al. A Novel AURKA Mutant-Induced Early-Onset Severe Hepatocarcinogenesis Greater than Wild-Type via Activating Different Pathways in Zebrafish. Cancers. 2019 Jul;11(7):927.

73 Fadaka AO, Sibuyi NRS, Madiehe AM, Meyer M. MicroRNA-based regulation of Aurora A kinase in breast cancer. Oncotarget. 2020 Nov;11(46):4306–24.

74 Liu R, Jiang Z, Kong W, Zheng S, Dai T, Wang G. A Novel Nine-Gene Signature Associated With Immune Infiltration for Predicting Prognosis in Hepatocellular Carcinoma. Frontiers in Genetics. 2021 [cited 2023 Apr 7]. ;12. Available from: https://www.frontiersin.org/articles/10.3389/fgene.2021.730732

75 Guo J, Li W, Cheng L, Gao X. Identification and Validation of Hub Genes with Poor Prognosis in Hepatocellular Carcinoma by Integrated Bioinformatical Analysis. Int J Gen Med. 2022 Apr;15:3933–41.

76 Guo L, Wang Z, Du Y, Mao J, Zhang J, Yu Z, et al. Random-forest algorithm based biomarkers in predicting prognosis in the patients with hepatocellular carcinoma. Cancer Cell Int. 2020 Jun;20:251.

77 Xu L, Tong T, Wang Z, Qiang Y, Ma F, Ma X. Identification of Hub Genes and Analysis of Prognostic Values in Hepatocellular Carcinoma by Bioinformatics Analysis. The American Journal of the Medical Sciences. 2020 Apr;359(4):226–34.

78 Meng Z, Wu J, Liu X, Zhou W, Ni M, Liu S, et al. Identification of potential hub genes associated with the pathogenesis and prognosis of hepatocellular carcinoma via integrated bioinformatics analysis. J Int Med Res. 2020 Jul;48(7):0300060520910019.

79 Yang T, Chen Y, Xu J, Li J, Liu H, Liu N. Bioinformatics screening the novel and promising targets of curcumin in hepatocellular carcinoma chemotherapy and prognosis. BMC Complement Med Ther. 2022 Jan;22:21.

80 Yang Z, Wu X, Li J, Zheng Q, Niu J, Li S. CCNB2, CDC20, AURKA, TOP2A, MELK, NCAPG, KIF20A, UBE2C, PRC1, and ASPM May Be Potential Therapeutic Targets for Hepatocellular Carcinoma Using Integrated Bioinformatic Analysis. IJGM. 2021 Dec;Volume 14:10185–94.

81 Su W-L, Chuang S-C, Wang Y-C, Chen L-A, Huang J-W, Chang W-T, et al. Expression of FOXM1 and Aurora-A predicts prognosis and sorafenib efficacy in patients with hepatocellular carcinoma. CBM. 2020 Jul;28(3):341–50.

82 Xie W, Wang B, Wang X, Hou D, Su H, Huang H. Nine hub genes related to the prognosis of HBV-positive hepatocellular carcinoma identified by protein interaction analysis. Ann Transl Med. 2020 Apr;8(7):478.

83 Ji Y, Yin Y, Zhang W. Integrated Bioinformatic Analysis Identifies Networks and Promising Biomarkers for Hepatitis B Virus-Related Hepatocellular Carcinoma. Int J Genomics. 2020;2020:2061024.

84 Zhang Y, Tang Y, Guo C, Li G. Integrative analysis identifies key mRNA biomarkers for diagnosis, prognosis, and therapeutic targets of HCV-associated hepatocellular carcinoma. Aging (Albany NY). 2021 May;13(9):12865–95.

85 Li C, Ding J, Mei J. Comprehensive Analysis of Epigenetic Associated Genes on Differential Gene Expression and Prognosis in Hepatocellular Carcinoma. J Environ Pathol Toxicol Oncol. 2022;41(1):27–43.

86 Zhang L, Makamure J, Zhao D, Liu Y, Guo X, Zheng C, et al. Bioinformatics analysis reveals meaningful markers and outcome predictors in HBV-associated hepatocellular carcinoma. Exp Ther Med. 2020 Jul;20(1):427–35.

87 Hao J, Peng Q, Wang K, Yu G, Pan Y, Du X, et al. Antitumor Effect of Lenvatinib Combined with Alisertib in Hepatocellular Carcinoma by Targeting the DNA Damage Pathway. Biomed Res Int. 2021 Jul;2021:6613439.

88 Shen Z, Yin L, Zhou H, Ji X, Jiang C, Zhu X, et al. Combined inhibition of AURKA and HSF1 suppresses proliferation and promotes apoptosis in hepatocellular carcinoma by activating endoplasmic reticulum stress. Cell Oncol. 2021 Oct;44(5):1035–49.

89 Liu F, Wang G, Wang X, Che Z, Dong W, Guo X, et al. Targeting high Aurora kinases expression as an innovative therapy for hepatocellular carcinoma. Oncotarget. 2017 Mar;8(17):27953–65.

90 Chen C, Song G, Xiang J, Zhang H, Zhao S, Zhan Y. AURKA promotes cancer metastasis by regulating epithelial-mesenchymal transition and cancer stem cell properties in hepatocellular carcinoma. Biochemical and Biophysical Research Communications. 2017 Apr;486(2):514–20.

91 Li G, Tian Y, Gao Z. The role of AURKA/miR-199b-3p in hepatocellular carcinoma cells. Clinical Laboratory Analysis. 2022 Dec;36(12). DOI: 10.1002/jcla.24758

92 Hanahan D, Weinberg RA. The Hallmarks of Cancer. Cell. 2000 Jan;100(1):57–70.

93 Donnella HJ, Webber JT, Levin RS, Camarda R, Momcilovic O, Bayani N, et al. Kinome rewiring reveals AURKA limits PI3K-pathway inhibitor efficacy in breast cancer. Nat Chem Biol. 2018 Aug;14(8):768–77.

94 Yin Y, Kong D, He K, Xia Q. Aurora kinase A regulates liver regeneration through macrophages polarization and Wnt/β-catenin signalling. Liver International. 2021 Feb;42(2):468–78.

95 Lu L, Han H, Tian Y, Li W, Zhang J, Feng M, et al. Aurora kinase A mediates c-Myc's oncogenic effects in hepatocellular carcinoma: A c-Myc-AURKA FEEDBACK LOOP IN HEPATOCARCINOGENESIS. Mol Carcinog. 2015 Nov;54(11):1467–79.

96 Wu M, Zhou Y, Fei C, Chen T, Yin X, Zhang L, et al. ID1 overexpression promotes HCC progression by amplifying the AURKA/Myc signaling pathway. Int J Oncol. 2020 Jul;57(3):845–57.

97 Cui S-Y, Huang J-Y, Chen Y-T, Song H-Z, Huang G-C, De W, et al. The role of Aurora A in hypoxia-inducible factor 1α-promoting malignant phenotypes of hepatocelluar carcinoma. Cell Cycle. 2013 Sep;12(17):2849–66.

98 Shen H-M, Zhang D, Xiao P, Qu B, Sun Y-F. E2F1-mediated KDM4A-AS1 up-regulation promotes EMT of hepatocellular carcinoma cells by recruiting ILF3 to stabilize AURKA mRNA. Cancer Gene Ther. 2023 Jul;30(7):1007–17.

99 Luedde T, Schwabe RF. NF-κB in the liver—linking injury, fibrosis and hepatocellular carcinoma. Nat Rev Gastroenterol Hepatol. 2011 Feb;8(2):108–18.

100 Briassouli P, Chan F, Savage K, Reis-Filho JS, Linardopoulos S. Aurora-A regulation of nuclear factor-kappaB signaling by phosphorylation of IkappaBalpha. Cancer Res. 2007 Feb;67(4):1689–95.

101 Zhang K, Chen J, Chen D, Huang J, Feng B, Han S, et al. Aurora-A promotes chemoresistance in hepatocelluar carcinoma by targeting NF-kappaB/microRNA-21/PTEN signaling pathway. Oncotarget. 2014 Dec;5(24):12916–35.

102 Liu P, Han B, Zhang Y, Wang X. Network Pharmacology-Based Strategy to Investigate the Mechanisms of Lenvatinib in the Treatment of Hepatocellular Carcinoma. Comput Intell Neurosci. 2022;2022:7102500.

103 Burgess SG, Oleksy A, Cavazza T, Richards MW, Vernos I, Matthews D, et al. Allosteric inhibition of Aurora-A kinase by a synthetic vNAR domain. Open Biol. 2016 Jul;6(7):160089.

104 Rawson TE, Rüth M, Blackwood E, Burdick D, Corson L, Dotson J, et al. A Pentacyclic Aurora Kinase Inhibitor (AKI-001) with High in Vivo Potency and Oral Bioavailability. J Med Chem. 2008 Aug;51(15):4465–75.

105 Yu T, Tagat JR, Kerekes AD, Doll RJ, Zhang Y, Xiao Y, et al. Discovery of a Potent, Injectable Inhibitor of Aurora Kinases Based on the Imidazo-[1,2-a]-Pyrazine Core. ACS Med Chem Lett. 2010 Aug;1(5):214–8.

106 Hsu YC, Coumar MS, Wang W-C, Shiao H-Y, Ke Y-Y, Lin W-H, et al. Discovery of BPR1K871, a quinazoline based, multi-kinase inhibitor for the treatment of AML and solid tumors: Rational design, synthesis, in vitro and in vivo evaluation. Oncotarget. 2016 Dec;7(52):86239–56.

107 Manfredi MG, Ecsedy JA, Chakravarty A, Silverman L, Zhang M, Hoar KM, et al. Characterization of Alisertib (MLN8237), an Investigational Small-Molecule Inhibitor of Aurora A Kinase Using Novel *In Vivo* Pharmacodynamic Assays. Clinical Cancer Research. 2011 Dec;17(24):7614–24.

108 Zhu Q, Yu X, Zhou Z-W, Zhou C, Chen X-W, Zhou S-F. Inhibition of Aurora A Kinase by Alisertib Induces Autophagy and Cell Cycle Arrest and Increases Chemosensitivity in Human Hepatocellular Carcinoma HepG2 Cells. CCDT. 2017 Apr;17(4):386–401.

109 Ren B-J, Zhou Z-W, Zhu D-J, Ju Y-L, Wu J-H, Ouyang M-Z, et al. Alisertib Induces Cell Cycle Arrest, Apoptosis, Autophagy and Suppresses EMT in HT29 and Caco-2 Cells. IJMS. 2015 Dec;17(1):41.

110 Mossé YP, Fox E, Teachey DT, Reid JM, Safgren SL, Carol H, et al. A Phase II Study of Alisertib in Children with Recurrent/Refractory Solid Tumors or Leukemia: Children's Oncology Group Phase I and Pilot Consortium (ADVL0921). Clinical Cancer Research. 2019 Jun;25(11):3229–38.

111 O'Connor OA, Özcan M, Jacobsen ED, Roncero JM, Trotman J, Demeter J, et al. Randomized Phase III Study of Alisertib or Investigator's Choice (Selected Single Agent) in Patients With Relapsed or Refractory Peripheral T-Cell Lymphoma. JCO. 2019 Mar;37(8):613–23.

112 Hahn NM, Sarantopoulos J, Higano C, Zhou X, Zhang B, Leonard EJ, et al. MLN8237 (ALISERTIB), An Investigational Aurora a Kinase (AAK) Inhibitor, in Patients with Advanced Solid Tumors Including Castration-Resistant Prostate Cancer (CRPC) Receiving a Standard Docetaxel Regimen: Preliminary Phase 1 Results. Annals of Oncology. 2012 Sep;23:ix303–4.

113 Sehdev V, Katsha A, Ecsedy J, Zaika A, Belkhiri A, El-Rifai W. The combination of alisertib, an investigational Aurora kinase A inhibitor, and docetaxel promotes cell death and reduces tumor growth in preclinical cell models of upper gastrointestinal adenocarcinomas: Alisertib & Docetaxel Inhibit Tumor Growth. Cancer. 2013 Feb;119(4):904–14.

114 Falchook G, Coleman RL, Roszak A, Behbakht K, Matulonis U, Ray-Coquard I, et al. Alisertib in Combination With Weekly Paclitaxel in Patients With Advanced Breast Cancer or Recurrent Ovarian Cancer: A Randomized Clinical Trial. JAMA Oncol. 2019 Jan;5(1):e183773.

115 Du J, Yan L, Torres R, Gong X, Bian H, Marugán C, et al. Aurora A–Selective Inhibitor LY3295668 Leads to Dominant Mitotic Arrest, Apoptosis in Cancer Cells, and Shows Potent Preclinical Antitumor Efficacy. Mol Cancer Ther. 2019 Dec;18(12):2207–19.

116 Gong X, Du J, Parsons SH, Merzoug FF, Webster Y, Iversen PW, et al. Aurora A Kinase Inhibition Is Synthetic Lethal with Loss of the RB1 Tumor Suppressor Gene. Cancer Discov. 2019 Feb;9(2):248–63.

117 Sun S, Zhou W, Li X, Peng F, Yan M, Zhan Y, et al. Nuclear Aurora kinase A triggers programmed death-ligand 1-mediated immune suppression by activating MYC transcription in triple-negative breast cancer. Cancer Commun (Lond). 2021 Jul;41(9):851–66.

118 Takchi A, Haddad TC. Effect of DUAL pharmacological blockade of AURKA and PD-L1 pathways on plasticity and metastasis for triple negative breast cancer. JCO. 2023 Jun;41(16_suppl):e13100–e13100.

119 Meng B, Zhao X, Jiang S, Xu Z, Li S, Wang X, et al. AURKA inhibitor-induced PD-L1 upregulation impairs antitumor immune responses. Front Immunol. 2023;14:1182601.

120 Wang X, Huang J, Liu F, Yu Q, Wang R, Wang J, et al. Aurora A kinase inhibition compromises its antitumor efficacy by elevating PD-L1 expression. J Clin Invest. 2023 May;133(9). DOI: 10.1172/JCI161929

121 Katsha A, Arras J, Soutto M, Belkhiri A, El-Rifai W. AURKA regulates JAK2–STAT3 activity in human gastric and esophageal cancers. Mol Oncol. 2014 Dec;8(8):1419–28.

122 Islam B, Yu H-Y, Duan T-Q, Pan J, Li M, Zhang R-Q, et al. Cell cycle kinases (AUKA, CDK1, PLK1) are prognostic biomarkers and correlated with tumor-infiltrating leukocytes in HBV related HCC. Journal of Biomolecular Structure and Dynamics. 2023 Jan;0(0):1–17.

123 Chen H, Wu J, Lu L, Hu Z, Li X, Huang L, et al. Identification of Hub Genes Associated With Immune Infiltration and Predict Prognosis in Hepatocellular Carcinoma via Bioinformatics Approaches. Front Genet. 2020;11:575762.

124 Kleiner DE, Brunt EM, Van Natta M, Behling C, Contos MJ, Cummings OW, et al. Design and validation of a histological scoring system for nonalcoholic fatty liver disease. Hepatology. 2005 Jun;41(6):1313–21.

125 Chisari FV, Klopchin K, Moriyama T, Pasquinelli C, Dunsford HA, Sell S, et al. Molecular pathogenesis of hepatocellular carcinoma in hepatitis B virus transgenic mice. Cell. 1989 Dec;59(6):1145–56.

126 Caruso S, Calatayud A-L, Pilet J, La Bella T, Rekik S, Imbeaud S, et al. Analysis of Liver Cancer Cell Lines Identifies Agents With Likely Efficacy Against Hepatocellular Carcinoma and Markers of Response. Gastroenterology. 2019 Sep;157(3):760–76.

127 Das BK, Kannan A, Nguyen Q, Gogoi J, Zhao H, Gao L. Selective Inhibition of Aurora Kinase A by AK-01/LY3295668 Attenuates MCC Tumor Growth by Inducing MCC Cell Cycle Arrest and Apoptosis. Cancers (Basel). 2021 Jul;13(15):3708.

128 Numata Y, Akutsu N, Ishigami K, Koide H, Wagatsuma K, Motoya M, et al. Synergistic effect of IFN-γ and IL-1β on PD-L1 expression in hepatocellular carcinoma. Biochem Biophys Rep. 2022 Jul;30:101270.

129 Bustin SA, Benes V, Garson JA, Hellemans J, Huggett J, Kubista M, et al. The MIQE guidelines: minimum information for publication of quantitative real-time PCR experiments. Clin Chem. 2009 Apr;55(4):611–22.

130 Li C-W, Lim S-O, Xia W, Lee H-H, Chan L-C, Kuo C-W, et al. Glycosylation and stabilization of programmed death ligand-1 suppresses T-cell activity. Nat Commun. 2016 Aug;7(1):12632.

131 Li C-W, Lim S-O, Chung EM, Kim Y-S, Park AH, Yao J, et al. Eradication of triple negative breast cancer cells by targeting glycosylated PD-L1. Cancer Cell. 2018 Feb;33(2):187-201.e10.

132 Young S, Sanghvi T, Lake JJ, Rubin N, Golzarian J. Predicting post-transarterial chemoembolization outcomes: A comparison of direct and total bilirubin serums levels. Diagnostic and Interventional Imaging. 2020 Jun;101(6):355–64.

133 Guerra Ruiz AR, Crespo J, López Martínez RM, Iruzubieta P, Casals Mercadal G, Lalana Garcés M, et al. Measurement and clinical usefulness of bilirubin in liver disease. Adv Lab Med. 2(3):352–61.

134 Wang Y, Dong F, Sun S, Wang X, Zheng X, Huang Y, et al. Increased INR Values Predict Accelerating Deterioration and High Short-Term Mortality Among Patients Hospitalized With Cirrhosis or Advanced Fibrosis. Front Med (Lausanne). 2021 Nov;8:762291.

135 Shah KN, Bhatt R, Rotow J, Rohrberg J, Olivas V, Wang VE, et al. Aurora kinase A drives the evolution of resistance to third generation EGFR inhibitors in lung cancer. Nat Med. 2019 Jan;25(1):111–8.

136 Caputo E, Miceli R, Motti ML, Taté R, Fratangelo F, Botti G, et al. AurkA inhibitors enhance the effects of B-RAF and MEK inhibitors in melanoma treatment. J Transl Med. 2014 Jul;12:216.

137 Umstead M, Xiong J, Qi Q, Du Y, Fu H. Aurora kinase A interacts with H-Ras and potentiates Ras-MAPK signaling. Oncotarget. 2017 Apr;8(17):28359–72.

138 Wang-Bishop L, Chen Z, Gomaa A, Lockhart AC, Salaria S, Wang J, et al. Inhibition of AURKA Reduces Proliferation and Survival of Gastrointestinal Cancer Cells With Activated KRAS by Preventing Activation of RPS6KB1. Gastroenterology. 2019 Feb;156(3):662-675.e7.

139 Dar AA, Belkhiri A, El-Rifai W. The Aurora kinase A Regulates GSK-3β in Gastric Cancer Cells. Oncogene. 2009 Feb;28(6):866–75.

140 Li Y, Li X, Pu J, Yang Q, Guan H, Ji M, et al. c-Myc Is a Major Determinant for Antitumor Activity of Aurora A Kinase Inhibitor MLN8237 in Thyroid Cancer. Thyroid. 2018 Dec;28(12):1642–54.

141 Li L, Song Y, Liu Q, Liu X, Wang R, Kang C, et al. Low expression of PTEN is essential for maintenance of a malignant state in human gastric adenocarcinoma via upregulation of p-AURKA mediated by activation of AURKA. Int J Mol Med. 2018 Jun;41(6):3629–41.

142 Wu J, Yang L, Shan Y, Cai C, Wang S, Zhang H. AURKA promotes cell migration and invasion of head and neck squamous cell carcinoma through regulation of the AURKA/Akt/FAK signaling pathway. Oncol Lett. 2016 Mar;11(3):1889–94.

143 Jin X, Wang J, Zou S, Xu R, Cao J, Zhang Y, et al. Cinobufagin Triggers Defects in Spindle Formation and Cap-Dependent Translation in Liver Cancer Cells by Inhibiting the AURKA-mTOR-eIF4E Axis. Am J Chin Med. 2020;48(3):651–78.

144 Wei T-YW, Wu P-Y, Wu T-J, Hou H-A, Chou W-C, Teng C-LJ, et al. Aurora A and NF-κB Survival Pathway Drive Chemoresistance in Acute Myeloid Leukemia via the TRAF-Interacting Protein TIFA. Cancer Res. 2017 Jan;77(2):494–508.

145 Tavernier N, Sicheri F, Pintard L. Aurora A kinase activation: Different means to different ends. Journal of Cell Biology. 2021 Jul;220(9):e202106128.

146 Bertolin G, Sizaire F, Herbomel G, Reboutier D, Prigent C, Tramier M. A FRET biosensor reveals spatiotemporal activation and functions of aurora kinase A in living cells. Nature Communications. 2016 Sep;7:12674.

147 Zhang H, Zhang W, Jiang L, Chen Y. Recent advances in systemic therapy for hepatocellular carcinoma. Biomarker Research. 2022 Jan;10(1):3.

148 Kim T, Issa D, Onyshchenko M. Analyzing TCGA Data to Identify Gene Mutations Linked to Hepatocellular Carcinoma in Asians. Gastrointestinal Tumors. 2022 Apr;9(2–4):43–58.

149 Toh MR, Wong EYT, Wong SH, Ng AWT, Loo L-H, Chow PK-H, et al. Global Epidemiology and Genetics of Hepatocellular Carcinoma. Gastroenterology. 2023 Apr;164(5):766–82.

150 Sim YK, Chong MC, Gandhi M, Pokharkar YM, Zhu Y, Shi L, et al. Real-World Data on the Diagnosis, Treatment, and Management of Hepatocellular Carcinoma in the Asia-Pacific: The INSIGHT Study. Liver Cancer. 2023 Oct;1–16.

151 Liu Z, Wu B, Liu X, Wu X, Du J, Xia G, et al. CD73/NT5E-mediated ubiquitination of AURKA regulates alcohol-related liver fibrosis via modulating hepatic stellate cell senescence. Int J Biol Sci. 2023;19(3):950–66.

152 Grisetti L, Saponaro AA, Sukowati CHC, Tarchi P, Crocè LS, Palmisano S, et al. The expression of Aurora Kinase A and its potential role as a regulator of Programmed Death-Ligand 1 in hepatocellular carcinoma: Implications for immunotherapy and immune checkpoint regulation in hepatocarcinogenesis. Digestive and Liver Disease. 2023 Sep;55:S219–20.

153 Jeong GU, Ahn B-Y. Aurora kinase A promotes hepatitis B virus replication and expression. Antiviral Research. 2019 Oct;170:104572.

154 Bao Z, Lu L, Liu X, Guo B, Zhai Y, Li Y, et al. Association between the functional polymorphism Ile31Phe in the AURKA gene and susceptibility of hepatocellular carcinoma in chronic hepatitis B virus carriers. Oncotarget. 2017 Aug;8(33):54904–12.

155 Sumida Y, Nakajima A, Itoh Y. Limitations of liver biopsy and non-invasive diagnostic tests for the diagnosis of nonalcoholic fatty liver disease/nonalcoholic steatohepatitis. World J Gastroenterol. 2014 Jan;20(2):475–85.

156 Shin SO, Lee KH, Kim JH, Baek S-H, Park J-W, Gabrielson EW, et al. Alternative splicing in 5'-untranslational region of STK-15 gene, encoding centrosome associated kinase, in breast cancer cell lines. Exp Mol Med. 2000 Dec;32(4):193–6.

157 Lai C-H, Tseng JT, Lee Y-C, Chen Y-J, Lee J-C, Lin B-W, et al. Translational up-regulation of Aurora-A in EGFR-overexpressed cancer. J Cell Mol Med. 2010 Jun;14(6B):1520–31.

158 Cacioppo R, Akman HB, Tuncer T, Erson-Bensan AE, Lindon C. Differential translation of mRNA isoforms underlies oncogenic activation of cell cycle kinase Aurora A. Elife. 2023 Jun;12:RP87253.

159 Li J, Guo W, Xue W, Xu P, Deng Z, Zhang D, et al. Long noncoding RNA AURKAPS1 potentiates malignant hepatocellular carcinoma progression by regulating miR-142, miR-155 and miR-182. Sci Rep. 2019 Dec;9(1):19645.

160 Jiang M, Bai M, Xu S, Wang T, Lei J, Xu M, et al. Blocking AURKA with MK-5108 attenuates renal fibrosis in chronic kidney disease. Biochim Biophys Acta Mol Basis Dis. 2021 Nov;1867(11):166227.

161 Yang Y, Santos DM, Pantano L, Knipe R, Abe E, Logue A, et al. Screening for Inhibitors of YAP Nuclear Localization Identifies Aurora Kinase A as a Modulator of Lung Fibrosis. Am J Respir Cell Mol Biol. 2022 Jul;67(1):36–49.

162 Huang D-H, Jian J, Li S, Zhang Y, Liu L-Z. TPX2 silencing exerts anti-tumor effects on hepatocellular carcinoma by regulating the PI3K/AKT signaling pathway. Int J Mol Med. 2019 Dec;44(6):2113–22.

163 Wang H, Chu F, Zhang X, Zhang P, Li L, Zhuang Y, et al. TPX2 enhances the transcription factor activation of PXR and enhances the resistance of hepatocellular carcinoma cells to antitumor drugs. Cell Death Dis. 2023 Jan;14(1):1–17.

164 Hsu C-W, Chen Y-C, Su H-H, Huang G-J, Shu C-W, Wu TT-L, et al. Targeting TPX2 Suppresses the Tumorigenesis of Hepatocellular Carcinoma Cells Resulting in Arrested Mitotic Phase Progression and Increased Genomic Instability. Journal of Cancer. 2017 May;8(8):1378–94.

165 Asteriti IA, Polverino F, Stagni V, Sterbini V, Ascanelli C, Naso FD, et al. AurkA nuclear localization is promoted by TPX2 and counteracted by protein degradation. Life Sci Alliance. 2023 May;6(5):e202201726.

166 Fu J, Bian M, Xin G, Deng Z, Luo J, Guo X, et al. TPX2 phosphorylation maintains metaphase spindle length by regulating microtubule flux. Journal of Cell Biology. 2015 Aug;210(3):373–83.

167 Kettenbach AN, Schweppe DK, Faherty BK, Pechenick D, Pletnev AA, Gerber SA. Quantitative Phosphoproteomics Identifies Substrates and Functional Modules of Aurora and Polo-Like Kinase Activities in Mitotic Cells. Science Signaling. 2011 Jun;4(179):rs5–rs5.

168 Jančík S, Drábek J, Radzioch D, Hajdúch M. Clinical Relevance of KRAS in Human Cancers. J Biomed Biotechnol. 2010;2010:150960.

169 Huang L, Guo Z, Wang F, Fu L. KRAS mutation: from undruggable to druggable in cancer. Sig Transduct Target Ther. 2021 Nov;6(1):1–20.

170 Gomes-Filho SM, Dos Santos EO, Bertoldi ERM, Scalabrini LC, Heidrich V, Dazzani B, et al. Aurora A kinase and its activator TPX2 are potential therapeutic targets in KRAS-induced pancreatic cancer. Cell Oncol (Dordr). 2020 Jun;43(3):445–60.

171 dos Santos EO, Carneiro-Lobo TC, Aoki MN, Levantini E, Bassères DS. Aurora kinase targeting in lung cancer reduces KRAS-induced transformation. Molecular Cancer. 2016 Feb;15(1):12.

172 Sharma RK, Chafik A, Bertolin G. Aurora kinase A/AURKA functionally interacts with the mitochondrial ATP synthase to regulate energy metabolism and cell death. Cell Death Discov. 2023 Jun;9(1):1–12.

173 Cabral LKD, Giraudi PJ, Giannelli G, Dituri F, Negro R, Tiribelli C, et al. Network Analysis for the Discovery of Common Oncogenic Biomarkers in Liver Cancer Experimental Models. Biomedicines. 2023 Jan;11(2):342.

174 Falchook GS, Bastida CC, Kurzrock R. Aurora Kinase Inhibitors in Oncology Clinical Trials: Current State of the Progress. Seminars in Oncology. 2015 Dec;42(6):832–48.

175 Bavetsias V, Linardopoulos S. Aurora Kinase Inhibitors: Current Status and Outlook. Frontiers in Oncology. 2015 [cited 2024 Jan 17]. ;5. Available from: https://www.frontiersin.org/articles/10.3389/fonc.2015.00278

176 Yang Y, Ding L, Zhou Q, Fen L, Cao Y, Sun J, et al. Silencing of AURKA augments the antitumor efficacy of the AURKA inhibitor MLN8237 on neuroblastoma cells. Cancer Cell International. 2020 Jan;20(1):9.

177 Ju X, Zhang H, Zhou Z, Wang Q. Regulation of PD-L1 expression in cancer and clinical implications in immunotherapy. Am J Cancer Res. 2020 Jan;10(1):1–11.

178 Zhong F, Cheng X, Sun S, Zhou J. Transcriptional activation of PD-L1 by Sox2 contributes to the proliferation of hepatocellular carcinoma cells. Oncology Reports. 2017 May;37(5):3061–7.

179 Yadollahi P, Jeon Y-K, Ng WL, Choi I. Current understanding of cancer-intrinsic PD-L1: regulation of expression and its protumoral activity. BMB Rep. 2021 Jan;54(1):12–20.

180 Deng J, Jiang W, Liu L, Zhan W, Wu Y, Xu X. Research progress on the intrinsic non-immune function of PD-L1 in tumors (Review). Oncology Letters. 2023 Jan;25(1):1–13.

181 Wang Y, Wang H, Zhao Q, Xia Y, Hu X, Guo J. PD-L1 induces epithelial-to-mesenchymal transition via activating SREBP-1c in renal cell carcinoma. Med Oncol. 2015 Aug;32(8):212.

182 Cui P, Jing P, Liu X, Xu W. Prognostic Significance of PD-L1 Expression and Its Tumor-Intrinsic Functions in Hypopharyngeal Squamous Cell Carcinoma. Cancer Manag Res. 2020;12:5893–902.

183 Qiu XY, Hu DX, Chen W-Q, Chen RQ, Qian SR, Li CY, et al. PD-L1 confers glioblastoma multiforme malignancy via Ras binding and Ras/Erk/EMT activation. Biochim Biophys Acta Mol Basis Dis. 2018 May;1864(5 Pt A):1754–69.

184 Chang C-H, Qiu J, O'Sullivan D, Buck MD, Noguchi T, Curtis JD, et al. Metabolic Competition in the Tumor Microenvironment Is a Driver of Cancer Progression. Cell. 2015 Sep;162(6):1229–41.

185 Kim S, Jang J-Y, Koh J, Kwon D, Kim YA, Paeng JC, et al. Programmed cell death ligand-1-mediated enhancement of hexokinase 2 expression is inversely related to T-cell effector gene expression in non-small-cell lung cancer. J Exp Clin Cancer Res. 2019 Nov;38(1):462.

186 Almozyan S, Colak D, Mansour F, Alaiya A, Al-Harazi O, Qattan A, et al. PD-L1 promotes OCT4 and Nanog expression in breast cancer stem cells by sustaining PI3K/AKT pathway activation. Int J Cancer. 2017 Oct;141(7):1402–12.

187 Zhang X, Li F, Zheng Y, Wang X, Wang K, Yu Y, et al. Propofol Reduced Mammosphere Formation of Breast Cancer Stem Cells via PD-L1/Nanog In Vitro. Oxid Med Cell Longev. 2019;2019:9078209.

188 Chen RQ, Xu XH, Liu F, Li CY, Li YJ, Li XR, et al. The Binding of PD-L1 and Akt Facilitates Glioma Cell Invasion Upon Starvation via Akt/Autophagy/F-Actin Signaling. Front Oncol. 2019;9:1347.

189 Gao H, Zhang J, Ren X. PD-L1 regulates tumorigenesis and autophagy of ovarian cancer by activating mTORC signaling. Biosci Rep. 2019 Dec;39(12):BSR20191041.

190 Jiang X, Wang J, Deng X, Xiong F, Ge J, Xiang B, et al. Role of the tumor microenvironment in PD-L1/PD-1-mediated tumor immune escape. Molecular Cancer. 2019 Jan;18(1):10.

191 Li Q, Han J, Yang Y, Chen Y. PD-1/PD-L1 checkpoint inhibitors in advanced hepatocellular carcinoma immunotherapy. Front Immunol. 2022 Dec;13:1070961.

192 Kudo M. Adjuvant atezolizumab-bevacizumab after curative therapy for hepatocellular carcinoma. Hepatobiliary Surg Nutr. 2023 Jun;12(3):435–9.

193 Lawson NL, Dix CI, Scorer PW, Stubbs CJ, Wong E, Hutchinson L, et al. Mapping the binding sites of antibodies utilized in programmed cell death ligand-1 predictive immunohistochemical assays for use with immuno-oncology therapies. Mod Pathol. 2020;33(4):518–30.

194 Lee H-H, Wang Y-N, Xia W, Chen C-H, Rau K-M, Ye L, et al. Removal of N-Linked Glycosylation Enhances PD-L1 Detection and Predicts Anti-PD-1/PD-L1 Therapeutic Efficacy. Cancer Cell. 2019 Aug;36(2):168-178.e4.

195 Liu C-Q, Xu J, Zhou Z-G, Jin L-L, Yu X-J, Xiao G, et al. Expression patterns of programmed death ligand 1 correlate with different microenvironments and patient prognosis in hepatocellular carcinoma. Br J Cancer. 2018 Jul;119(1):80–8.

196 Yang Z, Zhang L, Liu J, Yang L, Xue H, Bai S, et al. PD-L1 combined with HDAC9 is a useful prognostic predictor in hepatocellular carcinoma. Translational Cancer Research. 2021 May;10(5). DOI: 10.21037/tcr-20-3415

197 Tanaka T, Koga H, Suzuki H, Iwamoto H, Sakaue T, Masuda A, et al. Anti-PD-L1 antibodies promote cellular proliferation by activating the PD-L1–AXL signal relay in liver cancer cells. Hepatol Int. 2023 Aug DOI: 10.1007/s12072-023-10572-3

Research dissemination

List of publications

Published:

- **Grisetti L**, Võ NVT, Nguyễn NNQ, Crocè LS, Visintin A, Tiribelli C, Pascut D. MiR-3201 as a Prognostic Blood Biomarker for Curative Treatments in Hepatocellular Carcinoma. Technol Cancer Res Treat. 2022 Jan-Dec;21:15330338221132924. doi: 10.1177/15330338221132924. PMID: 36537076; PMCID: PMC9772976.
- **Grisetti L**, Cabral LKD, Pratama MY, Tiribelli C, Pascut D. Biomarkers for the Detection and Management of Hepatocellular Carcinoma in Patients Treated with Direct-Acting Antivirals. Cancers (Basel). 2022 May 30;14(11):2700. doi: 10.3390/cancers14112700. PMID: 35681679; PMCID: PMC9179595.
- **Grisetti L**, Saponaro AA, Sukowati CHC, Tarchi P, Crocè LS, Palmisano S, Rosso N, Giraudi PJ, Anfuso B, Tiribelli C, Pascut D. The expression of Aurora Kinase A and its potential role as a regulator of Programmed Death-Ligand 1 in hepatocellular carcinoma: Implications for immunotherapy and immune checkpoint regulation in hepatocarcinogenesis. Digestive and Liver Disease, volume 55, supplement 3, s219-s220. September 2023. doi: 10.1016/j.dld.2023.08.021.

Under review:

- **Grisetti L**, Garcia CJC; Saponaro AA, Tiribelli C, Pascut D. The role of Aurora kinase A in hepatocellular carcinoma: Unveiling the intriguing functions of a key but still underexplored factor in liver cancer. Cell proliferation.

Oral presentations

- The potential combination of oncogene-targeted therapy and immunotherapy for the treatment of hepatocellular carcinoma. Shark Tank: Young Investigator research competition for the best clinical or translational proposal achievable in one year. ILCA 2023, 17th annual conference. Amsterdam, The Netherlands. September 7-9, 2023.

- Eziologia e caratteristiche genomiche ed epigenomiche dell'epatocarcinoma. Ricerca scientifica, medicina personalizzata e multidisciplinarietà: come ottimizzare la cura dei tumori dell'apparato digerente. Castellana Grotte (BA), Italy. February 9, 2024.

Poster presentations

- Exploring the effects of Aurora Kinase A inhibition in liver cancer: A possible link to PD-L1 regulation. ILCA 2022, 16th annual conference. Madrid, Spain. September 1-4, 2022.
- The role of Aurora kinase A in hepatocellular carcinoma: possible regulation of Programmed death–ligand 1. EASL 2023, Liver Cancer Summit. Estoril, Portugal. April 20-22, 2023.
- The expression of Aurora kinase A in hepatocarcinogenesis and its role in Programmed Death–Ligand 1 regulation. ILCA 2023, 17th annual conference. Amsterdam, The Netherlands. September 7-9, 2023.
- The expression of Aurora Kinase A and its potential role as a regulator of Programmed Death-Ligand 1 in hepatocellular carcinoma: implications for immunotherapy and immune checkpoint regulation in hepatocarcinogenesis. AISF 2023 Monothematic Conference. Liver oncology: from basic science to liver transplantation. Padua, Italy. September 28-29, 2023.

Acknowledgments

Liver samples were generously provided by the Surgery Department of the University Hospital of Trieste and Azienda Sanitaria Universitaria Giuliano Isontina (ASUGI). Special thanks to Dr. Deborah Bonazza, Dr. Michela Giuricin, Dr. Paola Tarchi, Prof. Silvia Palmisano, and Prof. Fabrizio Zanconati for their valuable contributions. Prof. Saveria Lory Crocè and Dr. Paola Tarchi provided essential demographic, clinical, and pathological data for HCC patients.

For human samples, sincere appreciation goes to other members of the Italian Liver Cancer Foundation, including Ph.D. Caecilia H.C. Sukowati (Liver Cancer Unit) for HCC and healthy samples, and Ph.D. Natalia Rosso and Ph.D. Pablo J. Giraudi (MASLD Group) for MASLD samples. Special acknowledgment to Ph.D. Beatrice Anfuso (International Centre for Genetic Engineering and Biotechnology (ICGEB)) and Ph.D. Caecilia H.C. Sukowati for providing mouse samples from a previous project conducted at the Italian Liver Foundation.

Thanks to the pathology department of ASUGI for performing the immunohistochemical staining of KI67 and PD-L1. Dr. Deborah Bonazza (Surgical Pathology, ASUGI) and Emilana Giacomello (Department of Medical, Surgical, and Health Sciences, University of Trieste) played a fundamental role in the analysis and interpretation of the results.

Special gratitude to Ph.D. Loraine Kay Cabral and Ph.D. Caecilia H.C (Liver Cancer Unit, Italian Liver Cancer Foundation) for providing mRNA expression results of PD-L1 knockdown in JHH6 and the siRNA targeting PD-L1 used in their study.

Heartfelt thanks to the members of my group at the Italian Liver Foundation. To my supervisor, Dr. Prof. Claudio Tiribelli, for consistent support, encouragement, and trust. To my co-supervisor, Devis Pascut, for exemplary leadership and guidance, shaping me into a researcher. This study is the expression of your efforts in training me and the hours spent discussing intricate project results.

Special thanks to Matteo Barbaglia for teaching GraphPad software usage, Anna Alessia Saponaro for assistance during her master's internship, Clarissa Garcia for conducting experiments to set conditions for atezolizumab treatments, and Vivien Josol for help with the luciferase assay. Gratitude also extends to other past and present group members involved in various other research

projects (Inah Marie Aquino, Giulia Maiorana, and Therriz Mamerto) and all the members of the Italian Liver Foundation for their support and help.